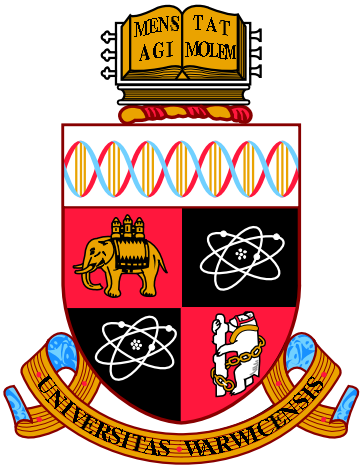

Threaded Network of Ring Polymers

by

Nart Noodee

Thesis

Submitted to the University of Warwick

for the degree of

Doctor of Philosophy

Department of Physics

April 2021

Contents

Acknowledgments

First and foremost, I would like to express my sincere gratitude to my supervisor, Matthew Turner, for dedicating his time to guide me during the years of my study, for patiently letting me learn at my pace, and for keeping me on track. His expertise and insight have helped me gain the understanding of how to be a good researcher. I am forever grateful.

I would like to thank Varagorn and Naraphorn (Physics Chula) who introduced me to the world of soft condensed matter and encouraged me to pursue a PhD in this field. I would also like to thank my family and friends for their love, support and sacrifices throughout my study. I am fortunate to have such wonderful people around me.

Finally, I gratefully acknowledge the funding from the Development and Promotion of Science and Technology Talents Project (DPST), Thailand. Without their support, my PhD journey would not have been possible.

Declarations

I declare that this thesis submitted in support for the application for the degree of Doctor of Philosophy is my own work and has not been submitted for a degree at another university.

Abstract

A system of highly entangled ring polymers embedded in a gel was studied using Monte Carlo simulation and analytic approaches using the techniques of statistical mechanics. The rings are assumed to be flexible, unlinked and unknotted at synthesis. The gel confines the ring polymers to adopt "duplex" structures in which any mesh volume of the gel occupied by the polymer contains both an outgoing and returning segment of the ring. These duplex structures are further assumed to be unbranched for simplicity. The emergence of effective "ends" on these linear duplex configurations offers the possibility of utilising the standard tube model and reptation dynamics, developed for linear polymers. This helps to simplify the dynamics of the rings, that can then be treated as reptating linear chains. Inter-ring threadings have been confirmed to exist in recent molecular dynamics (MD) simulations. These can be incorporated in the present work by the process of one end of a duplex chain threading through (between the two strands of) a second duplex ring. This generates a pair of threadings, an "active" one on the threading ring and a partner "passive" threading on the threaded ring. Threadings are included in our Monte Carlo simulations and are shown to have very different properties. The main advantage of this approach is that we can access a regime in which there are many threadings per ring, a regime that remains inaccessible to brute force MD or, indeed, any other technique. The simulation results suggests that threadings play a vital role in reducing the ring polymer mobilities, resulting

in an increase in the stress relaxation time that is exponential in the number of threadings per polymer. Several other novel features are identified, including a heavy tailed distribution of stress relaxation times and a sub-diffusive plateau in the mean squared curvilinear displacement of the polymers as a function of time. The data presented in this thesis supports the hypothesis that the fundamental mechanism behind the slowing down of ring dynamics is pinning provided by passive threadings. The distribution of the active penetrations reveals the previously unexplored role of an entropy associated with the network of inter-ring threadings. Some threading configurations are topologically inaccessible and bias the positions of the active threadings on their corresponding chain contours, enriching them near the chain ends. We explore an analytic approach to understand the driven diffusion of polymers relative to the active threading sites. In one limit, where the network entropy is small, we recover threading lifetimes consistent with Doi-Edwards theory of linear polymer. In the limit where the network entropy plays an important role the agreement is less good. This may indicate that mean-field approaches are fundamentally inadequate to study this problem and motivates possible future studies, e.g. based on retaining information at the level of distribution functions.

Chapter 1

Introduction

Polymers are macromolecules composed of repeating subunits called “monomers". These substances are abundant in nature and play an important role in human society. They are found in the DNA of living cells, a very long molecule containing genetic code, to other biological constituents, such as proteins and carbohydrates [Lodish et al., 2008]. In fact, humans were familiar with polymeric materials a long time ago, without knowing about their microscopic structure. Many of these were in the forms of naturally occurring materials, such as cotton, silk fibres, leather and natural rubber *(Hevea brasiliensis)*. The development of Polymer Chemistry in the early 20th-century improved our microscopic knowledge and triggered a huge amount of research. Polymer Physics emerged in order to study the mechanical, statistical and dynamical properties of polymers. Many of these are unique and cannot be found in other materials, for example, a polymeric liquid can behave like a liquid by changing its shape to fill containers, however, it still has a rubber-like property as it performs temporary contraction after a small strain is applied. This property is called “viscoelasticity".

Polymers can appear in various architectures, such as linear, ring and branched, depending on the molecular arrangement [Flory, 1953, Rubinstein and Colby, 2003, Carraher, 2017]. The simplest type is arguably the linear chains - with monomeric units formed in a linear sequence from start to finish. Due to this simplicity, understanding linear polymers is a sensible starting point for those who want to study polymers. Some aspects of the physics of other polymer architectures are mirrored in the behaviour of linear chains,

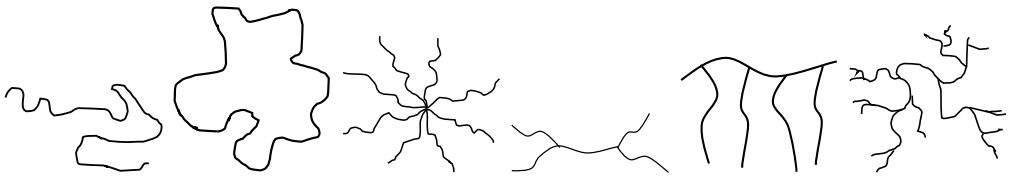

Figure 1.1: Polymers in various architectures: (a) linear, (b) ring, (c) star, (d) H-shaped, (e) comb and (f) random branched

which is not surprising as they are made up of linear chains joined to each other. To investigate the statistical properties of flexible polymers, one might start with so-called "ideal chain" conformations in which the interactions of the polymer with itself are neglected and the solvent is correspondingly neutral. Due to the lack of self-interactions the polymer configurations then adopt the statistics of a random walk, this maximising the configurational entropy. Models corresponding to this limit include the "freely joined chain" model in which monomers are treated as inextensible (rods) connected by freely-jointed connections (hinges) [Kuhn, 1934, Kuhn, 1936, Kuhn, 1939]. A related model is the "freely rotating chain" in which the hinges cannot bend but can freely rotate while preserving a fixed angle between neighbouring segments. In both cases it has been shown that the size of the polymer R, measured as the root mean square of the end-to-end vector, written $\sqrt{\langle \mathbf{R} \cdot \mathbf{R} \rangle}$ depends on the degree of polymerisation M as $R \sim M^{1/2}$ [Volkenstein, 1958, Birshtein and Ptitsyn, 1966, Flory, 1969] in the limit where M is very large. The exponent $1/2$ is characteristic of random walks and diffusive processes in general. The distribution of the end-to-end vector in this large M limit is Gaussian. The size of polymers is also often measured by using the radius of gyration R_g, defined by analogy with the rotational inertia of the corresponding chain configurations. A similar scaling holds for this measure of chain size [Berne and Pecora, 2000]. The bead-and-spring model for a polymer chain has monomeric "beads" connected by harmonic "springs" [Flory, 1953, Rubinstein and Colby, 2003]. In the ideal limit this model also recovers the same exponent of $1/2$.

The behaviour of real polymers can diverge from that of ideal chains in the presence of interactions such as steric effects, van der Waals attraction or the effect of solvents. Flory approached the problem in the presence of

good solvents for the polymer (where chain repulsion is most apparent) by constructing a crude mean-field theory [Flory, 1949,Flory, 1953]. This balanced two effects that control the coil size: the size of the random chain configuration, related to the entropy of those configurations, and a repulsive excluded volume interaction. The result suggested that the good-solvent, or excluded volume, corresponding to the size of the linear polymer $r \sim M^{\nu}$, approaches $\nu \approx 3/5$ [Flory, 1953, Bhattacharjee et al., 2013], i.e. the polymer coil swells in size. In spite of the crude approximations used, this value is very close to that found in experiments [Wall et al., 1963, Cotton, 1980], and is reasonably close to simulation results [Domb et al., 1965].

There are also a number of models for the dynamical properties of polymers, many based on a model by Rouse [Zimm, 1956,Edwards, 1967,de Gennes, 1971, Edwards, 1977]. Here the dynamics of the bead-spring chain in dilute solution is approached by treating the motion of each bead as overdamped, such as might arise from friction with a viscous solvent, but stopping short of including a more faithful description of the system hydrodynamics, in which the motion of one bead sets up flows that influence the motion of others.

This approach provided a prediction for the correlation time of the end-to-end vector τ_R, scaling with M as $\tau_R \propto M^2$ [Rouse, 1953]. This finding is only partially consistent with experiments in which the stress relaxation time is proportional to $M^{\frac{3}{2}}$ [King et al., 1974, Nose and Chu, 1979]. A more accurate treatment of hydrodynamic effects was later provided by the Zimm model [Zimm, 1956], resolving this discrepancy.

The study of polymer physics has not been limited to the case of single (dilute) linear polymers, but has also been extended to systems containing many chains in close proximity. The mutually entangled systems that result include the melt (no solvent) and concentrated solutions, as well as cross-linked states, such as the gel phase. The dynamics of these systems are all rather different from isolated linear chains. In particular, topological constraints arise due to the presence of inaccessible configurations. These seriously affect the dynamical properties of polymers. One example of how topological constraints can affect the dynamics of linear polymers is the case of a linear polymer embedded in a fixed network in which it can move freely subject to the constraint that no chain crossings are allowed, see Fig. 1.2. An extremely sim-

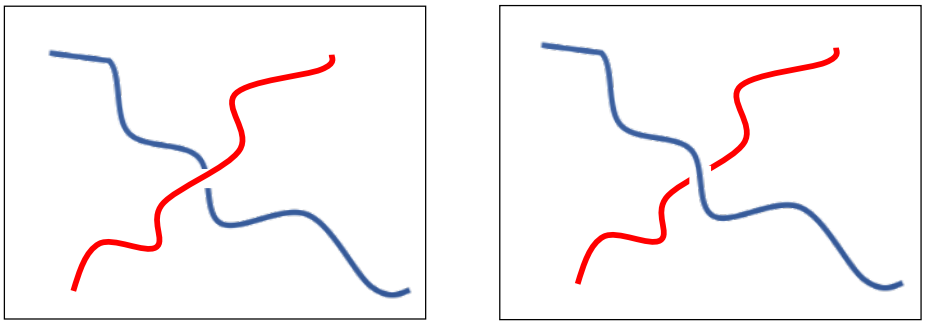

(a) (b)

Figure 1.2: A sketch showing a forbidden dynamical transition. The red polymer cannot cut through the middle section of the blue chain and interchange the order from state (a) to state (b). This is the essential nature of an "entanglement". Many such entanglements results in the emergence of an entanglement "tube" in concentrated systems.

ilar situation occurs in concentrated polymer solutions, well above the overlap concentration $c^\star$. In this regime the polymers are in a highly mutually entangled state. The lateral motion of one polymer is therefore substantially impeded by the presence of its neighbours, in a similar way to that which occurs in the gel (although the entanglements are not strictly permanent). The dynamics in both of these situations have been understood in terms of two concepts: the tube model and *reptation*. This framework assumes that the motion of the polymer chain is primarily directed (symmetrically) by its two ends and occurs inside a tube-like region confined by the surrounding chains. This model involves the concept of the primitive chain, which connects the terminal segments of the polymer along the tube mid-line, and ignores the precise configuration, or configurational rearrangements, occurring inside the tube [de Gennes, 1971, Doi and Edwards, 1986, Doi, 1996]. By solving an effective diffusion equation for the motion of the polymer along the primitive path an understanding of the polymer dynamics can be derived. The solution to this shows that the reptation time τ_d is larger than the correlation time from the Rouse model, roughly depending on M^3 rather than M^2.

A natural modification of linear polymers is to join their ends together to form rings. This seemingly minor alteration significantly changes both the dynamic and static properties of the polymers. Essentially, linear polymers

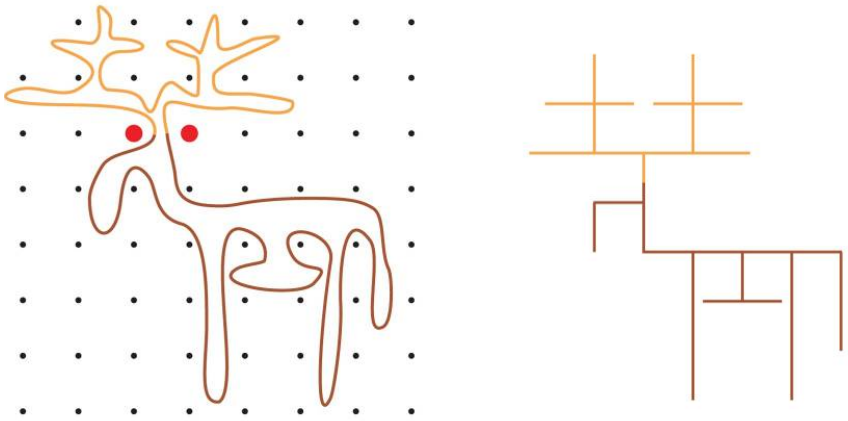

(a) (b)

Figure 1.3: Ring polymer embedded in a gel. The moose-like conformation in (a) is formed by double folded segments of ring polymer which are confined by uncrossable obstacles shown in dots. (b) The ring can be mapped onto a "lattice animal" structure. The images are taken from [Kapnistos et al., 2008].

protrude and retract their ends to explore their surrounding environment. Unlike their linear counterpart, ring polymers do not contain such terminal end segments. Rings spatially relocate themselves by generating temporary double folded segments. An example of such a configuration is shown in Fig. 1.3. Such conformations are sometimes called "lattice animals", analogous to annealed branched polymers. As well as being of interest for the profound role that their topology has on the physical properties, ring polymers are also ubiquitous in most prokaryotic cells, where they are found as Bacterial plasmids, formed from rings of DNA [Drew et al., 2004, Bates and Maxwell, 2005], see Fig.1.4.

In the past few decades, understanding the static and dynamic properties of long, unlinked ring polymers in the concentrated regime remains perhaps the most challenging open problem in polymer physics. As such it has attracted significant contemporary research interest. For instance, studies on how entangled ring polymers relax corresponding stress [Kapnistos et al., 2008] and the static and dynamic properties of nonconcatenated ring polymers in a melt [Halverson et al., 2011a, Halverson et al., 2011b, Rosa and Everaers, 2014]. If rings are synthesised in a state in which they are mutually unknotted and unlinked then they are uncrossable. These systems are difficult to analyse

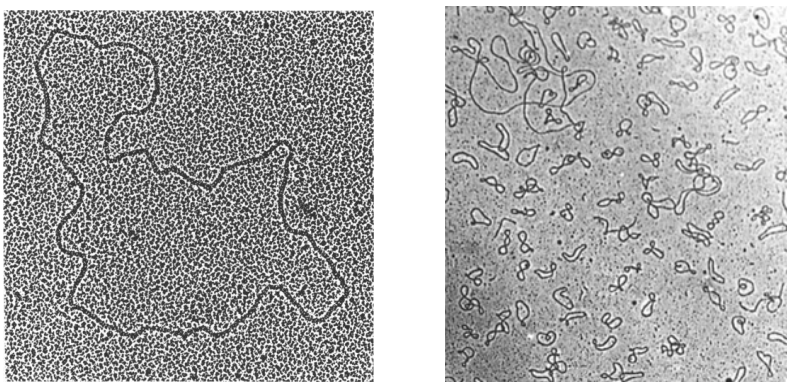

(a) (b)

Figure 1.4: Examples of ring polymers in biological systems. Electron micrographs of (a) circular DNA from Escherichia alcalescens MMCA 96 (Ref. [Christiansen et al., 1973]) and (b) a network of topoisomerase II-decatenated circular DNAs. The images are taken from [Shapiro et al., 1999].

theoretically due to the essentially non-local nature of these topological constraints. To our knowledge no practical method to incorporate this exists, short of exhaustive molecular dynamics simulations that are necessarily restricted in the polymer lengths that can be explored. Simulation studies [Halverson et al., 2011a, Grosberg, 2014] confirm that the statistics of ring polymers in concentrated solutions are different from those of linear chains. Ring polymers have a spatial size as measured by the radius of gyration R_g , showing asymptotic scaling close to $R_g \sim M^{1/3}$, even further from the ideal scaling of $R_g \sim M^{1/2}$ for linear polymers than was proposed in earlier scaling estimates [Grosberg et al., 1988]. Ring polymers have many intra-chain contacts and are thought to collapse spatially as a result of topological constraints with their neighbours. The dynamics is also quite unusual, with evidence for the onset of a slowed state for the longest chains that is sometimes referred to as a "topological glass" [Lo and Turner, 2013, Michieletto and Turner, 2016, Michieletto et al., 2017a, Smrek et al., 2020]. The lack of analytic theory is a major conceptual roadblock in deeper understanding of these systems and this motivates us to analyse a highly simplified model for the chain statistics. We adopt a model of ring polymers in the concentrated state in which the polymers are assumed to collapse, extending into a linear "duplex" structure, in which each outgoing chain segment has a returning chain segment in the same tube segment, and

further assume, purely for simplicity, that this state has no branches. The model is clearly an idealisation, although a similar collapsed state is thought to arise when rings are embedded in a polymer gel, leading to configurations reminiscent of a lattice animal [Rubinstein, 1986, Kapnistos et al., 2008, Smrek and Grosberg, 2015] with branches that arise with a rate that is controlled by the chain stiffness and gel mesh size. It may well be that we neglect important features of the chain configurations in the concentrated state when we adopt this strong assumption. However, several considerable advantages follow from it. Firstly, we adopt a set of chain configurations that have a reference state that is naturally unlinked: one can take (any) microstate of concentrated linear polymers and swell the chains locally to a duplex structure (preserving uncrossability) without changing the system topology. Quasi-topological interactions can be supported in this system by permitting the duplex rings to "thread" through each other. This does not change the system topology provided no chain crossing occurs. Such threadings are thought to play a role in the emergence of any topological glass. Networks of mutual threadings must be (un)done in specific sequences, leading to dramatically slowed dynamics [Michieletto et al., 2014, Lo and Turner, 2013]. This construction allows us to apply the considerable technical tools developed for linear polymers to the analysis of systems of mutually threaded ring polymers. Our model therefore represents at least a candidate for a framework within which we might hope to make analytic progress. We are further encouraged by the fact that polymer physics has many success stories involving models based on extremely crude approximations that have nonetheless proved to be highly informative.

This thesis aims to contribute to our understanding of systems of entangled ring polymers in several ways. We investigate the system by conducting extensive Monte Carlo simulations. To do so, we consider double folded, unbranched duplex rings, such as previously studied in [Lo and Turner, 2013]. By treating rings as linear (duplex) chains, the ring architecture resembles a linear polymer residing in a confined tube-like region formed by the entanglements with surrounding polymers or any gel into which the polymers may be embedded.

Several methods have now been developed to study the role of threadings in simulations. One approach is to employ fully 3D molecular dynam-

ics (MD) simulations and employ a minimal surface, constructed on the ring contour as a threshold for threading by other rings [Smrek and Grosberg, 2016, Smrek et al., 2019]. This provides a surface through which other rings might penetrate, then being recorded as threadings (under this definition) see Fig.1.5. Another involves examining the effect of artificially "freezing" poly-

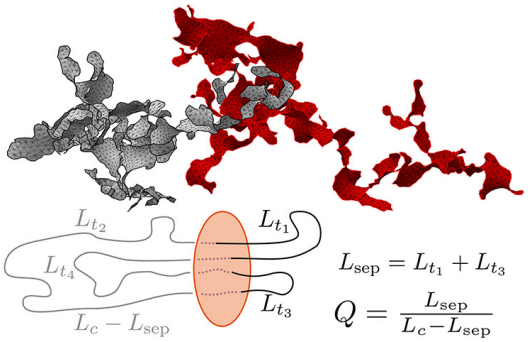

Figure 1.5: Minimal surfaces of two neighbouring ring polymers. The bottom cartoon pictures shows a ring coloured in grey and black threads into the minimal surface of another ring painted in orange. The visible labels present the relative contour length fraction Q. The image is taken from [Smrek et al., 2019].

mers to infer the presence of threadings via the "caging" effect on the dynamics of other chains, thereby inferred to be threaded by the frozen chain [Michieletto and Turner, 2016]. Yet another approach is to perform molecular dynamics of ring polymers in a gel, as shown in Fig.1.6, and to exploit a cutting-and-pasting approach that exploits the gel architecture to construct a topological test of threading [Michieletto et al., 2014].

In this thesis, we choose to adopt a method that incorporates inter-ring threading within a model of linear duplex chains, in which the ring is folded back on itself, as previously described. More detail on this mechanism will be provided in Chapter 3 but, briefly, we make the assumption that duplex rings can thread each other (while remaining otherwise duplex). The threading rate is assumed to be extensive in the length of the target polymer (all segments are equally likely to be threaded) and otherwise depends on non-universal microscopic parameters which we do not attempt to model, rather we postulate a rate p per end-move of a single tube segment. We only incorporate space in the sense that each polymer moves along its own primitive path. Otherwise, all chains are assumed to occupy the same coarse-grained volume. Alternative

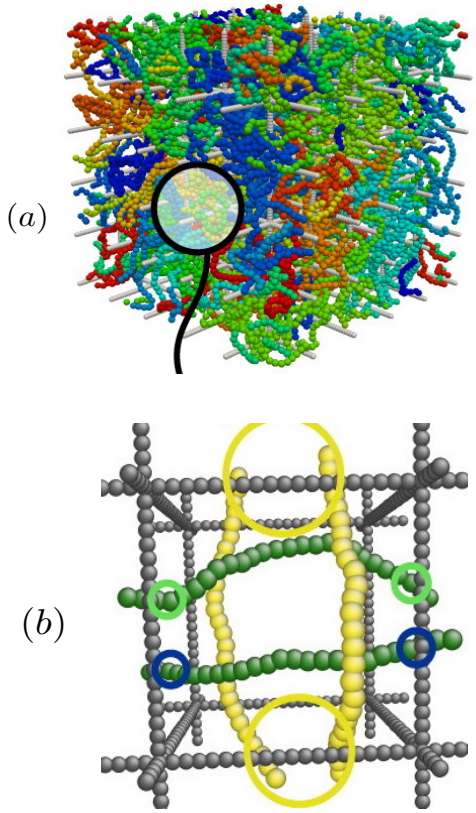

Figure 1.6: Ring polymers in a gel studied by using Molecular dynamics (MD). The image is taken from [Michieletto et al., 2014]. The above 3D picture in (a) represents a condensed system of 50 rings while the bottom sketch (b) shows the method of identifying the threading by counting the possible close loops.

approaches that assign a probabilistic weight to inter-ring threadings based on their physical locations are also possible but are not the focus of this work. This kind of setting is comparatively efficient in terms of computational run-time and, most importantly, can generate equilibrated systems with a large number of threadings: microscopically faithful MD simulations are limited to system sizes that correspond to only 1-2 threadings, insufficient to access any kind of universal regime that may exist for large numbers of threadings per chain [Michieletto et al., 2014]. By adopting this approach we can measure the stress relaxation function corresponding to the threaded network. We use this to construct a tube disengagement time and a disengagement rate, effectively probing opposite ends of the stress relaxation function and use these to attempt to build a better understanding of the mechanism of stress relaxation. We

can also study the rate and lifetime of threadings and the distribution of threadings, and their ages, along the primitive path. A significant new result in the present work is the identification of entropy associated with the network of threadings that has not previously been studied. We believe that this plays a central role in breaking the mean-field equivalence of the loss of stress per tube segment and the loss of threadings per tube segment. Motivated by this we seek to understand the system by constructing an analytic theory that incorporates the effect of the network entropy. This involves solving a Fokker-Planck equation for the motion of threading chains in the presence of a potential that arises due to the entropy of the threading network.

The content of this thesis is divided into five main chapters. Chapter 2 will provide the background theories and a review of the prior studies of rings in various conditions, mainly in gel and concentrated solution. Chapter 3 will be focused on the Monte Carlo simulation of duplex rings. The simulation procedure and measurement techniques are described in detail. The fourth chapter will describe how we analyse the results of the simulation, including the use of an analytic approach. Finally, in Chapter 5, I will draw some conclusions and summarise the main findings from this thesis.

Chapter 2

Static Conformation and Dynamics of Rings

2.1 Static conformation of rings and universal exponent

In polymer solutions the molecules begin to overlap and engage with others for concentrations above the overlap concentration $c^* \propto N^{1-3\nu}$ where N is the number of polymer segments. In the universal regime of large N polymers can be in entangled states, even at very low concentrations. In what follows we assume that our ring polymers are at concentrations well above c^* and are highly overlapping, with N_c chains occupying the same coil volume. MD simulations reveal that even when the exponent is close to 1/3 many chains can occupy the same coil volume, with single-chain volume fractions as small as $\sim 1\%$ [Halverson et al., 2011a, Michieletto and Turner, 2016]. In linear polymer melts it is well understood that entanglement plays no part when N is lower than the entanglement length N_e [de Gennes, 1979, Rubinstein and Colby, 2003]. For ring melts, a mean-field theory [Sakaue, 2012] predicts an intermediate regime $N_1 \lesssim N \lesssim N_2$ with the chains approximately ideal (exponent 1/2) for $N \lesssim N_1$ and compactified (exponent 1/3) for $N \gtrsim N_2$. These work suggests that N_1 and N_2 depend on the coordination number N_R, which can be thought of as the number of neighbouring rings [Kavassalis and Noolandi, 1987]. The simulation results found in [Vettorel et al., 2009,

Halverson et al., 2011b] suggest that $N_R(N_1) \sim 6$ chains and $N_R(N_2)$ is about $15 - 17$ chains. In the crossover regime the apparent exponent is around $2/5$ although identifying an unambiguous scaling regime in such a small window of N is challenging.

Microscopically faithful models of polymers can exhibit jamming. For example, the jammed packings of freely jointed chains made up of chains of hard spheres in contact with one another has been studied as a function of concentration [Karayiannis et al., 2009]. These result showed that the organisation was similar to that found in packings of single (monomeric) hard spheres. The jamming transition in macroscopic chains of granular particles (metal spheres) has also been studied [Lopatina et al., 2011]. They found that the jamming density decreased with chain length and was reduced in mixtures of granular chains and rings.

2.2 Reptation dynamics in melts, concentrated solutions and polymers embedded in gels

Polymer chains can be chemically conjugated to cross-link with one another, forming a three-dimensional network called a polymer gel. This gel does not dissolve in dilute solvent due to the permanent bonds connected the polymers. The gel itself can be formed at arbitrarily low volume fraction in a solvent, this fraction depending on the length of polymer between each cross-link. As a result additional polymers can be introduced into the gel. These can be linear polymers or rings - our interest lies in ring polymers embedded in a gel. The gel has a relatively small effect if linear polymers are embedded in it. They must live in a tube made up, at least in part, of entanglements with the gel polymer but are otherwise free to move to adopt any spatial configuration. However, the gel has a much more profound effect on embedded ring polymers. This is because ring polymers synthesised as unlinks are, and must remain, unlinked with the gel. This means that no "open" spatial configurations are allowed that would break this topological protection by encircling (any) covalently closed contours that can be traced through the gel. As shown in Fig.1.3, this results in the polymer adopting a

"duplex" configuration in which each gel mesh volume contains two strands and the polymer remains unlinked with the gel. Such duplex configurations are only rigorously preserved in this ensemble (ring + gel) and while this is therefore arguably the most relevant for our work we hope that our results may also have some relevance for ring melts in which any parts of the duplex pair form loops that mostly small, although large excursions do sometimes occur [Michieletto, 2016]. Edwards originally introduced the tube model [Edwards, 1967,Edwards, 1977], which is the tube-like region formed by entanglements with neighbouring polymeric strands, to describe the dynamics of polymers in rubbers. Using a similar idea, we can schematically draw a tube-like region to include fixed obstacles, see Fig.2.1. This tube is formed by the surrounding polymers and/or gel segments. De Gennes proposed the term *reptation* to describe the end-directed motion of polymers in this environment [de Gennes, 1971], see Fig.2.2.

In polymer melts or concentrated solutions all polymers are moving simultaneously. We imagine choosing one polymer arbitrarily from the system. If we try to drag this polymer in the direction perpendicular to its contour, we will find that this polymer meets resistance due to its entanglements with other polymers. However, if we attempt a move along the polymer contour, the situation will be completely different. Therefore, we picture the polymer as moving in a confining tube made up of surrounding polymers. This is the concept of reptation. To understand reptation dynamics one typically studies the dynamics of a polymer in a fixed array of obstacles.

Duplex rings also undergo a form of reptation (in what follows we neglect branches of the duplex chain for simplicity): They are assumed to move by duplex-end directed curvilinear diffusion, much like linear polymers. In what follows we neglect all relaxation mechanisms faster than reptation, focussing on long time behaviour.

Following the approach in [Doi and Edwards, 1986] we consider a linear polymer chain consisting of N segments with bond length b. The chain is moving in a fixed tube, formed by entanglements with its neighbours (and/or any gel present). A primitive path connects two ends of the polymer and represents the average contour, relevant for the dynamics of the chain on the longest time-scales. The primitive path/chain is characterised by the length

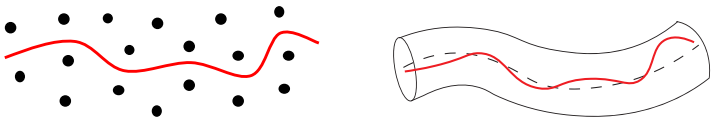

(a) (b)

Figure 2.1: A linear polymer in a fixed network formed by entanglements with surrounding polymers (a) can be represented by a chain in an entanglement tube (b), where the dashed line represents the primitive path.

L, the diffusion constant D_c and the correlation length of the primitive chain a, of the order of the tube radius.

$$L = \frac{Nb^2}{a} \tag{2.1}$$

According to the Einstein relation [Einstein, 1905], the diffusion constant D_c can be expressed as

$$D_c = \frac{k_B T}{N\zeta} \tag{2.2}$$

in which the friction constant is the product of a friction per segment ζ and the number of segments N, i.e. is assumed to be extensive in the polymer length.

Let us consider an entanglement tube segment at position s (fixed), with the polymer diffusing within it. The stress associated with this tube segment is lost if either end of the primitive chain passes through it. The probability of finding this segment surviving at time t is defined as $\psi(s,t)$. This is therefore the probability that neither end of the polymer chain have reached this segment at that time. We now define $\Psi(\xi, s, t)$ as the probability that a primitive chain has moved a distance ξ while neither end has reached the segment of the original tube at position s, see Fig.2.3. Clearly,

$$\psi(s,t) = \int_{s-L}^{s} \Psi(\xi, s, t) d\xi. \tag{2.3}$$

The stress is associated with the remaining length $\sigma(t)$ of the original tube. Therefore, the average length of unrelaxed tube remaining can be estimated using

$$\langle \sigma(t) \rangle = \int_0^L \psi(s,t) ds. \tag{2.4}$$

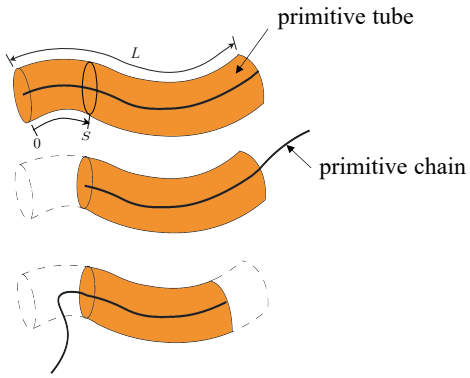

Figure 2.2: A diagram showing a linear polymer diffusing in a network of entanglements (not shown). Here the primitive tube is formed by the surrounding obstacles. The contour shown in black that we imagine diffusing along the tube is called the primitive chain. The motion of this chain can be parameterised by the curvilinear coordinate s, measured along its path. If the system is perturbed, e.g. by applying a strain, stress is associated with unrelaxed tube segments, and is therefore proportional to the fraction of the original tube remaining, shown in orange. The top panel shows the situation just after the application of a small step strain - the entire tube is stressed. Shown in the middle panel is the result of a move a distance s to the right. Whenever the chain moves out of the original tube segment the stress associated with that segment relaxes. The orange section shows the original tube remaining. The tube is lost when the chain leaves it and new, equilibrium (zero stress) tube is created at the leading end. The bottom panel shows a later move to the left, further reducing the stress.

As we are considering the diffusion of the primitive chain, $\Psi(\xi, s, t)$ satisfies the one dimensional diffusion equation

$$\frac{\partial \Psi}{\partial t} = D_c \frac{\partial^2 \Psi}{\partial \xi^2}. \tag{2.5}$$

The primitive chain is located at $\xi = 0$ with certainty when $t = 0$, therefore the initial condition is

$$\Psi(\xi, s, 0) = \delta(\xi). \tag{2.6}$$

To relax the primitive tube segment locating at position s, either ends of the primitive chain must reach that segment imposing the boundary conditions

$$\Psi(\xi, s, t) = 0 \quad \text{at} \quad \xi = s \quad \text{and} \quad \xi = s - L. \tag{2.7}$$

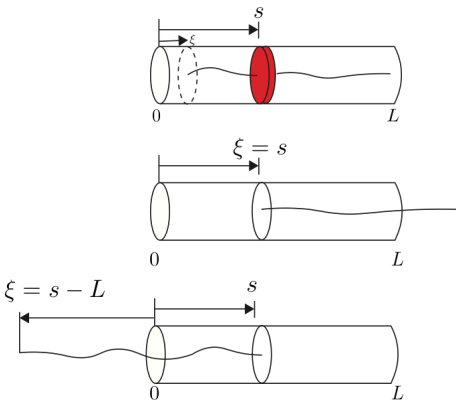

Figure 2.3: Illustration to show the analytical set-up of the primitive chain diffusion. The segment coloured in red is an original tube segment, locating at position s. The primitive chain position is now specified by the variable ξ. The stress related to that segment relaxes when either ends of the polymer reaches it at $\xi = s$ and $\xi = s - L$.

The solution of equation 2.5 together with the preceding conditions is

$$\Psi(\xi, s, t) = \sum_{n=1}^{\infty} \sin\left(\frac{n\pi s}{L}\right) \sin\left(\frac{n\pi(s-\xi)}{L}\right) \exp\left(-\frac{n^2 t}{\tau_{DE}}\right) \tag{2.8}$$

where

$$\tau_{DE} = \frac{L^2}{D_c \pi^2}. \tag{2.9}$$

is the Doi-Edwards time.

The probability that the primitive tube segment remains at time t is defined by

$$\begin{aligned} \psi(s,t) &= \int_{s-L}^{s} \Psi d\xi \\ &= \sum_{n;odd} \frac{4}{n\pi} \sin\left(\frac{n\pi s}{L}\right) \exp\left(-\frac{n^2 t}{\tau_{DE}}\right). \end{aligned} \tag{2.10}$$

Figure 2.4 shows the plot between the probability $\psi(s,t)$ and the curvilinear position s and suggests that the segments distributing around the middle of the chain remain longer than those who reside at the ends of the primitive tube. To calculate the fraction of stress remaining we define the stress relaxation function $G(t)$ (scaled by the initial stress so that $G(0) = 1$) by integrating this

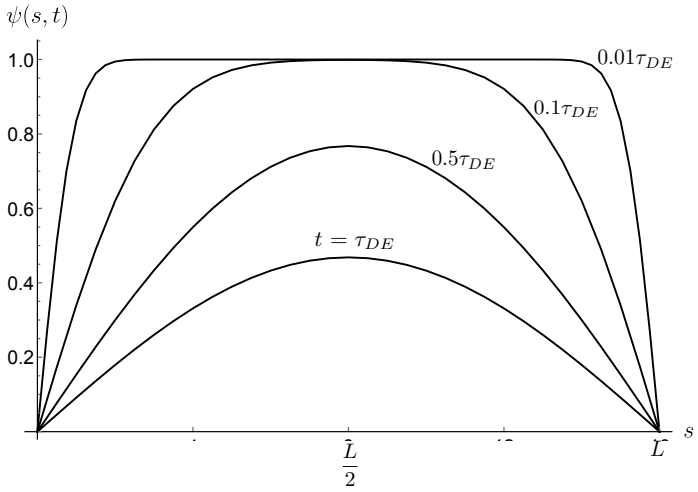

Figure 2.4: The probability $\psi(s,t)$ that the original tube segment at s survives to later time: $t = \tau_{DE}$, $0.5\tau_{DE}$, $0.1\tau_{DE}$ and $0.01\tau_{DE}$.

probability over the contour length to obtain

$$\begin{aligned} G(t) &= \frac{1}{L}\int_0^L \psi(s,t)ds \\ &= \sum_{n;odd} \frac{8}{n^2\pi^2} \exp\left(-\frac{n^2 t}{\tau_{DE}}\right). \end{aligned} \tag{2.11}$$

The first moment of the stress relaxation function is defined as

$$\begin{aligned} \tau_d &= \mathcal{N}\int_0^\infty tG(t)dt \\ &= \mathcal{N}\int_0^\infty t\sum_{n;odd} \frac{8}{n^2\pi^2} \exp\left(-\frac{n^2 t}{\tau_{DE}}\right) dt \\ &= \mathcal{N}\sum_{n;odd} \frac{8}{n^2\pi^2}\int_0^\infty t\exp\left(-\frac{n^2 t}{\tau_{DE}}\right) dt \\ &= \mathcal{N}\sum_{n;odd} \frac{8}{n^2\pi^2}\left(\frac{\tau_{DE}^2}{n^4}\right) \\ &= \mathcal{N}\frac{8\tau_{DE}^2}{\pi^2}\sum_{n;odd}\frac{1}{n^6} \\ &= \mathcal{N}\frac{8\tau_{DE}^2}{\pi^2}\frac{\pi^6}{960}, \end{aligned} \tag{2.12}$$

where $\mathcal{N}$ is a normalising factor and can be written as

$$\begin{aligned}
\frac{1}{\mathcal{N}} &= \int_0^\infty G(t)dt \\
&= \int_0^\infty \sum_{n;odd} \frac{8}{n^2\pi^2} \exp\left(-\frac{n^2 t}{\tau_{DE}}\right) dt \\
&= \sum_{n;odd} \frac{8}{n^2\pi^2} \int_0^\infty \exp\left(-\frac{n^2 t}{\tau_{DE}}\right) dt \\
&= \sum_{n;odd} \frac{8}{n^2\pi^2} \left(\frac{\tau_{DE}}{n^2}\right) \\
&= \frac{8\tau_{DE}}{\pi^2} \sum_{n;odd} \frac{1}{n^4} \\
&= \frac{8\tau_{DE}}{\pi^2} \frac{\pi^4}{96}.
\end{aligned} \tag{2.13}$$

Therefore, the stress relaxation time can be written in terms of the number of polymer segments N such that

$$\begin{aligned}
\tau_d &= \frac{\pi^2}{10}\tau_{DE} \\
&= \frac{1}{\pi^2}\frac{\zeta N^3 b^4}{k_B T a^2},
\end{aligned} \tag{2.14}$$

recovering $\tau_d \sim N^3$. On the other hand, the Rouse stress relaxation time is given by

$$\tau_R = \frac{\zeta N^2 b^2}{3\pi^2 k_B T}, \tag{2.15}$$

clearly indicating that $\tau_R \sim N^2$. Therefore, τ_d is essentially bigger than τ_R in the limit of large N signifying the crucial role of entanglements in the dynamics.

2.3 Dynamics of ring polymers

2.3.1 Stress relaxation in entangled melts of unlinked ring polymers

Experiments on polystyrene (PS) ring melts [Kapnistos et al., 2008] have been carried out on samples of unlinked and highly entangled ring polymers and show a power-law dependence of stress relaxation $G(t) \sim t^{-1/2}$, rather different from the mixed exponential decay of eq 2.11. In order to try to understand these results [Milner and Newhall, 2010] proposed a model based on ring configurations resembling a lattice animal, combined with a version of Edwards tube model to investigate the characteristic stress relaxation function $G(t)$. Generally, stress relaxation in entangled polymer systems can be measured via the probability of tube segments surviving to time t. This can be applied to various entangled polymers, whether linear or branched. In the linear case, this can be understood to be a result of reptation while in the branched case, it is determined by the retraction and extension of branches. The model developed by [Milner and Newhall, 2010] is a system of branched ring polymers living in a fixed network formed by background. Moreover, each bond of the ring has its own mass and is allowed to subtract or move to it nearby. Then, they perform Monte Carlo simulations of ring dynamics and specify its position by considering centrality c of the ring. Let us consider the definition of centrality. From Fig.2.5, each polymer bond divides the ring polymer into left and right parts. The right part has mass m, and the left part has mass $N-m$, where N is the total mass of this animal. Then, the centrality of a segment of the animal is defined by $c = \mathrm{Min}(m, N-m)$. These researchers investigated the diffusion of segments with different centralities through time and how this relates to the relaxation time. They predict that the maximum relaxation time obeys a power-law behaviour and, as a consequence, the variance of centrality increases in time as $t^{3/4}$ which is characteristic of non-Fickian diffusion. They conclude that their theory for stress relaxation in a melt of unlinked polymer are in good agreement with the experimental result because of the existence of power-law diffusion of centrality c and finally claim that the stress relaxation function corresponding to the dynamics of lattice animal

has the form of the power law, $G(t) \sim t^{-1/2}$, consistent with the experimental results. It is important to realise that this study completely neglected the possible role of inter-ring threadings, the primary motivation for the work reported in this thesis.

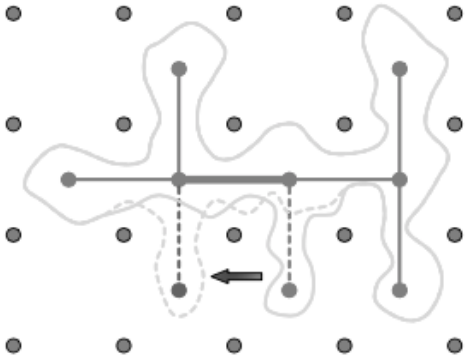

Figure 2.5: An illustration of a lattice animal formed by a ring polymer moving among fixed obstacles, e.g. provided by a gel. Shown is the dynamic scheme in which excursions can retract and extend elsewhere. The image is taken from [Milner and Newhall, 2010].

2.3.2 A speculative topological glass in entangled rings

The glass transition in Physics is still not yet well understood. 25 years ago P. W. Anderson famously wrote the following about it, "The deepest and most interesting unsolved problem in solid state theory is probably the theory of the nature of glass and the glass transition" [Anderson, 1995]. In the glass transition the microscopic mobilities of liquids are exponentially reduced as the temperature decreases towards a glass transition temperature T_g. Although their broad characteristics, such as the absence of signatures of thermodynamic phase transitions and the lack of crystalline structures, have long been known, there is no quantitative theory describing the microscopic behaviour. We speculate that a similar transition may occur in ring polymers, well above the classical glass transition temperature for the polymer itself. [Lo and Turner, 2013] studied rings that are long, semi-flexible, unlinked and unknotted with concentration well above an overlap concentration that are embedded in gel (although some arguments may carry over to ring

melts, as mentioned previously). Although the ring configurations correspond to a coil that is substantially compacted, they are still mobile, and the hypothesis of this work is that the significant slowing down of ring dynamics may be associated with interpenetration between each ring.

The model investigated here is constructed by using Edward's Tube model for a polymer (here a duplex ring) diffusing along a tube formed by surrounding polymers and/or gel segments. This is combined with de Gennes's idea of reptation - a kind of motion in which a polymer wriggles out of its primitive tube to a new equilibrium region, leaving the tube segment empty to be replaced by a new equilibrium tube at the leading end. This represents a model that allows us to measure relaxation time or disengagement time. For the sake of simplicity, a duplex structure is introduced by reducing the structure of rings to one that mimics linear polymer chains. These duplex chains are assumed to be able to open enough to be threaded or penetrated by the end of another duplex chain. The dynamics of the system of rings is then investigated by considering the simultaneous curvilinear diffusion of each chain within the tube. In order to include the inter-ring threadings they introduce the probability p that a duplex chain end threads through a neighbouring duplex chain on moving a single tube diameter. This then acts as a parameter controlling how often rings thread through each other. They neither seek to study the threading process in microscopic detail nor relate p to such physics. The parameter p essentially ends up setting a distance between threadings (large when p is small, smaller when p is large) and, for chains of fixed length, it thereby controls how many threadings are present on any ring on average, written m in what follows. They then perform collective Monte Carlo simulations by choosing random diffusive movements for all chains and then updating the polymers positions to either the left or the right in the curvilinear coordinates. Each move is assumed to result in a mean-squared curvilinear displacement of a duplex chain by one tube diameter, this being the length scale on which all dynamics are coarse-grained. Each successful trial move may create a new penetration, with probability p, or may be rejected if the trailing segment of the duplex ring is pinned by being threaded by another ring. There are thus two kinds of threading, one that is assigned to the chain that provides the threading (an "active" threading) and the other

that lives on the chain that is threaded (a "passive" threading). Threadings always exist in pairs like this and are created and annihilated together. If there are many threadings then the system can reach a transiently jammed state, in which the threadings must be undone in a specific order to fully relax the stress. This can take a very long time and, as we will see, can result in stress relaxation times that are exponential in m (and hence N) due to the increasing number of penetrations in the system [Lo and Turner, 2013, Michieletto et al., 2014, Michieletto and Turner, 2016]. In this picture m plays a stronger role than N and it will sometimes be computationally convenient to choose a very large value of p, so as to reach larger values of m. Ultimately their interest is in the physics of the network of inter-ring threadings that emerges and the distance between the threadings in terms of absolute contour length is relatively unimportant. A glass-like transition, characterised by exponential slowing down (in m or N, rather than $T-T_g$) can therefore emerge in a system of concentrated ring polymers.

An approximate relationship between the number of penetrations and the threading probability p can be constructed by using a mean-field approximation that neglects correlations. This gives the change in number of penetrations as shown in the following equation

$$\frac{d\langle m_a\rangle}{dt} \simeq p\left(1-\frac{\langle m_p\rangle}{N}\right)\left(1-\frac{\langle m\rangle}{N}\right)-\frac{\langle m_a\rangle}{N} \tag{2.16}$$

where m_p and m_a are the numbers of passive and active penetrations per ring, respectively [Lo and Turner, 2013]. Globally, across the whole system the numbers of active and passive threadings are equal and they are approximately equal on any chain so we can set $m_p = m_a$ here. m is a total number of threading and so $m = m_p + m_a$. Let us consider the right-hand side of this equation in detail. The term $1 - \langle m_p\rangle/N$ represents the probability that a polymer successfully diffuses without blocking where the term $1 - \langle m\rangle/N$ is the probability of finding unoccupied segments. Combining these two terms with p, one obtains the chance of introducing a new active penetration. On the other hand, an active penetration is lost with probability $\langle m_a\rangle/N$. At steady state, the left-hand side vanishes, and from the fact that $\langle m_p\rangle = \langle m_a\rangle = \langle m\rangle/2$

the solution for the average number of penetrations is

$$\frac{\langle m \rangle}{N} = \frac{3p + 1 - \sqrt{p^2 + 6p + 1}}{2p}. \tag{2.17}$$

Another research study that focussed on the role of threading between rings is [Michieletto et al., 2014]. In this research, large-scale three-dimensional molecular dynamics simulations were performed to study a system of ring polymers diffusing through a background gel which is formed by a three-dimensional lattice. The polymers are unlinked and unknotted and are at concentrations above the overlap concentration. A molecular dynamics engine (LAMMPS) is employed to model the Langevin dynamics at constant temperature and volume. There is a different notational convention in this work - the number of rings is labelled by N (in our work N_c is the equivalent) and the length of each chain is defined by M (here N). All rings are moving simultaneously within a three-dimensional cubic lattice of total linear size L and lattice spacing l shown in Fig.2.6. In order to study threadings which are local properties of rings conformation, a cubic lattice labelled by c was considered. If there is a threading of polymer i by polymer j within this cell a closed-loop i_c and strands j_c will be created, see Fig.2.6. The liking numbers, defined as $L_c(i_c, j_c; t)$, is counted from the number of closed loops created from j_c with i_c. Then, the local number of threadings is defined by

$$Th_c(i, j; t) = \sum_{j_c} \frac{|L_c(i_c, j_c; t)|}{2} \tag{2.18}$$

representing a penetration of ring i by ring j at time t. The total possible threading can be calculated using the summation over every cubics,

$$Th(i, j; t) = \sum_{c} \sum_{j_c} \frac{|L_c(i_c, j_c; t)|}{2}. \tag{2.19}$$

For a passive penetration of ring i by ring j, $Th_c(i, j; t) = 1$ and $Th_c(j, i; t) = 0$ while an active penetration is identified when $Th_c(i, j; t) = 0$ and $Th_c(j, i; t) = 1$. From the simulation, the result shows that the average number of penetrations per chain $\langle th \rangle / N$ extensively increase with M as shown in Fig.2.7

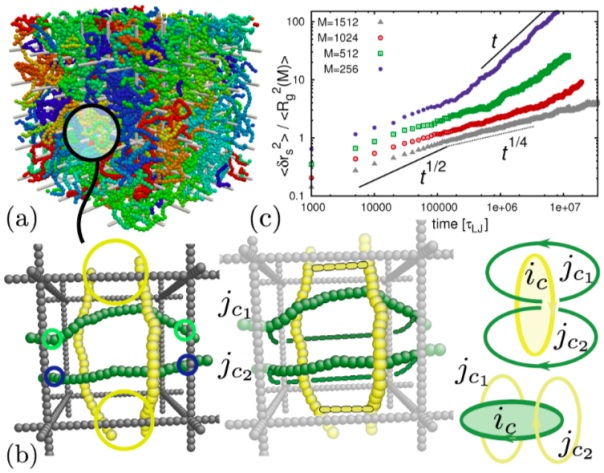

Figure 2.6: (a) A snapshot of the system with $N = 50$ and $M = 256$. (b) Procedure to identify threadings residing in a given unit cell c. (c) Mean squared curvilinear displacement of the rings increases in time according to an approximate power law. The presented images are taken from ref. [Michieletto et al., 2014].

[Michieletto et al., 2014]. Segmental mean squared displacements were also measured in [Michieletto et al., 2014], as reproduced in Fig.2.6. These were found to have a power-law character.

The system rearranges itself due to the relaxation of threading and then freely diffuses at late enough times. To understand inter-ring threading, a time correlation function is constructed with the claim that the existence of penetrations influences the dynamics of the rings by pinning a chain segment.

$$P_p(t) = \left\langle \frac{\sum_j Th(i,j;t_0)Th(i,j;t_0+t)}{\sum_j Th(i,j;t_0)} \right\rangle_{i,t_0} \tag{2.20}$$

A stress relaxation associated with rings can be calculated as follows

$$G(t) = \left\langle \frac{\sum_c g(i,c;t_0)g(i,c;t_0+t)}{\sum_c g(i,c;t_0)} \right\rangle_{i,t_0} \tag{2.21}$$

where $g(i,c;t_0)$ is equal to 1 if ring i is in cell c at time t and vanishes otherwise. After comparing this these two quantities, the result shows that the spatial stress relaxes faster than the threadings. This infers that the penetrations still exist after the time that the stress completely relaxes.

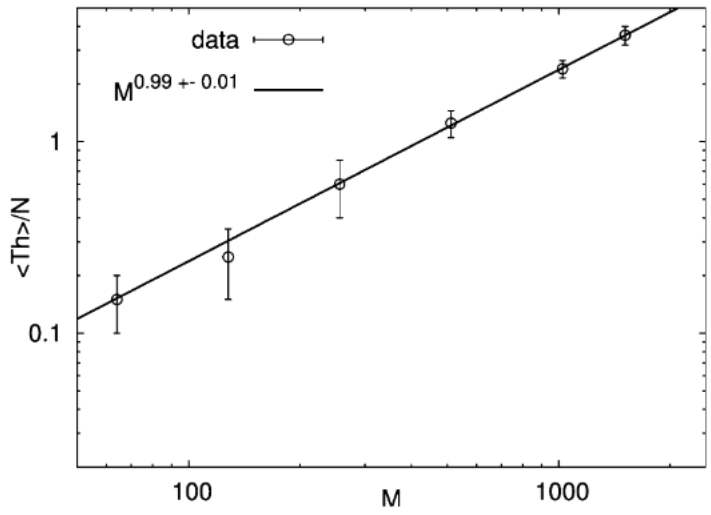

Figure 2.7: The number of threading per chain $\langle Th \rangle / N$ grows up with the length of the chain M. The simulation data presented here is taken form [Michieletto et al., 2014].

A major advance in [Michieletto et al., 2014] was the development of a technique to use the gel architecture to construct abstract test contours on polymer configurations that can be analysed to establish the existence of threadings. The stress relaxation can also be qualitatively measured by observing the diffusion of the polymers through a primitive tube. The existence of the interpenetration between polymer rings fundamentally change the stress relaxation process. Unfortunately, these simulations can only marginally reach the regime in which rings are inter-threaded – the limit of computational resources allows only 1–3 threadings per chain. As we will see below, the crossover value, after which the network becomes fully developed, is closer to $m = 10$ at least in our study of duplex rings. This provides a central motivation for the present work. If MD simulations cannot access the most interesting regime when $m \gg 1$, probably the only candidate for any universal regime in the problem, then other approaches must be explored. The Monte Carlo approach outlined in the next chapter provides a possible candidate with which we can access this regime.

Chapter 3

Monte Carlo Simulations of Ring Polymers in a Gel

In this chapter, I will introduce the underlying concepts of how Monte Carlo sampling can be applied to study the dynamics of ring polymers in a gel. Here, before we move to the more detailed description, it is worth mentioning that the system that we are interested in is the system of duplex ring polymers. Such a conformation has been useful in preceding research [Cates and Deutsch, 1986, Lo and Turner, 2013, Rosa and Everaers, 2019] and also offers us a few advantages. First of all, the duplex ring segments all resemble "linear" polymers and therefore can be said to have "ends" in this picture. The ring polymers can now navigate space using their terminal segments. Secondly, in a particular situation, such as when the chain are unbranched. It can be treated in a similar way as linear polymer and allow us to implement the tools developed for linear polymers, as discussed in Chapter 2, to the problem of rings. Last but not least, it provides the possibility of introducing threadings between rings with the benefit that we can now specify precisely the position at which the threading resides at the level of a tube segment (see Fig.3.1b). This approach has the major advantage that it is the only technique that we are aware of that can be used to study highly interpenetrating (duplex) ring networks. The computational limitations of more microscopically faithful simulations, e.g. Brownian dynamics, mean that the regime where the number of threadings $m \gg 1$ is inaccessible. In the present work we are able to generate fully equilibrated systems up to $m \approx 20$.

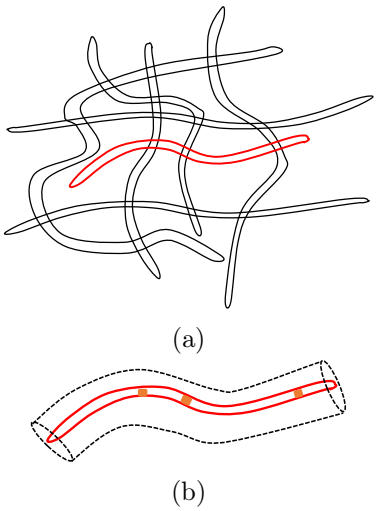

Figure 3.1: (a) A test (duplex) chain, coloured in red, is shown moving in a gel (not shown). The configurations are assumed to be unbranched for simplicity. (b) This can be depicted as a polymer chain reptating in a tube. The tube is the effect of the quasi-topological entanglement constraints provided by the surrounding obstacles (not shown). The strict uncrossability constraints provided by the gel segments confines the rings to adopt these duplex structures.

There are several ways to simulate the dynamics of ring polymer solutions. The popular approach is to perform Molecular dynamics simulations [Halverson et al., 2011b, Rosa and Everaers, 2014, Michieletto et al., 2014, Smrek and Grosberg, 2016, Michieletto, 2016, Michieletto and Turner, 2016, Michieletto et al., 2017a, Michieletto et al., 2017b, Smrek et al., 2019]. Another method, which is relatively straightforward, is to utilise Monte Carlo simulation. It can be done by sampling ring motion. In each simulation time step, for each ring, there is a controlled chance of introducing a new pair of penetrations to the system, as well as of losing a pre-existed threading. We will utilise a similar methodology as was discussed in [Lo and Turner, 2013] by considering rings as duplex polymers shown in Fig.3.1. As can be seen in the figure, a test ring coloured in red moves in a gel together with other ring polymers. The gel, which we assume to be present here, is treated as static with zero fluctuations and plays no part in the computer simulation. However, it provides a constraint that confines the polymer motion and allows them to move restrictedly along their own contours without cutting through the surrounding gel meshwork. Therefore, we can picture the test polymer as

moving inside a tube-like region (see Fig.3.1b). The threading between rings is simply replaced by a special (pair of) segment(s) as will be explained in the next section.

3.1 Simulation procedures

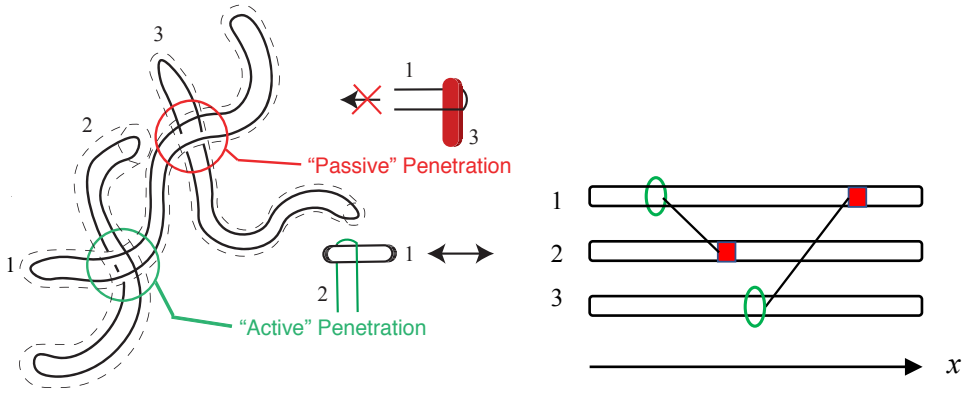

Figure 3.2: (a) A schematic diagram showing three mutually threaded ring polymers (solid lines), residing in entanglement tubes (dashed lines) formed by surrounding rings or gel segments (not shown). The ring polymers are shown as idealised, "duplex" structures in which an outgoing segment of any ring polymer always has a returning segment as a neighbour within the same entanglement tube. Polymer 1 actively threads through the contour of polymer 2 (green circle), creating an **active threading on polymer 1** and a partner passive threading on polymer 2 at the same site. Threadings are always created or lost in such active-passive pairs. The nearby cartoon emphasises that this threading places no restrictions on the movement of polymer 1; it remains free to slide through a loop of polymer 2. The pair is lost if the end of the active chain, here polymer 1, ever passes beyond the tube segment containing the site of the threading. New threadings are formed whenever a reptation-like end move of one tube diameter threads a neighbouring polymer loop. Elsewhere, polymer 3 actively threads through polymer 1 (red circle) forming a **passive threading through polymer 1**. (b) These threadings can be shown as active-passive pairs with termini at the appropriate curvilinear coordinate on the threaded chains. Our simulation does not record spatial information in the form of panel (a), rather it merely records the curvilinear position of the polymers and the threadings that live on them.

Our framework is limited to the problem of ring polymers that have double folded conformations with no branches. The extension of this approach to branched polymers is reserved for future work. The concentration of the

polymers is assumed to be above the overlap concentration $c^\star$. Due to the high concentration of the system, the rings polymers interact with each other in each simulation time step, chosen so that they diffuse a root mean squared distance equal to a tube diameter (entanglement length). For the purposes of our simulation the only relevant interactions in this model are therefore provided by the inter-ring threadings. Moreover, the temperature of the system is set at above the glass transition temperature T_g to guarantee that the rings still retain their motilities. Furthermore, we consider the ring polymers that are flexible, unlinked and unknotted.

We explored this type of entangled system by performing a series of computer simulations. Throughout the thesis, the following notation will be used for the simulation parameters. The number of ring polymer chains in the system is defined to N_c. Each of these chains is identical and has equal length, corresponding to N tube segments. Furthermore, in order to simplify the complexity of the system, the rings are considered as linear duplex chains. To understand threadings between rings, let us focus on Fig.3.2. The figure illustrates the mutual threading between three duplex polymer rings called Polymer 1, Polymer 2 and Polymer 3, respectively. These polymers live in their own primitive tubes made by entanglements with the surrounding rings and gel. If we carefully look into the entire system, we will notice that there are two kinds of penetrations in the system. One is an "active" penetration (on the penetrating chain). This kind of threading does not limit the moves of the active, threading polymer. Conversely, another type of penetration can block moves by the penetrated polymer and is only removed when its active partner is annihilated (slides off the end of the active polymer). This is called a "passive" penetration (on the penetrated chain). In the figure, Polymer 1 threads into Polymer 2 and forms an active penetration on Polymer 1, and at the same site its passive pair is created on Polymer 2. On the other hand, Polymer 1 is threaded by Polymer 3 creating a passive penetration on Polymer 1 and also the active partner penetration on Polymer 3. In terms of stress relaxation, Polymer 1 cannot completely relax its corresponding stress as long as the passive penetration on the chain still persists (remains "alive"). If there is only a single passive penetration, then end moves in both directions can remove all stress except that carried by the passively threaded tube segment. If there

are multiple segments then only the tube segments outside the region between the left-most and right-most passive threadings can relax, unless and until these passive threadings are lost. Therefore, we form a hypothesis that the passive penetration will play a significant role in slowing down the dynamics of the system. A cartoon picture presenting in Fig.3.2b shows a mapping of the entangled rings on the left panel into a curvilinear representation of the three linear chains containing threading segments in which the curvilinear coordinate is shown on a straight linear axis for simplicity. The red squared blocks represent the passive penetrations while the green circles symbolise the active penetrations. This representation underlies the computer simulation discussed below.

We define a simulation time step t_h as a time it takes to diffuse the distance equal to a unit of polymer segment. Therefore,

$$t_h = \frac{a^2}{2D_c} \tag{3.1}$$

where D_c is a curvilinear diffusion constant, equivalent to the diffusion constant appearing in the Doi-Edwards model for linear polymers reviewed in chapter 2. In the simulation we measure all lengths in units of the tube diameter, setting $a = 1$. Thus,

$$t_h = \frac{1}{2D_c}. \tag{3.2}$$

Time is then often shown in units of t/t_h with t_h defined in 3.2.

At some $t = 0$, the positions of each polymer i, $i = \{1, 2, 3, ..., N_c\}$ are located at an (arbitrary) origin in their respective curvilinear coordinates. In each simulation time step, the position of the polymer will be sequentially updated. Let x be the curvilinear position along the polymer contour. As discrete time progresses in t_h units, the following update rule apply:

1. The direction of motion for a diffusive displacement attempt by chain i is sampled by selecting either $-x$ or $+x$ with equal probability for each chain. The chains then generally move in a mixture of negative and positive x directions at each timestep.

2. If a right move is chosen, meaning the polymer attempts a move in the positive direction, we check whether its tail (here the leftmost segment) is

occupied by a penetration or not. If there is no threading at the tail, the chain move is successful and the chain position is updated one unit in the positive direction. However, if there is a penetration present in the tail segment, we proceed to test the type of the penetration. If it is a passive penetration the move will be rejected as this threading is blocking the polymer movement. However, if the penetration is active the polymer move is accepted but it will lose that threading. Thus the threading pair is annihilated and, simultaneously, its partner passive penetration on another chain is removed. We will apply the similar update (in the opposite direction) if a left move was first selected.

3. If the displacement attempt succeeds, there is a chance that the leading end will have randomly threaded through other polymer during this displacement. Consequently, with probability p, a new pair of penetrations will be introduced, inserted as follows. The active penetration will be generated at the leading (terminal) tube segment on chain i, that has undergone this move. The passive partner penetration will be created on a randomly chosen chain $j \neq i$. The creation of the new threading will be rejected if the chosen segment at which it is to be injected is already occupied by another threading.

4. The polymer i update is complete. The same procedure is applied to all polymer chains.

There are effectively no boundaries in our simulations as the polymers curvilinear coordinates are unbounded. Our simulation therefore represents a mean-field approach in which space is only represented through these curvilinear coordinates and all polymers are assumed to share the same physical space.

3.2 Stress relaxation

According to the Doi-Edwards theory of linear polymers, the stress relaxation function is proportional to the remaining primitive tube segment of

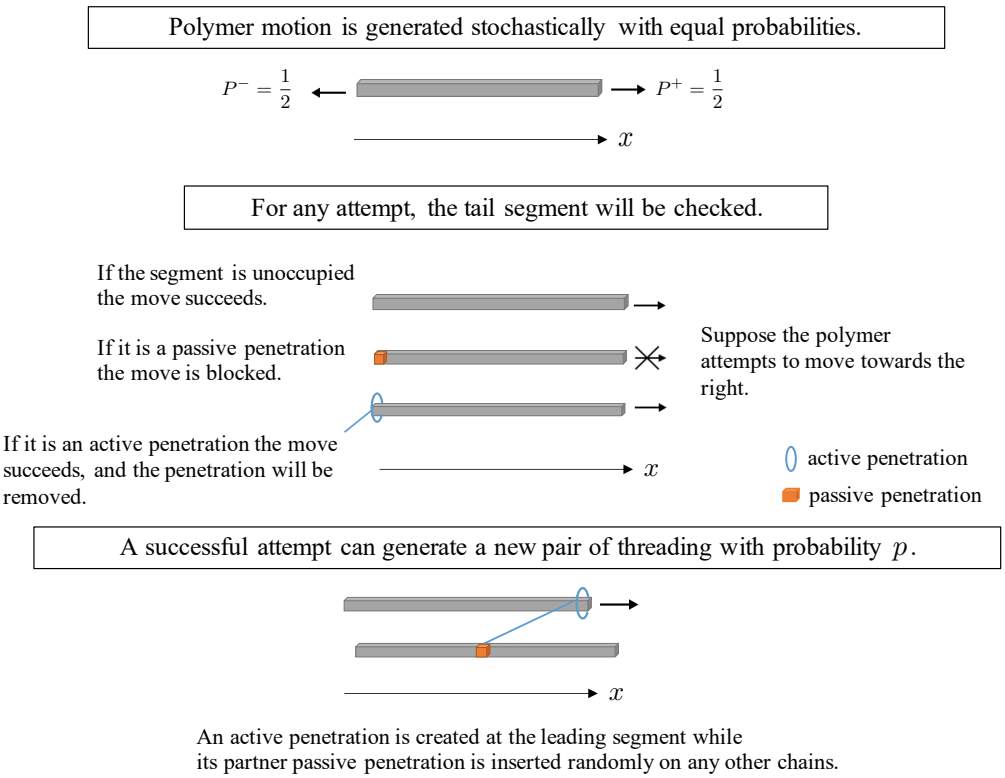

Figure 3.3: A diagram showing how the motion of ring polymers is generated during each Monte Carlo time step. In the first stage the polymer trial move direction is chosen to be towards positive x and negative x with equal probabilities $P^+ = P^- = \frac{1}{2}$. Suppose a polymer is moving in the positive direction by using its leading segment. To perform the position update, the algorithm checks at the tailing segment the three possible conditions: (i) no penetration present at this segment, (ii) occupied by a passive penetration and (iii) hosting an active penetration. The attempt will fail if the segment is passively threaded and will succeed if it is occupied by an active threading or is unoccupied. In case (ii) the active penetration will then be lost, as well as its partner passive penetration on another chain (not shown).

length L. We recall the relationship between L and N,

$$L = \frac{Nb^2}{a}. \tag{3.3}$$

In the simulation we set the polymer mesh size $a = 1$ and the bond length $b = 1$. Thus, N and L are interchangeable and the stress relaxation function $G(t)$ can be calculated by counting the number of unrelaxed segments. At time $t = 0$, the stress relaxation function is equal to the original tube length which

is the polymer contour length and when $t \to \infty$, the function has reached zero and all stress has been lost. However, it is computationally inefficient to relax one single chain over the entire runtime like this. So, we define t_f as the time that the stress relaxation function reaches zero. To give an idea of how $G(t)$ is measured consider the example shown in 3.4. This diagram shows how $G(t)$ decreases with time for a system with eight segments $N = 8$. Conventionally $G(t)$ is normalised so that $G(0) = 1$. Here we instead show it in terms of unrelaxed tube segments so that, at $t = 0$, the stress relaxation function $G(0) = 8$ as no segments have yet relaxed. It is reduced by one unit whenever an original primitive tube segment is lost. It first vanishes at $t = t_f$,i.e. $G(t_f) = 0$ with $G(t < t_f) > 0$. The conventional (normalised) stress relaxation function is simply the $G(t)$ shown here divided by N.

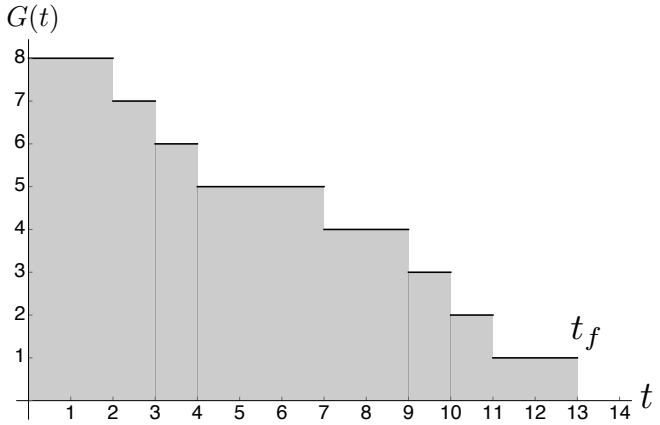

Figure 3.4: An example of a stress relaxation function $G(t)$, here measured as the number of unrelaxed tube segments, from a simulation with $N = 8$. According to the tube model, the length of the primitive tube is equal to the length of the primitive chain N. $G(t)$ decreases one step whenever the test polymer loses the original tube segment and disappears at $t = t_f$. In this graph $t_f = 13$.

In the simulation, stress relaxation functions of each chain relaxation processes are recorded after the system has equilibrated. The method of equilibrating the system will be presented in the next section. We use the index j to specify the j^{th} relaxation event of the total number of relaxation processes n_{relax}. The $i \in [1, N_c]$ chains fully relaxing its stress; chains that remain partially unrelaxed at the end of the simulation run are not included in the data set since their stress relaxation functions are not complete. Also, the number of unrelaxed is comparatively small compared with the number of entirely

relaxed events. We usually managed to collect about 10^3 to 10^6 complete relaxation events on each simulation run. The number of unrelaxed chains at the end of the simulation is exactly the number of rings in the system. This is because the program always maintains N_c (unrelaxed) chains in the simulation process and so, by construction, these will remain unrelaxed at termination. The j^{th} complete stress relaxation process contributes the normalised stress relaxation function $G_j(t)$. We define the average relaxation time of the j^{th} process as

$$\tau_d^j = \frac{\int_0^{t_f} t\, G_j(t) dt}{\int_0^{t_f} G_j(t) dt} \tag{3.4}$$

with an implied index j on t_f. This gives an ensemble average value of the mean chain disengagement, or stress relaxation, time as

$$\tau_d = \frac{1}{n_{relax}} \sum_{j=1}^{n_{relax}} \tau_d^j. \tag{3.5}$$

A system with a higher number of penetrations m (equivalently a large value of p) takes a longer time to relax. For example, in the case of $m \approx 20$, it typically takes 10 hours to achieve 10^4 complete stress relaxation processes, although the runtime would be different on other computer architectures.

3.3 Equilibrating the system

We are interested in the equilibrium properties of these entangled ring polymer systems. Equilibrating the system within the simulation needs care since we do not know the statistics of an equilibrium network of threadings *a priori*, and hence how to initialise the system. In this section, I will explain how we developed a criterion to measure the equilibration time t_{eq}. This is the time taken for the system to reach equilibrium. We know that in an equilibrium system the principle of detailed balance means that there should be no changes in any measurable quantities (on average, in the thermodynamic limit of many rings). We use this to establish a criterion for equilibration, assuming that the stress relaxation time is the slowest relaxing quantity. Thus when there are no further changes in the stress relaxation time (on average) the system is

assumed to have fully equilibrated. We initialise the system in a state with zero threadings because the initial condition does not affect the equilibrium development. Furthermore, one has to be careful introducing a (network of) threadings at random as it is possible to initialise states that are not undoable (violate global unlinking of the rings). We then let the system evolve until it reaches an equilibrium. To measure this period, we carried out parallel simulations from the no-threading initial condition and estimate the ensemble average of τ_d. When the mean stress relaxation time has reached a steady state the system will be equilibrated. Figure 3.5 shows a sketch of $\ln \tau_d$ versus time. To identify t_{eq}, we first create a moveable bin at time t_{bin}, as shown in grey. The bin is moved from $t = 0$ to the end of the run. The centre of the bin is used to identify its time-position. In each of these locations

$$x_{bin} = \langle \ln (\tau_d) \rangle_{bin} \tag{3.6}$$

where $\langle \dots \rangle_{bin}$ is the average of datapoints within this bin of relaxation times. The bin width is defined as Δt and satisfies the following condition.

$$\frac{\Delta t}{\langle \tau_d \rangle} \ll 1, \tag{3.7}$$

where $\langle \tau_d \rangle$ refers to the stress relaxation time of the simulation, averaged over all time bins. We further choose

$$\frac{\Delta t}{\langle \tau_d \rangle} = \frac{1}{100}. \tag{3.8}$$

For later times than each bin, as shown in Fig.3.5, the corresponding late time average of the logarithm of the stress relaxation time is calculated as

$$\overline{x} = \langle \ln (\tau_d) \rangle_l \tag{3.9}$$

where $\langle \dots \rangle_l$ is the average of time bins for times later than the current bin. The standard deviation of this over the n_l late time bins, with the average x

in each bin labelled with its index i, is

$$\sigma_l = \frac{1}{\sqrt{n_l - 1}} \sqrt{\sum_{i=1}^{n_l} (x_i - \overline{x})^2}. \tag{3.10}$$

To establish equilibration of the system at time t_{bin}, we carry out a test of whether we can be sure that x_{bin} is sampled from the stress relaxation time data with mean equal to $\bar{x}$ and standard deviation σ_l at the 90% confidence level. According to the central limit theorem, if n_{bin} is large enough, the sampling distribution of x_i will be approximately Gaussian. In section 3.5 we report on the distribution of τ_d and show that it shares some empirical similarity with a log-normal distribution. This gives some justification for using a normal distribution for $\ln \tau_d$. However, ours remains an approximate approach and more sophisticated alternatives that e.g. attempt to bootstrap the distribution itself as part of the test are possible.

To be 90% sure that the value of x from the current bin is drawn from the late time distribution, assumed to be Normal, the relevant criterion involves the usual $z = 1.645$ value for a one-sided Normal distribution at this confidence value

$$x_{bin} > \overline{x} + 1.645 \frac{\sigma_l}{\sqrt{n_{bin}}}. \tag{3.11}$$

The time t_{bin} at which the above condition is met is used as the equilibration time. If the measured value of x_{bin} does not meet this criterion the test for equilibration is not met and the subsequent bin is tested. This procedure is repeated until a bin that satisfies the convergence criterion (3.11) is identified (cases in which equilibration is not reach according to this definition are reported by the algorithm). This criterion is designed to identify an equilibration time from simulation runs that are long enough to provide a good estimate of the late time (fully equilibrated) relaxation times. It can fail if the simulation run is not long enough. The signature that a reliable estimate of the equlibration time has been obtained is that the equilibration time is much less than the total runtime. This condition is satisfied for data points included in all subsequent graphs, with data points corresponding to systems that may not have fully equilibrated being shown in red.

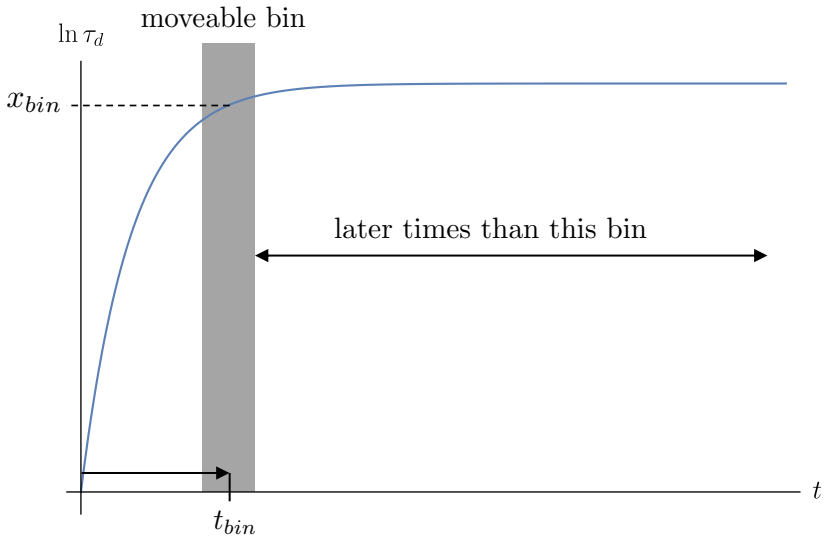

Figure 3.5: Outline of the method of estimating the equilibration time in our Monte Carlo simulations. The graph shows a sketch of the approximate relationship between a moving average of $\ln \tau_d$ and time t. The criterion for equilibration is established as follows. First, we construct a moveable bin (shaded). The bin starts at $t = 0$ and sequentially moves to later times. We calculate the average $\langle \ln \tau_d \rangle$ over the bin, defining x_{bin}. The late time is defined between t_{bin} and the ending time of the simulation. Over this time period, we calculate the average of the logarithm of the stress relaxation time, defining $\overline{x}$ and its standard deviation σ_l. To establish the time from which the system is equilibrated we identify the bin for which x_{bin} is drawn from a distribution with mean $\overline{x}$ and its standard deviation σ_l with 90% confidence. This corresponds to the first bin (smallest time) for which $x_{bin} > \overline{x} + 1.645 \frac{\sigma_l}{\sqrt{n_{bin}}}$.

3.4 Stress relaxation of threaded ring polymer networks

An instantaneous picture of the threading network can be obtained from the simulations. Figure 3.6 shows such simulation data for a system with $N_c = 4$ ring polymers. The threadings are represented by arrows, connecting the partner passive and active threadings.

Figure 3.7 represents the stress relaxation functions for two different cases, zero threadings (a) and $m \approx 17$ threadings (b). The time measured in the diagram is dimensionless in units of t_h. The first subfigure shows the Doi-Edwards equivalent case with $p = m = 0$ while the second subfigure displays the $p = 0.288$ equivalent to $m = 17$ penetration. The distinctive finding here is the time taken to entirely relax stress of the penetrated network is much

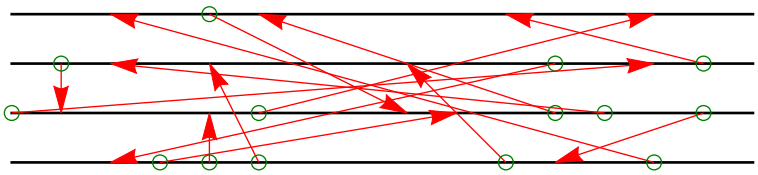

Figure 3.6: A snapshot of a network of four ring polymers showing the threadings between them represented as abstract arrows. The duplex rings are the solid black lines (the rings are co-aligned in curvilinear displacement for convenience here). The passive penetrations are represented by the red arrowheads while the green circles represent the partner active penetrations. Here $m \approx 6$ is the average number of the sum of both active and passive threadings per chain.

longer than the $p = 0$ case, signifying that the presence of threadings has strongly affected the stress relaxation.

3.5 Glassy behaviour

In classical linear polymers the stress relaxation time scales with a power of the length of the rings, roughly $\tau_d \sim N^3$. In the simulation time units t_h scales linearly with N (because D_c scales inversely with N), see eq 3.2. Thus, for linear polymers the Doi-Edwards result here corresponds to $\tau_d/t_h \sim N^2$. Figure 3.8 presents the stress relaxation time for several p cases. The presence of threadings results in a stress relaxation time that increases faster than a power law, reflecting the slowing down of the ring dynamics. To be more precise about the trend we examined the corresponding relaxation time on a semilogarithmic scale and compare it with an exponential increase in N, see Fig. 3.9. The comparison underlines the fact that the relaxation time appears to vary more strongly than with a power law in N. This reflects the slowing down due to the emergence of threadings.

We are conscious of the fact that the mean of the stress relaxation time is only a single parameter and the *distribution* of times is also potentially significant. Figures 3.10 and 3.11 shows histograms constructed from the individual stress relaxation times obtained for simulation. Figure 3.10 shows the case when $p = 0$, equivalent to Doi-Edwards, exhibiting approximately log-normal statistics, while Figure 3.11 shows a similar histogram for $m = 20$ that has a distinct "heavy tail" at large relaxation times. It seems as though thread-

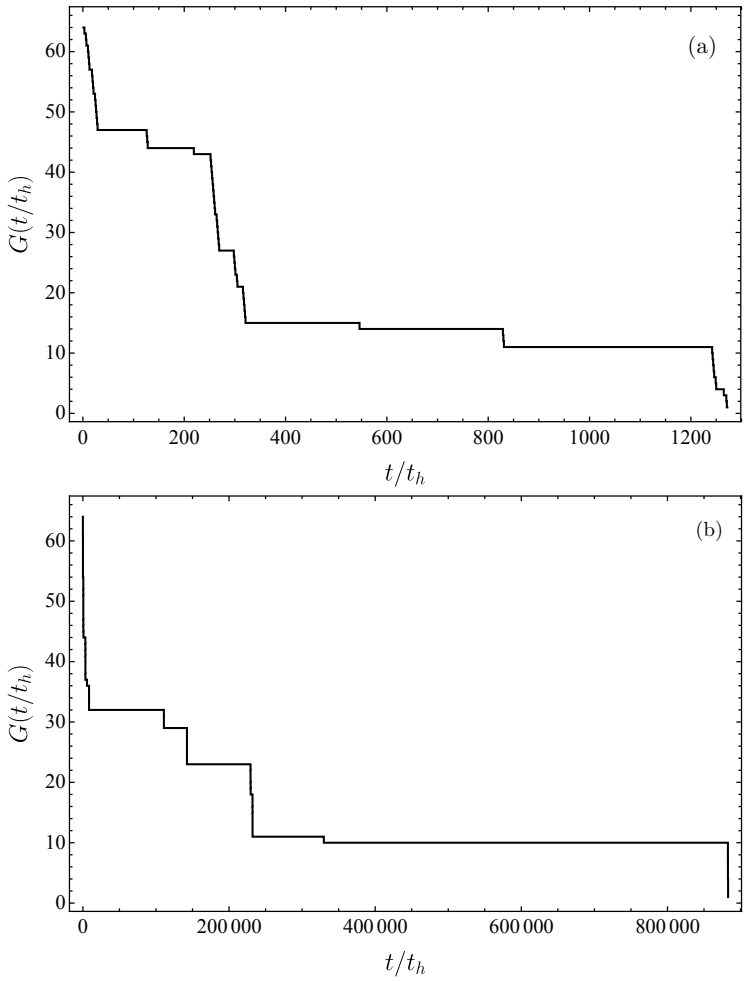

Figure 3.7: Threading significantly slows down the stress relaxation resulting in the longer decay time of $G(t)$ (again shown un-normalised, as number of stressed tube segments remaining). The graph compares between two sets of parameters. The first case (a) is $N_c = 40, N = 64$ and $p = 0$ and the second case (b) is $N_c = 40, N = 64, p = 0.228$ equivalently to $m \approx 17$.

ings significantly delay the stress relaxation but also result in a heavy-tailed distribution.

[Lo and Turner, 2013] proposed an estimate of the mean number of threadings per chain $\overline{m}$ using a mean-field approximation 2.17. We performed simulations to establish the relationship between p and m with a new approach developed by us that is based on imposing detailed balance, as should apply at equilibrium.

Let P_m be the equilibrium probability of finding a ring with m pene-

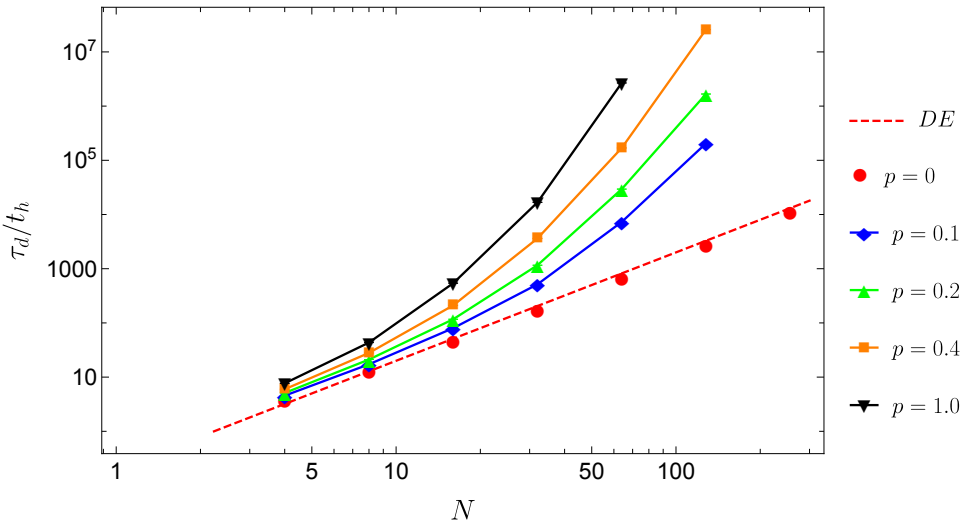

Figure 3.8: The mean stress relaxation time τ_d of the ring polymers increases with the probability p implying the significantly slowing down of ring dynamics due to the increase of threading. The effect is greater for longer chains (large N). Several values of p are shown (see key). The red-dashed line, labelled DE, represents the Doi-Edwards result for linear polymers, for which $\tau_d/t_h = 0.2N^2$.

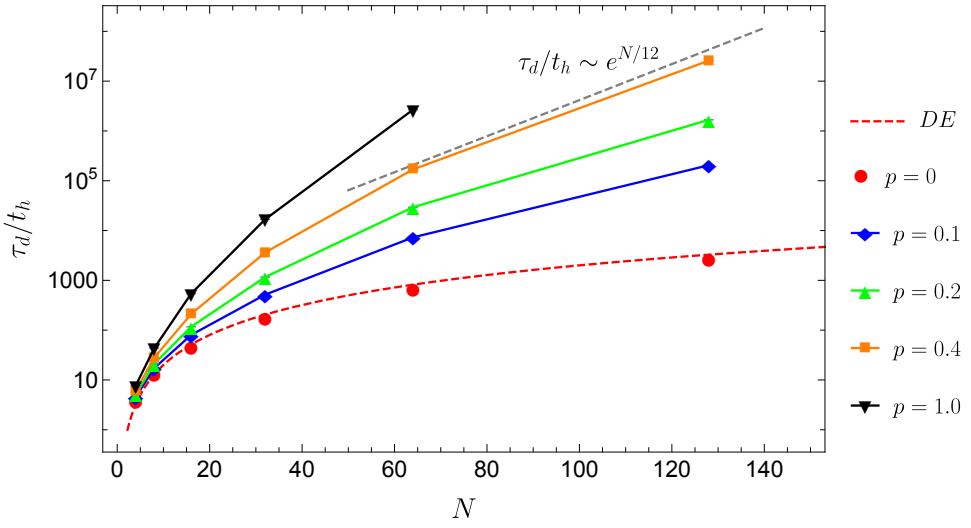

Figure 3.9: The mean stress relaxation time τ_d of ring polymers increases with the threading probability p (data shown on semilogarithmic axes). The data presented here is the same as in Fig.3.8. The trend is closer to linear at large N (a linear relationship indicating exponential dependence). We show $\tau_d/t_h \sim e^{N/12}$ as a dashed black line as a guide to the eye.

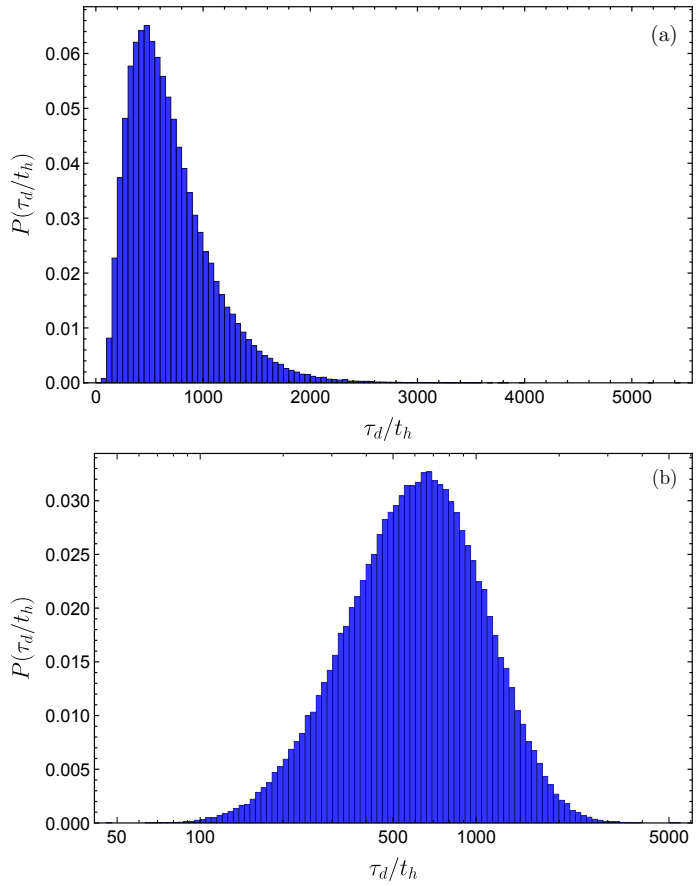

Figure 3.10: A histogram of individual stress relaxation times for the case of $N_c = 40$, $N = 64$ and $p = 0$ (a) in linear scale and (b) logarithmic scale. The distribution shows log-normal characteristic.

trations and $k_{l,m}$ be the transition rate from state with l threadings to state with m threadings. Hence, we can write the master equation for P_m as

$$\frac{dP_m}{dt} = k_{m-1,m}P_{m-1} + k_{m+1,m}P_{m+1} - k_{m,m+1}P_{m+1} + k_{m,m-1}P_{m-1}. \tag{3.12}$$

The detailed balanced condition corresponds to

$$k_{m-1,m}P_{m-1} + k_{m+1,m}P_{m+1} = k_{m,m+1}P_{m+1} + k_{m,m-1}P_{m-1}. \tag{3.13}$$

The argument employed in 2.16 suggests that

$$k_{m-1,m} = p\left(1 - \frac{m-1}{2N}\right)\left(1 - \frac{m-1}{N}\right) \tag{3.14}$$

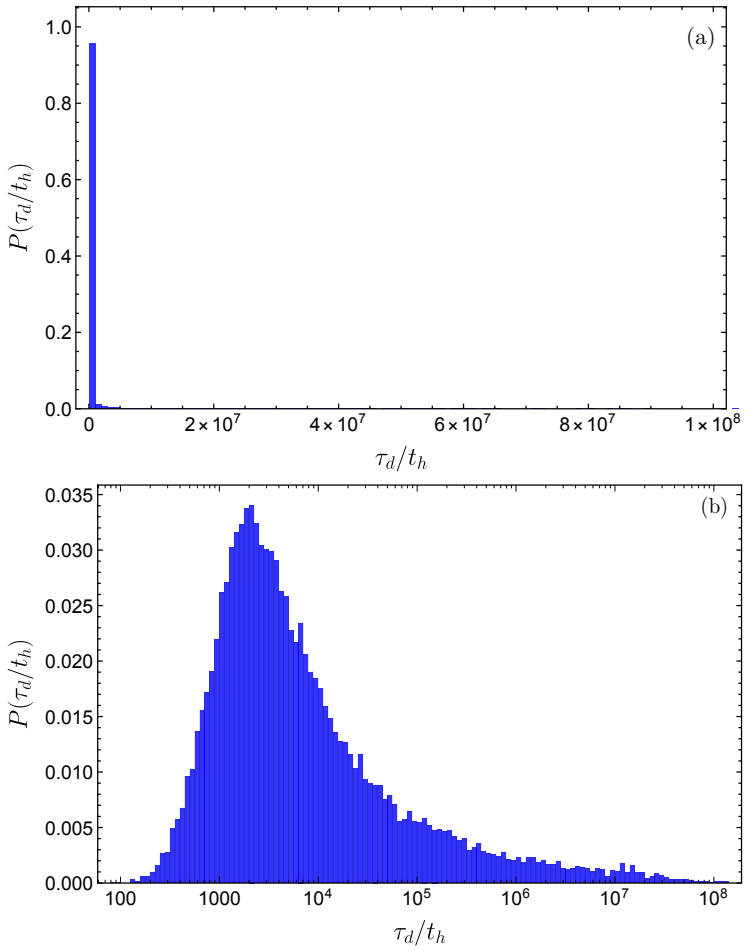

Figure 3.11: A histogram of individual stress relaxation times $N_c = 40$, $N = 64$ and $m = 20$ (a) in linear scale and (b) logarithmic scale. The distribution shows a heavy-tailed characteristic.

and

$$k_{m,m-1} = \frac{m}{2N}. \tag{3.15}$$

From the fact that $P_1 = (k_{0,1}/k_{1,0})P_0$, we can show that equation 3.13 can be rewritten as

$$P_m = P_0 \prod_{i=1}^{m} \frac{k_{i-1,i}}{k_{i,i-1}}. \tag{3.16}$$

The average number of penetrations per segment can then be calculated using

$$\overline{m} = \frac{1}{N} \frac{\sum_m m P_m}{\sum_m P_m}. \tag{3.17}$$

The result of this new approach is shown by the dashed line in Fig. 3.12 where it is seen to be in reasonable agreement with the simulation data.

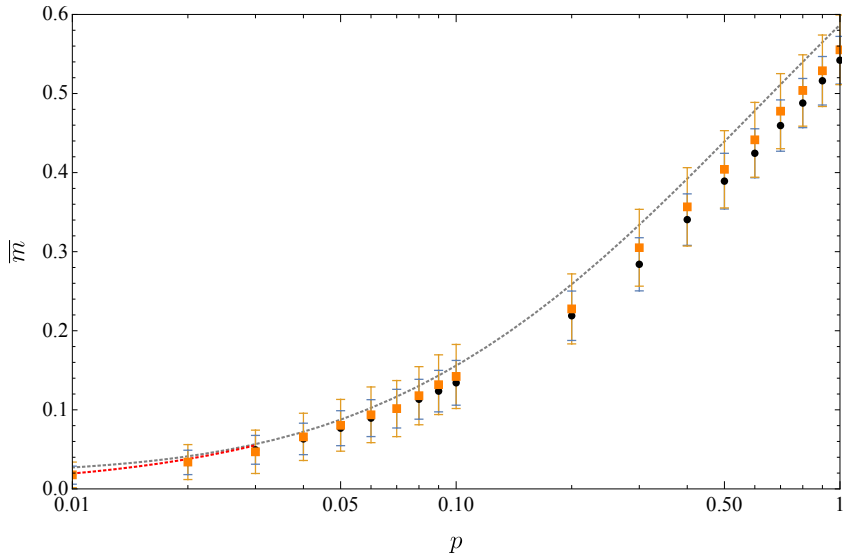

Figure 3.12: The average number of penetrations per segment $\overline{m}$ grows with the probability of creating a new pair of threadings per move p. A solution obtained using detailed balance shown by the grey-dashed line slightly deviates from [Lo and Turner, 2013] prediction shown in red at small p. The simulation results are shown as orange squares for a case of $N_c = 4, N = 32$ and black dots for $N_c = 4, N = 64$.

A naive assumption about stress relaxation in the system of inter-threaded duplex rings might be that the stress relaxation dynamics may follow a rescaled form of Doi-Edwards stress relaxation, derived for linear polymers. This assumption could be motivated on the basis that the rings have a double-folded duplex structure that is essentially linear and they still undergo some form of stochastic curvilinear motion, albeit one that is slowed by the presence of threadings. Could it be that the threadings merely renormalise D_c but that otherwise the relaxation remains essentially diffusive and therefore Doi-Edwards like? To test this hypothesis, we examined the first few moments of the stress relaxation function, using the definition

$$n^{th}\text{moment} = \langle \int_0^{t_f} t^n G(t) dt \rangle. \tag{3.18}$$

The result is shown in Fig. 3.13 where we calculate the moment of the threaded system with parameters $N_c = 4, N = 32$ and $p = 0.2$ (up to fifth moment)

and compare the result with the corresponding moments for the Doi-Edwards case of linear polymers where we artificially rescale the 1st moments to have the same relaxation time. If the relaxation of the rings was diffusive and Doi-Edwards like the moments would align under this rescaling. From the comparison it is apparent that the moments of the threaded network are deviating from the corresponding (rescaled) Doi-Edwards moments, indicating that the relaxation does not involve a standard diffusive process.

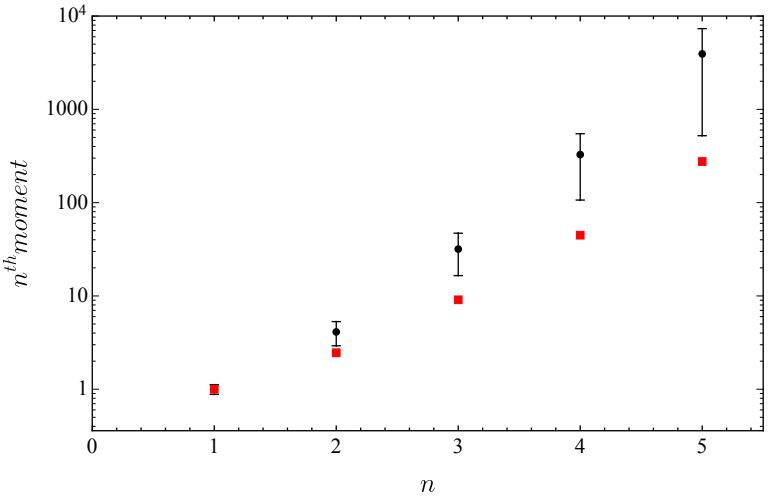

Figure 3.13: Normalised moments (black) measured in t_h^{n+1} unit from the simulation deviate from the prediction from the standard diffusion (red). The illustration presents the result for a system with $N_c = 4, N = 32, p = 0.2$.

To further understand this we measured the mean squared displacement of the duplex rings, defined as

$$\langle s^2 \rangle(t) = \frac{1}{N_c} \sum_{i=1}^{N_c} s_i(t)^2 \tag{3.19}$$

where $s_i(t)$ is the curvilinear position of the centre of mass of the i-th ring polymer at time t. Figure 3.14 shows the relationship between the average mean squared displacement $\langle s^2 \rangle$ and time. To calibrate this behaviour, we compare this result with the well-known result due to Doi-Edwards, presented in red, that is purely diffusive $\langle s^2 \rangle \sim t$. There is clearly a substantial departure between the motion of classical linear polymers and duplex rings. $m_p = m/2$, the number of passive threadings, appears on this plot (both as a label for the

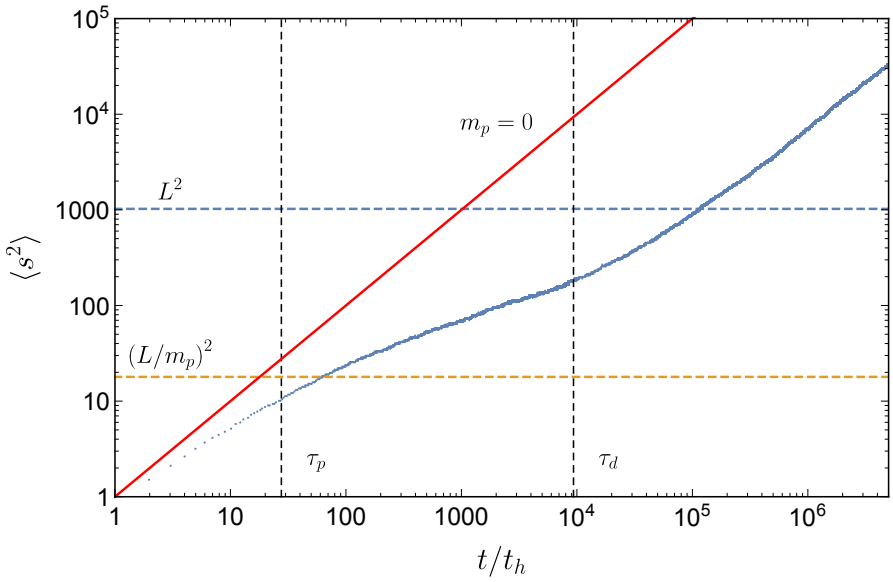

Figure 3.14: Mean squared displacement of ring polymers for the case of $N_c = 3$ rings, each of length $N = 32$ with a threading-per-move probability $p = 0.7$ (blue data points). The dynamics can be divided into 3 different regimes: Early diffusion ($t/t_h < \tau_p$), sub diffusive "plateau" ($\tau_p < t/t_h < \tau_d$) and late diffusion ($t/t_h > \tau_d$). Shown, for comparison, is the equivalent (Doi-Edwards) dynamics for rings with no threadings presented ($p = 0$), shown by the red line.

Doi-Edwards case $m_p = 0$ and in a displacement threshold $(L/m_p)^2$, roughly the square of the distance between passive threadings $\lambda = L/m_p$. The diffusion can be divided into different regimes. The slope of the graph represents the exponent of the diffusion, which is approximately equal to 1 at very late times in both cases. For rings, this regime emerges for timescales longer than the chain stress relaxation time τ_d. At early times the system does not encounter any threadings and behaves similarly to a linear polymer. This occurs for times $t \lesssim \tau_\lambda = (L/m_p)^2$ defined here as the time to diffuse the distance between passive threadings. This corresponds to the time when the solid red (freely diffusing) displacement intersects with the horizontal yellow dashed displacement. This is the time the ring takes to encounter a blocking passive penetration. In the simulation, τ_p is measured to be the lifetime of the terminal passive penetration, defined to be the passive threading nearest the ends of any chain. This is measured by sampling the ages of such threadings across all chains in the system after any relaxation process terminates (roughly the stress relaxation time). The reason that we use the terminal passive penetrations is

because they are the threadings that actually block the ring motion. Until the terminal passive threading is removed from the moving duplex ring it is pinned by these threadings and is unable to relax any more stress than that associated with tube segments close to either end, "outside" the region between these terminal passive threadings. The stress associated with these peripheral tube segments will relax extremely fast, as this process is governed by unimpeded diffusion, governed by the bare Doi-Edwards curvilinear diffusion constant D_c. In the next regime ($t/t_h > \tau_p$), after the polymer has diffused further than λ the graph gradually flattens into a sub-diffusive plateau regime that extends at least two order of magnitude in time, extending for more highly threaded systems. To understand this slowing-down one must appreciate that the system follows bare diffusion for short times but begins to experience blocking threadings that hinder its progress, becoming sub-diffusive. At very late times $t/t_h > \tau_d$ the system becomes diffusive again, albeit with a diffusion constant that is much smaller than the bare Doi-Edwards D_c. This evidences that the time before free diffusion is robustly recovered and the associated memory remains even longer than τ_d.

3.6 Lifetime of penetrations

A network of threadings exists in our system of ring polymers that contains active-passive threading pairs, as shown in Fig 3.6. One question that we might naturally ask about this threaded network is how long do these penetrations last? Indeed, this is a crucial question because we are now beginning to understand that the chain dynamics is controlled at a very deep level by the threadings. In section 3.7 we will discuss the reflexive nature of this relationship - that the threadings are merely tube segments on secondary chains that are lost by the same stress relaxation process that applies on the primary chain.

There are some features we might expect of the threading lifetimes (ages). First of all, we might expect their ages to vary, depending on where they are located on the chain. Active threadings are, by definition, created at the ends of the duplex chain, and those near an end are likely to be quickly annihilated, compared with those far from the ends. This means that active

threadings near the end of the active chain that created them are likely to be younger (and less long-lived) than those who reside closer to the centre of the chain contour, where they are likely to be older (and live longer). The reason is that small diffusion steps easily remove the active penetrations at the ends. The passive threadings are created (and lost) in a completely different way. They are introduced at random positions on some secondary chain, with the insertion position chosen from a uniform distribution along the (all) polymer length(s). The lifetime of these threadings might therefore be expected to be relatively insensitive to their position on the passive partner chain that hosts them.

A crude model to test this idea can be constructed by using a renormalised version of Doi-Edwards theory. We assume that rings undergo a genuine diffusion process (mean squared displacement is proportional to elapsed time) and that the role of the threadings can be captured, on average, merely by a renormalisation of the curvilinear diffusion constant, from the "bare" value D_c to a smaller effective value D_{eff}. We then construct a model describing the lifetime of an active penetration segment, see Fig.3.15. Let $\psi(x,t)$ be the

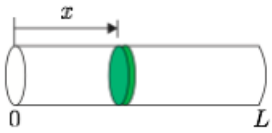

Figure 3.15: An active chain (not shown) moves in a tube of length L (equal to N in dimensionless units). It carries an active threading at the green tube segment (as usual, this generates a passive threading on some secondary chain). The lifetime of the passive threading is merely the lifetime of the tube segment that carries it.

probability of finding an active threading segment alive at position x and time t. $\psi(x,t)$ must satisfy the one-dimensional diffusion equation

$$\frac{\partial \psi(x,t)}{\partial t} = D_{eff} \frac{\partial^2 \psi(x,t)}{\partial x^2}. \tag{3.20}$$

New active penetrations are inserted into a system only at the end of the polymer chain. Because active threadings can be created at both ends of the chain the boundary condition and initial condition for this model can be

written as follows.

$$\psi(0,t) = 0, \psi(L,t) = 0 \text{ ,and} \tag{3.21}$$

$$\psi(x,0) = \delta(x-\epsilon) + \delta(x-(L-\epsilon)) \tag{3.22}$$

where ϵ is a small distance representing the location at which the threadings are injected (equal to one tube segment in the simulations). What we are therefore calculating is the (transient) motion of active threadings injected at (near) the chain ends. Given that this injection is a continuous process, and the equation is linear, we can use a single injection like this to infer the lifetime of a tube segment at x by calculating the probability of finding a segment alive at position x at later time and normalising appropriately.

Using boundary condition 3.21, we obtain

$$\psi(x,t) = \sum_{n}^{\infty} A_n \sin\left(\frac{n\pi x}{L}\right) e^{-\left(\frac{n\pi}{L}\right)^2 D_{eff} t} \tag{3.23}$$

where D_{eff} and A_n are an effective diffusion constant and the Fourier coefficient of the probability density, respectively. The A_n are calculated by using the initial condition 3.22. The solution can be written as

$$\psi(x,t) = \sum_{n;odd} \frac{4}{L} \sin\left(\frac{n\pi\epsilon}{L}\right) \sin\left(\frac{n\pi x}{L}\right) e^{-\left(\frac{n\pi}{L}\right)^2 D_{eff} t}. \tag{3.24}$$

The lifetime of active penetration $\tilde{a}(x)$ at position x can be determined using

$$\tilde{a}(x) = \frac{\int_0^\infty t\psi(x,t)dt}{\int_0^\infty \psi(x,t)dt}. \tag{3.25}$$

Using the fact that the number of active and passive penetrations are equivalent, we can derive the age of passively threading $\tilde{p}(x)$ (assumed independent of position x) as

$$\tilde{p}(x) = \tilde{p} = \frac{1}{L}\int_0^\infty \tilde{a}(x)dx. \tag{3.26}$$

In order to compare these calculations with simulation results, the lifetime of both active and passive penetration are measured using the following procedures. When any stress relaxation event occurs, a snapshot of the system is

taken. This includes information on the creation time (and hence ages) of all threadings that still remain alive in the system. By averaging over these snapshots we are able to compute an estimate of the mean age, equivalent to lifetime, of a threading at position x along the chain. The simulation results for the corresponding ages of active $\tilde{a}(x)$ and passive $\tilde{p}(x)$ threadings are reported in t_h units (hence dimensionless). Figures 3.16 and 3.17 show the results for a system at very small p. By choosing such extremely small values of p we are generating systems in which the chance that any chain bears more than one threading at any time is extremely small. The results therefore map to the Doi-Edwards limit in which tube segments (the rare active threadings) relax by standard reptation. We therefore expect, and confirm, agreement between the simulations and the Doi-Edwards lifetimes, as shown in red on these figures. The fit made in the illustrations is a least squared fit of the effective diffusion constant. The results emphasise that the active threading located around the middle of the chain are long-lived since they are more difficult to remove. Symmetry around the centre of the chain $x - L/2 \to L/2 - x$ is also apparent, as expected. In the case of passive threading, the picture here is somehow giving a new perspective. The lifetime of them are uniformly distributed along the primitive chain. The underlying reason may be the way we generate a passively penetrating is by random sampling the position. Increasing the number of threadings makes the age of penetration longer because the blocking of passive threading makes the network of rings slower to relax its associated stress, see Fig. 3.18 and 3.19). Thus, they live longer. Data from Fig. 3.18 and 3.19 shows hints that we are moving away from the Doi-Edwards limit, particularly in the fact that the lifetimes are now much longer than those when threadings are rare.

3.7 Relaxation times and rates

One of the most interesting questions to arise at this stage of our study is how the stress relaxation time τ_d is related to the average time to remove a terminal passive threading τ_p. This question, and attempts to resolve it, motivate much of the rest of this thesis.

The following thought experiment has been very revealing, even though

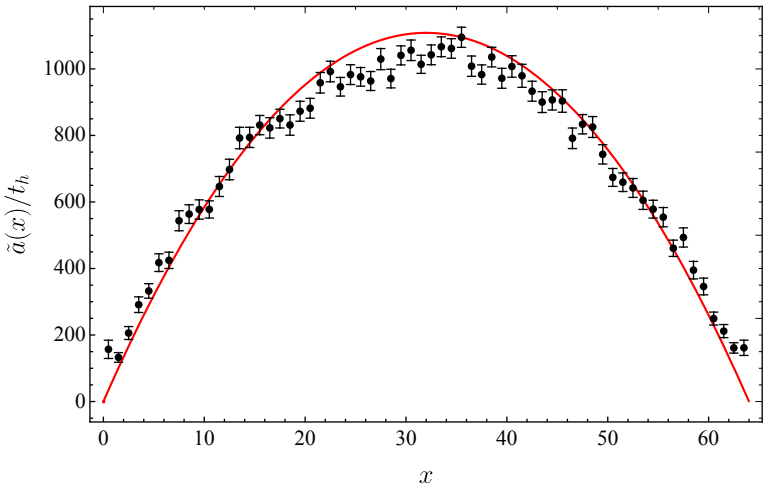

Figure 3.16: The lifetime of active penetration in the middle of the chain live longer than those near the ends. The simulation data presented in dots is taken from the system with $N_c = 40$, $N = 64$ and $p = 0.0001$. The red line represent the analytical solution from the diffusion of the active segment from equation 3.24 and3.25.

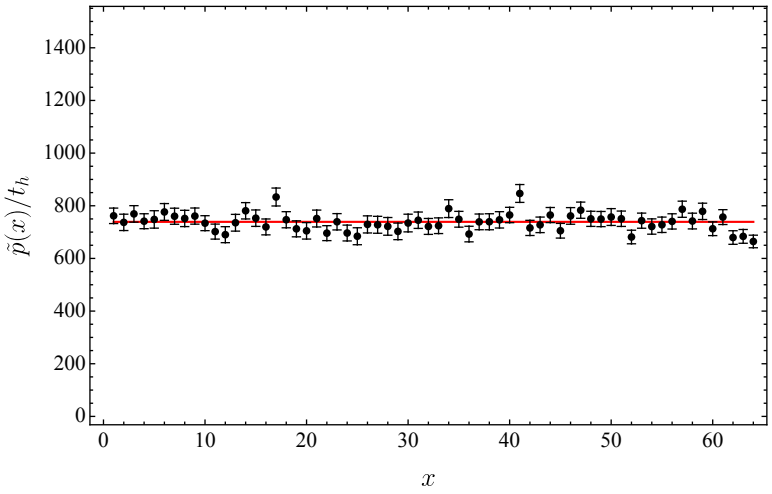

Figure 3.17: The lifetime of passive penetration is uniformly distributed along the polymer chain. The system parameters are $N_c = 40$, $N = 64$ and $p = 0.0001$. The red line indicates the theoretical calculation by applying the least squared fitting of the effective diffusion constant.

it only leads to an apparently paradoxical result. We are interested in a system in which the rings all have a significant number of threadings. If there is a universal regime in this problem then it is the regime where $m \gg 1$. We seek to understand the motion of a "primary" ring polymer in this regime, e.g. how the

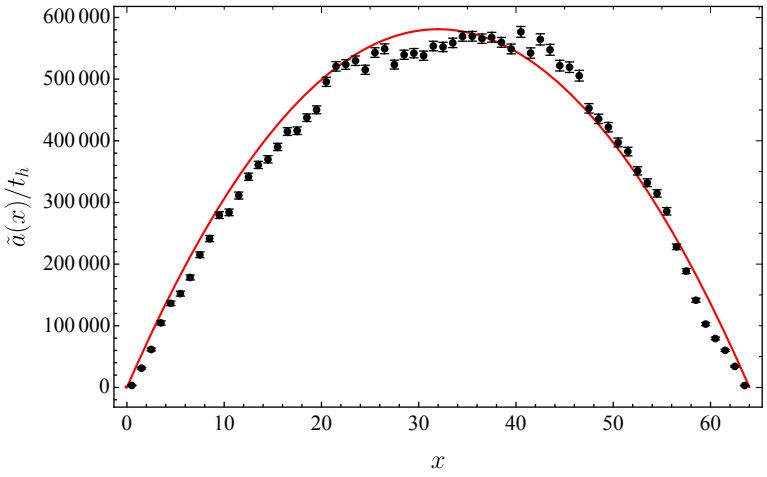

Figure 3.18: The lifetime of active penetrations increases when its position is closer to the centre of the chain, even when there are many threadings present. The system parameters are $N_c = 40$, $N = 64$ and $m \approx 13$. The overall relaxation times are much longer than in Fig 3.16.

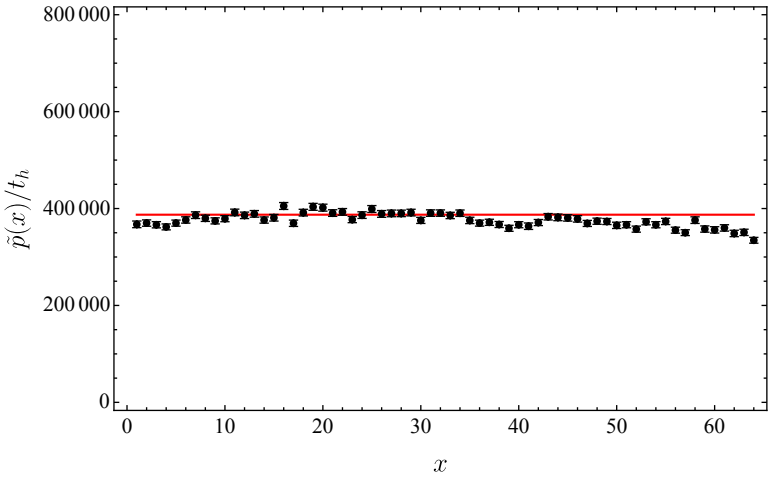

Figure 3.19: The lifetime of passive penetration is approximately uniformly distributed along the polymer chain, even when there are many threadings present. The system parameters are $N_c = 40$, $N = 64$ and $m \approx 13$. The overall relaxation times are much longer than in Fig 3.17.

stress associated with it relaxes. The motion of this primary polymer depends on the removal of passive threadings, each hosted by a "secondary" chain, where they appear as the partner active threading to the passive threading on the primary chain. The motion of the primary chain might be through to proceed as follows. The chain is caged (or pinned) by the terminal passive

threadings and has only limited freedom to move until one of the terminal passive threadings is removed. When this occurs the chain can "hop" one inter-threading length $\lambda = L/m_p$ with $m_p = m/2$. This hopping might be imagined to be approximately diffusive, with each hop occurring after a time τ_p. Such an argument leads to the following approximation for the stress relaxation time for the primary chain in terms of the lifetime of passive threadings on that chain

$$\tau_d \simeq \left(\frac{m}{2}\right)^2 \tau_p, \tag{3.27}$$

involving an unknown prefactor that is of order unity.

To incorporate the case where $m = 0$ as a limit, equation 3.27 might be adapted to include an additional time that corresponds to the bare curvilinear diffusion (in the absence of threadings). This involves τ_d^0, the stress relaxation time of the system with zero threadings. We could therefore rewrite the equation as

$$\tau_d - \tau_d^0 \simeq \left(\frac{m}{2}\right)^2 \tau_p, \tag{3.28}$$

noting that, for large m, the additional correction is likely negligible and eq 3.27 remains an adequate approximation.

The next stage of the argument involves thinking more carefully about the lifetime of the passive threadings. Each passive threading on this primary chain lives on a tube segment on a secondary chain, where it appears as an active threading. The lifetime of this active threading is therefore identical to that of the passive threading, by definition. The lifetime of the passive threading can therefore be estimated by constructing an argument for the lifetime of this active threading. We note that the active threading is lost whenever the tube segment that carries it is lost. This is exactly the same as saying it is lost when the *stress* associated with the tube segment hosting the active threading is lost. We now take a further step to suggest that the segment that carries the active threading is, on average, entirely typical. This argument means that the stress relaxation time of this segment should therefore be similar to the stress relaxation time of the typical chain that carries it. This statement implies that τ_d is of the same order as τ_p

$$\tau_d \simeq \tau_p. \tag{3.29}$$

However, these arguments, each seemingly plausible on its own, results in a paradox: 3.28 and 3.29 are obviously incompatible, even at this scaling level, for large m. This obviously reveals some flaw in the argument. A likely candidate is the breakdown of the mean-field assumption in which all threadings, and chains, are treated as "typical" (identical).

In order to explore these results we turned to our simulations. First, we examine the role of m on the stress relaxation time τ_d, as presented in Fig. 3.20. The result shows that the stress relaxation time scales exponentially with m, with an exponent (fitted from the data) with numerical value here of about 0.336. These results underscore the existence of this exponential scaling which has been described as analogous to a glass transition in which the divergence of the relaxation times is not exponential in temperature but rather in the number of threadings (equivalently the chain length N at fixed p). This can be thought of as some emergent slowing-down of the network of threadings.

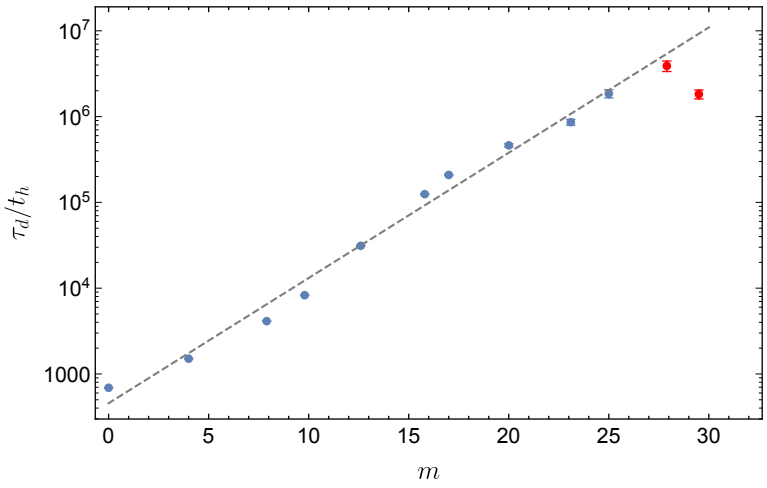

Figure 3.20: The stress relaxation time τ_d measured in t_h unit exponentially increases with the number of threading m with the exponent ≈ 0.336. The two highest m values (data points shown in red) are measured from systems that may not have fully equilibrated. We use this convention of showing datapoints from simulations that may not have fully equilibrated in red in all subsequent figures.

Next, we extend our investigation to the terminal passive penetration lifetimes τ_p. There are several ways this can be measured in simulation and we focussed on two methods. All the results shown in this chapter are obtained with the first method. In this method we measure τ_p by monitoring the events

when a chain undergoes a stress relaxation event, i.e. the time(s) when $G_i(t) = 0$. Whenever this occurs we sample the lifetimes (ages) of all terminal passive threadings across the entire network and calculate the average of those values. According to Fig. 3.21, τ_p measured in this way depends on m in a similar way as τ_d but with a different exponent ~ 0.515. A comparison of the exponents in these two cases suggest that τ_p becomes asymptotically longer than τ_d, indeed it is already larger for the m values we show in Figs. 3.20,3.21. This suggests that there may be some inconsistency in 3.29. The underlying reason why τ_p is larger than τ_d probably lies in the way we sample τ_p. In each simulation, there is a chance that a few very long-lived threadings arise. These threadings live for a long time and might be expected to reside deep within the network of threadings. This means that every time we sample we can include any very long-lived threadings, resulting in a correspondingly large value of τ_p. In Chapter 4 we discuss a second method of measuring τ_p that involves monitoring every threading. This provides an estimate that is much shorter with, $\tau_p \ll \tau_d$, because most threadings are indeed short lived.

Figure 3.22 represents an attempt to directly investigate 3.28. It shows the relationship between values of τ_d and values of $(m/2)^2\tau_p$ obtained for each simulation run, performed at a different p value. While this data is inconclusive as to the existence of an asymptotic relationship that may be linear, it clearly shows that the slope of any linear relationship that might exist is smaller than the expected value (of order unity) by a factor of 10^3 or more.

Clearly there is some deep contradiction between 3.28 and 3.29 but the underlying philosophy of relating stress relaxation to the removal of passive threadings (and vice versa) remains attractive and it is tempting to think that such an argument could be reconciled by somehow thinking a bit differently about the problem. In that spirit we consider the relaxation in terms of the *rates* associated with the process, rather than the times. We define the average rate of stress relaxation over n_{relax} simulated stress relaxation processes as

$$k_d = \frac{1}{n_{relax}} \sum_{j=1}^{n_{relax}} \frac{1}{\tau_d^j}. \tag{3.30}$$

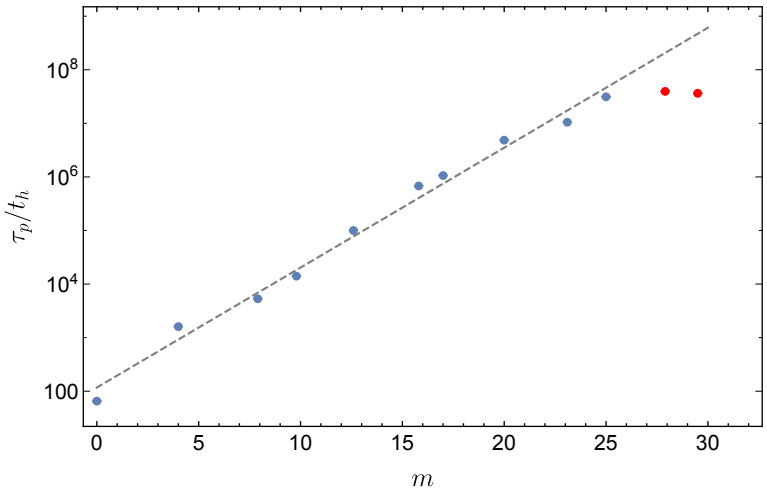

Figure 3.21: The average time taken to remove the terminal passive threading τ_p, measured in t_h units, grows exponentially with the number of threading m with the exponent ≈ 0.515.

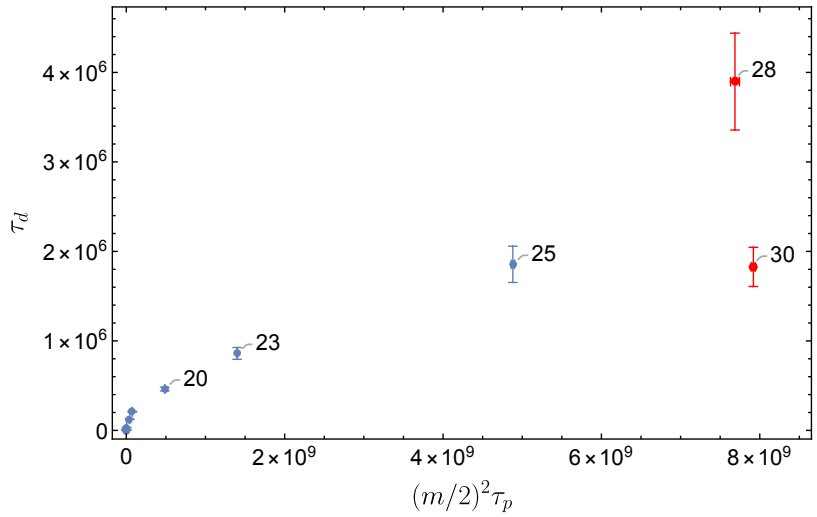

Figure 3.22: The stress relaxation time τ_d at large m varies extremely slowly with $(m/2)^2\tau_p$ (note the factor of 1000 difference in the scales of the axes), revealing a contradiction in equation 3.28.

In a similar way we define

$$k_p = \frac{1}{n_{relax}} \sum_{j=1}^{n_{relax}} \frac{1}{\tau_p^j} \tag{3.31}$$

where τ_p^j is the average lifetime of the terminal passive treading of the j^{th}

relaxation process. Using this definition will help us to mitigate the effect of long-lived penetrations lying in the tail of the distribution (see Fig.3.11). We now constructing the relationship between k_d and k_p by recalling 3.28 and rewrite in terms of rates

$$\frac{1}{k_d} \approx \left(\frac{m}{2}\right)^2 \frac{1}{k_p} + \frac{1}{k_d^0} \tag{3.32}$$

where k_d^0 is the stress relaxation rate of the system without threading. We compare this prediction with simulation results, as presented in Fig.3.23. From the graph, the data converges to a linear relationship with slope of order unity, when $m \geq 20$, confirming the relationship 3.32 with y-intercept $1/k_d^0 \approx 516$. There is an initial regime $0 < m \lesssim 10$ in which there is a steeper linear relationship than for larger m, with the trend appearing to revert back towards the fitted line for $m \gtrsim 10$. This suggests that the value $m \approx 10$ may represent some sort of crossover value between the "small m" and "large m" regimes.

Equation 3.32 still seems to holds if we consider the average over *all* passive threadings, rather than only the terminal threadings, see Fig. 3.24. The data for the associated times and rates are shown in table 3.1.

m	τ_d	k_d	τ_p	k_p
0	690.1 ± 0.9	$(1.976 \pm 0.003) \times 10^{-3}$	65.4 ± 1.8	0.571 ± 0.03
4	$(1.506 \pm 0.002) \times 10^{3}$	$(1.196 \pm 0.002) \times 10^{-3}$	$(1.604 \pm 0.002) \times 10^{3}$	$(2.57 \pm 0.01) \times 10^{-2}$
8	$(4.12 \pm 0.01) \times 10^{3}$	$(7.27 \pm 0.02) \times 10^{-4}$	$(5.313 \pm 0.009) \times 10^{3}$	$(2.479 \pm 0.009) \times 10^{-2}$
10	$(8.28 \pm 0.04) \times 10^{3}$	$(6.14 \pm 0.02) \times 10^{-4}$	$(1.405 \pm 0.003) \times 10^{4}$	$(2.477 \pm 0.009) \times 10^{-2}$
13	$(3.12 \pm 0.05) \times 10^{4}$	$(5.69 \pm 0.04) \times 10^{-4}$	$(9.99 \pm 0.02) \times 10^{4}$	$(2.494 \pm 0.009) \times 10^{-2}$
16	$(1.25 \pm 0.02) \times 10^{5}$	$(5.37 \pm 0.02) \times 10^{-4}$	$(6.78 \pm 0.02) \times 10^{5}$	$(2.669 \pm 0.009) \times 10^{-2}$
17	$(2.09 \pm 0.04) \times 10^{5}$	$(5.13 \pm 0.03) \times 10^{-4}$	$(1.061 \pm 0.003) \times 10^{6}$	$(2.762 \pm 0.009) \times 10^{-2}$
20	$(4.6 \pm 0.2) \times 10^{5}$	$(4.78 \pm 0.04) \times 10^{-4}$	$(4.86 \pm 0.01) \times 10^{6}$	$(2.98 \pm 0.01) \times 10^{-2}$
23	$(8.6 \pm 0.7) \times 10^{5}$	$(4.09 \pm 0.06) \times 10^{-4}$	$(1.049 \pm 0.005) \times 10^{7}$	$(3.24 \pm 0.02) \times 10^{-2}$
25	$(1.9 \pm 0.2) \times 10^{6}$	$(3.80 \pm 0.05) \times 10^{-4}$	$(3.12 \pm 0.01) \times 10^{7}$	$(3.35 \pm 0.02) \times 10^{-2}$
28	$(3.9 \pm 0.5) \times 10^{6}$	$(3.25 \pm 0.08) \times 10^{-4}$	$(3.95 \pm 0.03) \times 10^{7}$	$(3.57 \pm 0.02) \times 10^{-2}$
29	$(1.8 \pm 0.2) \times 10^{6}$	$(3.11 \pm 0.07) \times 10^{-4}$	$(3.64 \pm 0.01) \times 10^{7}$	$(3.67 \pm 0.01) \times 10^{-2}$

Table 3.1: Comparison between the mean stress relaxation time τ_d, the mean of the inverse of the stress relaxation time (rate) k_d, the average time of relaxing the terminal passive penetration τ_p and the rate of relaxing the terminal passive penetration k_p.

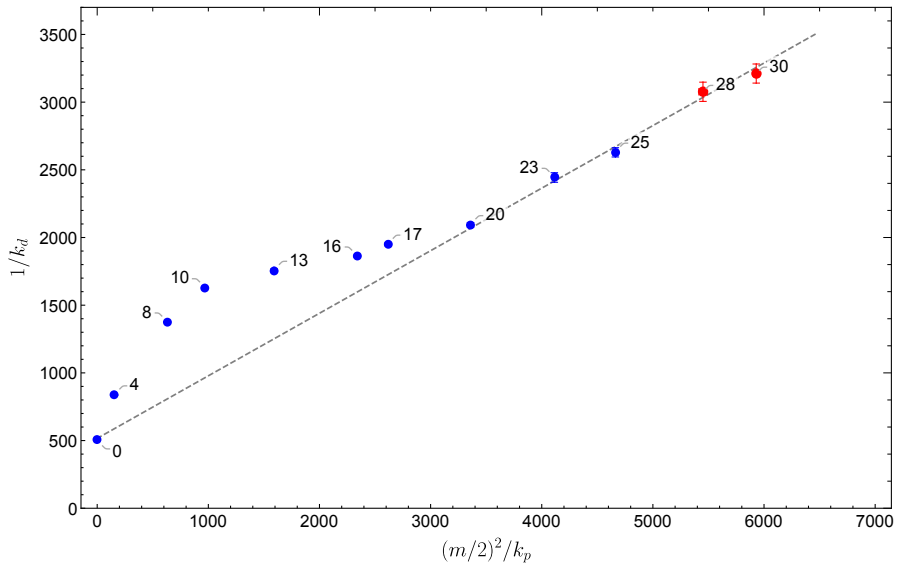

Figure 3.23: The inverse of the stress relaxation rate k_d is shown plotted against $(m/2)^2/k_p$, with $1/k_p$ the inverse of the terminal passive threading relaxation rate. The number next to each data point is the value of m for that simulation. All simulations involve duplex chains of length $N = 64$ but have a different threading probability p, giving rise to a mean number of threadings m as shown. The dashed line with slope 0.462 is a fit to the largest three m values that we are confident have fully converged, i.e. $m = 20, 23, 25$. The trend is initially a rapid increase up to a crossover around $m \approx 10$; for larger values of m the data seems to approach an asymptotically linear regime which may signify the emergence of a universal regime for large m in which the scaling of the stress relaxation time (inverse stress rate k_d) is $\sim m^2$ and therefore diffusion-like. The y-intercept at $1/k_d = 516.239$ corresponds roughly to the inverse of the bare (Doi-Edwards) stress relaxation time when $m = 0$ and the threadings play no role. Crucially, the slope here is of order unity, implying semi-quantitative equivalence between $1/k_d$ and $(m/2)^2/k_p$ at large m.

3.8 Chapter conclusion

Before moving to the next chapter, it is worth to review the information provided in this chapter. Some of the simulation results here will pave a way to an analysis in the next chapter. This chapter was dedicated mainly to the Monte Carlo simulation of dynamics of ring polymer in a gel. In the first part of the chapter I introduced the framework of our computational research. The structure of the ring polymer, which is duplex, unbranched, unlinked and unknotted, was carefully described, since our model relies on this kind of structure. The model preserves the topological constraints between

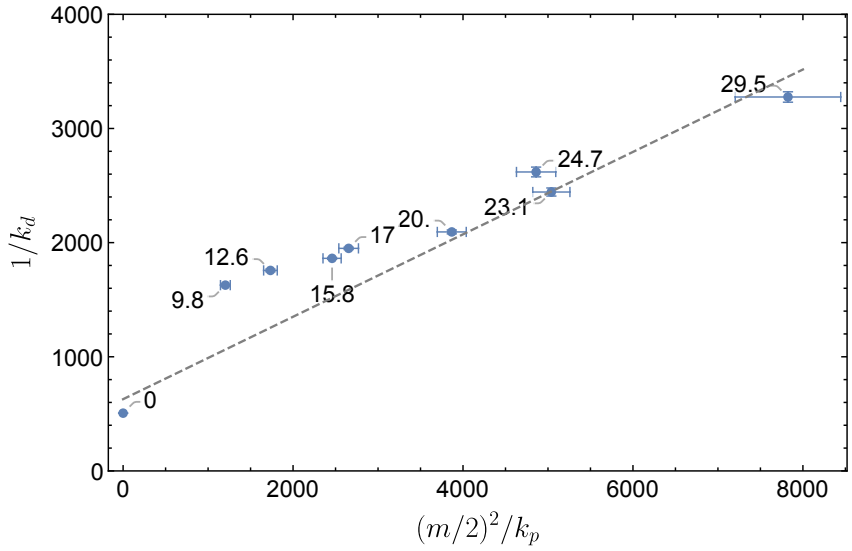

Figure 3.24: For all passive penetrations case, the relationship $1/k_d \sim (m/2)^2/k_p$ remains consistent in $m > 20$. The slope presented here is 0.361 and the y-intercept happens at $1/k_d = 628.528$.

the engagement gel and polymers. The gel in the model has no fluctuation and does not contribute directly to the simulation. Next, I established the definition of threading, both active and passive penetrations and clarified the role of them. I devoted the next part to describe the simulation procedures. Even though the simulation is performed by Monte Carlo sampling, it requires the proper update rules to perform the process. In this section, the role of the terminal passive penetration became significant due to the fact that it underlies rejection of certain polymer moves. The stress relaxation function $G(t)$ and average time τ_d played a central role in our research since they provided the information of the threaded rings system. Therefore, I dedicated a section to describe in detail their measurement.

Our system must be in an equilibrium to allow us to measured the properties mentioned above. In the simulation equilibrating the system is a significant issue as it affects the reliability of the simulations. The section 3.3 proposed a method of measuring the equilibration time by considering (the logarithm of) the mean stress relaxation time, as found in 3.5. The condition 3.11 ensured that we measured the equilibration time with 90% confidence.

The most important part of this chapter is where I presented the simulation results. One finding was the topological glass-like behaviour, in which

the dynamics of the ring polymers is slowed down by threading resulting in the growth of the stress relaxation time with the number of segments $\tau_d/t_h \sim \exp(\alpha N)$. The same behaviour was found later in the case of τ_d versus m. This is not surprising as $m \propto N$ with a proportionality constant that depends on the control parameter p. Moreover, the distribution of the mean stress relaxation time was studied and showed heavy-tailed statistics. The penetration significantly slowed down the dynamics of rings. The result also suggested that the motion of rings may not follow standard Fickian diffusion due to the difference of the moments of the stress relaxation function between the two cases. The mean squared displacement and time study added further evidence for this by showing a large sub-diffusive regime (plateau). In this region, the rings were slowed because they encountered the penetrations.

A study of the lifetime of threadings offered a new perspective regarding the stress relaxation. The active penetrations that are very close to the polymer ends are short-lived threading because they can be easily removed in a few time steps. Unlike the ones in the middle that remains longer. This is a stepping stone to an analysis of any thermodynamics of the threading network that we undertake in the next chapter. Also, the study also highlighted the role of the terminal passive penetration since it actually blocked the relaxation event.

Finally, I investigated the relationship between time τ_d and τ_p. To relax stress, the occupied passive threading needs to be successively removed. One can proposed that $\tau_d \simeq (m/2)^2\tau_p$. However, the results presented in section 3.7 revealed an inconsistency in this statement and suggested that there was some deep problem with the arguments, perhaps related to a breakdown of the mean-field assumptions that I used to understand the system of rings. On the other hand, considering rates k_d and k_p might be a more promising way of understanding the problem because the scaling $1/k_d \simeq (m/2)^2/k_p$ seems to instead be consistent in the large m limit.

Chapter 4

Mean-field Theory of Duplex Rings with Threading

The simulation results presented in Chapter 3 told a story of how the stress relaxation is slowed down by the presence of inter-ring threadings. The study of threading lifetimes was important given that the age, and type, of penetration is relevant to the relaxation process. The threadings that significantly slow down the relaxation process of the ring polymers network are the passive penetrations, especially, the "terminal" passive threadings, nearest to the polymer ends. We are interested in the terminal passive threadings because they provide the main mechanism that delays stress relaxation – in other words, they actually block the movement of other duplex rings, see Fig.4.1.

In order to relax the stress that might be associated with any polymer tube, these terminal threadings need to be removed. To do so the system must first remove their partner active threadings. Due to their central roles in the dynamics, we therefore investigate the properties of the active threadings paired with partner terminal passive threadings. We refer to these as "terminal-associated", rather than terminal, active threadings, to distinguish them from active threadings located closest to the ends of the polymers on which they live. These are unrelated.

We find that these terminal-associated threadings are not uniformly distributed along the primitive path of the active polymer that provides them but rather are statistically, and therefore thermodynamically, biased towards the ends, see Fig.4.2.

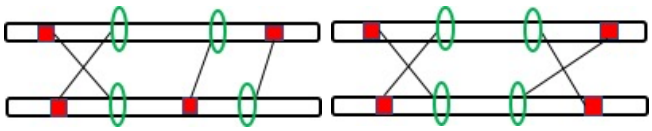

(a) (b)

Figure 4.1: Threading networks across two rings, with passive threadings shown in red and active in green. The lines connecting them identify pairs of threadings. (a) The polymer at the top contains a passive threading next to each polymer end. In order to relax the stress associated with this chain at least one of the two-terminal passive threadings, limiting the movement of its ends, need to first be removed. Its immediate prospects for substantial motion are therefore entirely "slave" to the motion of the other ring. In the case of the polymer shown on the bottom there are sequence(s) of moves that can achieve this stress relaxation: The bottom chain can move to the left, thereby losing its rightmost active threading and annihilating the rightmost passive-active pair. From that point additional moves allow the system to completely relax the stress on both chains. This configuration is therefore ergodically accessible: it can be *undone* and so it can be *"done"* (created). It is therefore topologically accessible for two ring unknots, with which it is topologically equivalent. (b) An example of an inaccessible arrangement of threadings, i.e. one that has a different topology to the initial state of two unknots. Here a "corona" of passive threadings on the outside of some part of the ring network (here the entire ring network) screens all active partner threadings in the interior, and so this configuration can never be (un)done. It cannot therefore be created. These microstates are inaccessible, breaking ergodicity. We propose that an entropy corresponding to limitations on accessible microstates is responsible for the emergence of an effective free energy $F(x)$ experienced by active threadings discussed in the text.

We analyse the positions of the active threadings on the primitive chain contour. While the threadings themselves are fixed in space, they move along the primitive path as the polymer undergoes random thermal moves along its tube. We consider only terminal-associated active threadings that connect to terminal passive penetrations. Fig.4.3 reveals that these active segments reside in a potential well roughly quadratic in nature that we approximate by

$$F(x) = -\frac{\beta}{2}\left(x - \frac{L}{2}\right)^2, \quad 0 \leq x \leq L. \tag{4.1}$$

Here, and in what follows, all energies are measured in units in which $k_B T = 1$. The parameter β is a parameter that controls the strength of the thermodynamic potential. Such a quadratic form corresponds to an equilibrium positional distribution that is in surprisingly close agreement with the results of

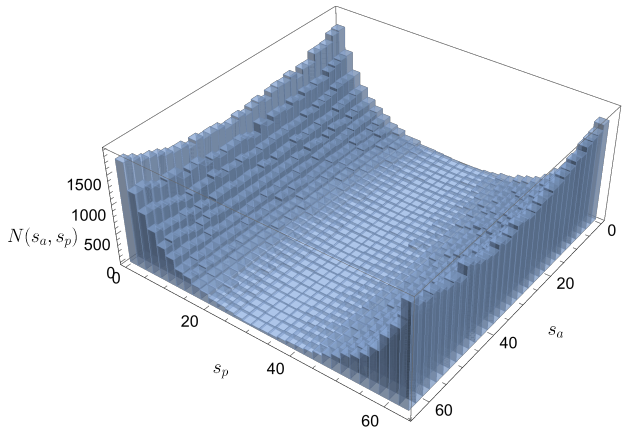

Figure 4.2: A histogram showing the equilibrium curvilinear positions of active penetrations s_a along the host chain that connect to terminal passive threadings at positions s_p on their partner polymers. Data acquired from Monte Carlo simulations of a system of $N_c = 40$ rings each containing $N = 64$ tube segments. Active threadings are created with a fixed probability following each successful chain move, here chosen to generate $m \approx 17$ threadings on each chain (including both passive and active). The simulation results reveal a bias in both distributions towards the end of their primitive contours. The bias in the position of the terminal passive threadings is trivial - we sample only the passive threadings closest to the end, and the distribution is approximately Poisson, as expected. The bias in the position of active threadings paired with the terminal passive threadings is non-trivial and becomes more pronounced as m increases (see below).

the kinetic Monte Carlo simulation in Fig.4.3. By fitting to results like this from simulations carried out over a range of values of m we can establish the depth of the free-energy potential, see Fig.4.4.

We are first interested in the lifetimes of the terminal-associated active threadings. Their mean lifetime can also be written τ_p to indicate that it is the same as the mean lifetime of a (terminal) passive threading (they are created and removed on a one-to-one basis with each other). This is therefore a fundamental microscopic timescale for the motion of polymers on length scales longer than the mean distance between threadings $\lambda \simeq L/m$: polymers move diffusively when $\langle x^2 \rangle \lesssim \lambda^2$, according to $\langle x^2 \rangle \simeq D_c t$ involving a "bare" Doi-Edwards curvilinear diffusion constant D_c. On longer timescales polymer motion involves random hops of mean squared distance $\simeq \lambda^2$ on the timescale on which terminal passive threading are lost (or added). If this motion was purely diffusive this would obey $\langle x^2 \rangle / \lambda^2 \simeq t/\tau_p$, corresponding to a diffusion

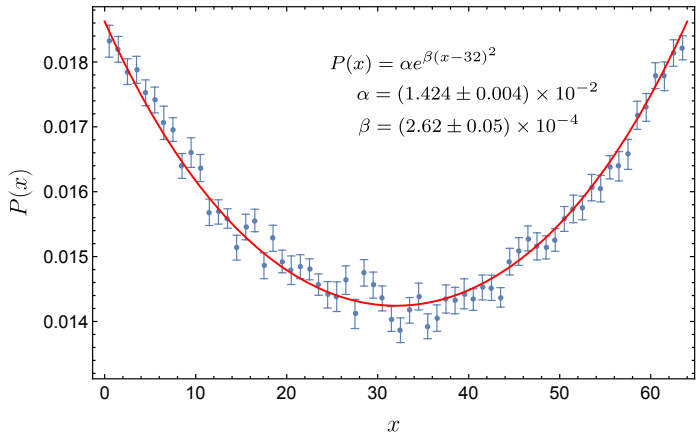

Figure 4.3: Active threadings paired with the terminal passive threadings are biased towards the ends of the polymer in a way that reflects an underlying entropic free energy that is quadratic about the polymer midpoint. Shown are the distribution of the curvilinear positions of the terminal-associated active threadings (blue points) for parameters $N_c = 40$, $N = 64$ and $m \approx 17$ as found by Monte Carlo simulation. This distribution is well fitted by a Boltzmann distribution involving a repulsive, rather than confining, quadratic potential $F(x) \sim -(x - L/2)^2$ (itself a free energy - it is entirely entropic in origin). This potential is inferred to arise from topological constraints associated with the network of threadings, see Fig.4.1.

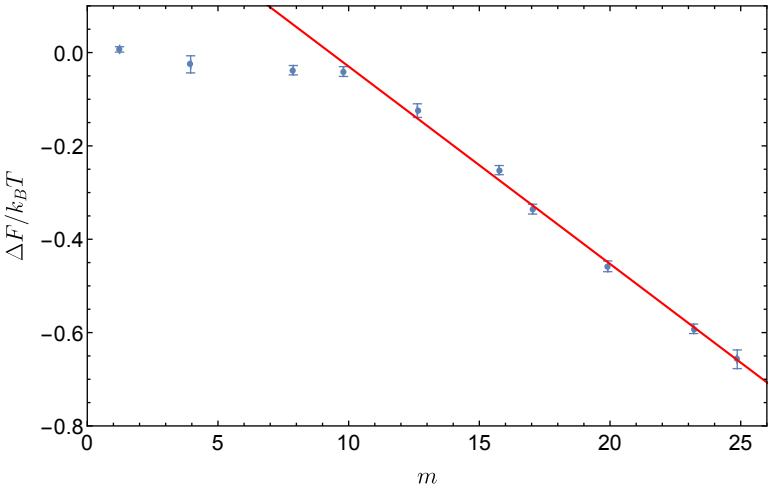

Figure 4.4: Free energy difference in k_BT units, between a terminal-associated active threading located at $x \approx L/2$ and $x \approx 0$, $\Delta F = F(L/2) - F(0)$. The origin of this free energy difference is in an entropy associated with the ring network topology. The large m scaling is linear $\Delta F/k_BT = \gamma(m_c - m)$ with $\gamma \approx 1/20$. The same crossover value of $m_c \approx 10$ as previously identified in Fig 3.23 appears here: this characterises the crossover to the large m regime.

constant $D \sim \frac{1}{m^2}L^2/\tau_p$ and a stress relaxation time $\tau \sim m^2\tau_p$. However, the loss of each passive threading occurs when the stress associated with the tube segment that hosts its partner active threading on another chain is lost. Assuming that this is a "typical" tube segment then it should be lost on the (same) stress relaxation timescale and hence $\tau \sim \tau_p$. Clearly, these last two equations for the stress relaxation time are completely inconsistent in their scaling with m. We believe that the resolution to this apparent paradox lies in the non-mean field distribution of active threadings along their host primitive path and the corresponding non-diffusive nature of the underlying dynamics of all ring polymers. There is an emergent free energy $F(x)$ associated with the position of active threadings, arising from the network topology, that acts to bias this motion by providing an advective component to the dynamics that moves the active threadings towards their nearest ends. We believe this non-uniformity to be behind the failure of the above mean-field argument and understanding this is a primary motivation in what follows.

To attempt to understand better the dynamics we compute the lifetimes of the terminal-associated active threadings. To do this we first consider the probability, at time t, that such a threading resides at curvilinear position x along the primitive path of the active chain that provides it. The generalisation of the diffusion equation for its movement can then be written as a Fokker-Planck equation that incorporates the free energy $F(x)$

$$\frac{\partial \Psi}{\partial t} = D\frac{\partial^2 \Psi}{\partial x^2} + \frac{1}{\zeta}\frac{\partial}{\partial x}\left(\frac{\partial F}{\partial x}\Psi\right) \tag{4.2}$$

where $\Psi = \Psi(x,t)$ is the probability of finding the active penetration at position x at time t and D is here some emergent curvlinear diffusion constant that we later hope to estimate self-consistently. We choose initial conditions that introduce newly born active threadings a (small) distance ϵ from the polymer ends and use this to compute its lifetime.

$$\Psi(x,0) = \delta(x-\epsilon) + \delta(x-L+\epsilon). \tag{4.3}$$

Much like the classical theory of reptation, the tube segment carrying the active threading, and therefore the threading itself, is lost when the end of the

diffusing chain reaches its position. Equivalently, the active threading can be seen to be diffusing along a chain contour in the frame of the polymer itself. It is lost when it reaches either polymer end. Therefore, the absorbing boundary conditions for this problem are

$$\Psi(0,t) = \Psi(L,t) = 0. \tag{4.4}$$

In order to more conveniently solve this problem, we extend the domain of our problem from $x \in [0, L]$ to $x \in [-L, L]$ with $\Psi(x,t)$ extended to be odd in x and $F(x)$ to be even in x. This is convenient for analysis using a Fourier transform of the diffusion equation and the method of images. We need to redefine the initial condition (4.3) to exploit the method of images to naturally satisfy 4.4 for all time.

$$\Psi(x,0) = \frac{1}{2}\left(\delta(x-\epsilon) + \delta(x-L+\epsilon) - \delta(x+\epsilon) - \delta(x+L-\epsilon)\right). \tag{4.5}$$

The Fokker-Planck equation then reads[1]

$$\frac{\partial \Psi}{\partial t} = D\frac{\partial^2 \Psi}{\partial x^2} - \frac{\beta}{\zeta}\frac{\partial}{\partial x}\left(\left(x + \frac{L}{2}\right)\Psi\right) \quad (-L \le x < 0) \tag{4.6}$$

and

$$\frac{\partial \Psi}{\partial t} = D\frac{\partial^2 \Psi}{\partial x^2} - \frac{\beta}{\zeta}\frac{\partial}{\partial x}\left(\left(x - \frac{L}{2}\right)\Psi\right) \quad (0 \le x \le L). \tag{4.7}$$

The preceding domain of the problem contains a symmetry around $x = L/2$. To satisfy that condition, the added domain must have symmetries around $x = -L/2$. The characteristic of the potential with the extended domain implies the Fourier sine series solution

$$\Psi(x,t) = \sum_{n=1}^{\infty} \psi_n(t) \sin\left(\frac{n\pi x}{L}\right) \tag{4.8}$$

[1]This equation also supports equilibrium solutions $\dot{\Psi} = 0$ corresponding to a Boltzmann distribution $\Psi \sim \exp[-F/k_BT]$ with the diffusion constant $D = k_BT/\zeta$, as can be checked by substitution.

with the time-dependent coefficient

$$\psi_n(t) = \frac{1}{L}\int_{-L}^{L} \Psi(x,t)\sin\left(\frac{n\pi x}{L}\right) dx. \tag{4.9}$$

The symmetric properties mentioned above suggest that the case of n even does not contribute to the solution 4.8. Therefore, we can rewrite

$$\Psi(x,t) = \sum_{n;odd}^{\infty} \psi_n(t)\sin\left(\frac{n\pi x}{L}\right). \tag{4.10}$$

We then apply the Fourier sine transform 4.9 to the diffusion equation 4.6 and 4.7. The Fokker-Planck equation reduces to a partial differential equation of the coefficient $\psi_n(t)$ with respect to n and time t as follows

$$\frac{\partial \psi_n}{\partial t} = -D\left(\frac{n\pi}{L}\right)^2 \psi_n + \beta^\star n\frac{\partial \psi_n}{\partial n} \tag{4.11}$$

with $\beta^\star = \beta/\zeta$. The partial differential equation can be solved analytically for the coefficient $\psi_n(t)$ by using the method of characteristics. Choosing the appropriate characteristic curve leads to

$$\psi_n(t) = A\sin\left(\frac{ne^{\beta^\star t}\pi\epsilon}{L}\right)\exp\left(\frac{n^2\pi^2 D}{2\beta^\star L^2}\left(1-e^{2\beta^\star t}\right)\right) \tag{4.12}$$

where A is a constant. $\psi_n(0)$ can be estimated using the definition 4.9 and the modified initial condition 4.5,

$$\psi_n(0) = \frac{4}{L}\sin\left(\frac{n\pi\epsilon}{L}\right). \tag{4.13}$$

By substituting this condition to 4.12, we find that

$$\psi_n(t) = \frac{4}{L}\sin\left(\frac{ne^{\beta^\star t}\pi\epsilon}{L}\right)\exp\left(\frac{n^2\pi^2 D}{2\beta^\star L^2}\left(1-e^{2\beta^\star t}\right)\right). \tag{4.14}$$

We recall that our motivation here was to derive an expression for the relaxation of the terminal-associated active threadings and we have achieved this in equation 4.14. It represents an expression for the relaxation of these terminal-associated active threadings through the n^{th} mode of the correspond-

ing real-space relaxation function defined by equation 4.8.

Reassuringly, this has the correct (diffusive) limit as $\beta^\star \to 0$ [Doi and Edwards, 1986]

$$\lim_{\beta^\star \to 0} \psi_n(t) = \frac{4}{L} \sin\left(\frac{n\pi\epsilon}{L}\right) \exp\left(-\left(\frac{n\pi}{L}\right)^2 Dt\right). \tag{4.15}$$

The solution is somehow reminiscent of equation 3.24 since the case $\beta^\star = 0$ recovers the physics of a Doi-Edwards linear chain, with D_{eff} the same as the diffusion constant D here. For the sake of simplicity, we define the timescale that appears in equations 4.14 and 4.15 as

$$\tau_D = \frac{L^2}{D}. \tag{4.16}$$

The time τ_D is the time taken to diffuse a distance $\sim L^2$ under a purely diffusive process with diffusion constant D.

To review: the dynamics of our system of threaded rings is controlled by the terminal passive threadings - substantial displacement moves can only occur when they are removed/renewed. In order to calculate the lifetime of these terminal passive threadings we can instead examine the lifetime of the terminal-associated active threadings, according to equation 4.14. This is because these two threadings always and identically appear in pairs and the lifetime of one is equal to the lifetime of the other by definition. This means that we can use equation 4.14, and equation 4.8, in order to compute the lifetime of the terminal passive threadings.

In order to make contact with equation 3.24 we can examine the corresponding lifetime of terminal-associated active threadings as a function of their position along the duplex chain contour, defined according to

$$\tilde{a}_{\mathrm{ta}}(x) = \int_0^\infty t\Psi(x,t)dt \Big/ \int_0^\infty \Psi(x,t)dt \tag{4.17}$$

by analogy with $\tilde{a}(x)$ appearing in equation 3.25. The quantity $\tilde{a}_{\mathrm{ta}}(x)$ represents the mean lifetime of a terminal-associated active threading located at x. As such it can be compared with the corresponding lifetime of an active threading in the absence of any advection $\tilde{a}(x)$ equation 3.25: the two results

should converge for small $\beta^\star$ (or β), the parameter that controls the strength of the advection of the terminal-associated active threadings in equation 4.11 (4.6 and 4.7).

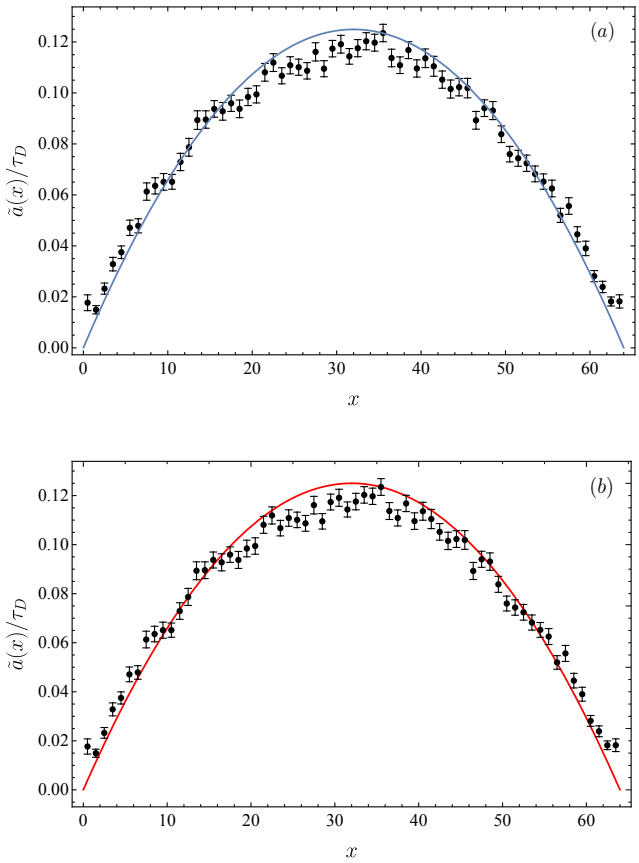

Figure 4.5: Lifetimes of active penetrations measured in τ_D unit from two different cases: (a) the result of the Fokker/Planck equation 4.14 with the approximation that $\beta^\star$ small (equivalent to $p = 10^{-4}$) shown in blue and (b) the standard diffusion of the active penetration 3.24. The result from both cases are consistent under this limit.

Equation 4.17 is difficult to solve exactly. However, we can compare the simulation result in the limit of small $\beta^\star$. Figure 4.5 shows the measurement of the lifetimes of active penetration $\tilde{a}(x)$ and $\tilde{a}_{\rm ta}(x)$ are in good agreement with each other in this limit. The lifetime in Fig. 4.5a was calculated from the active threadings that connects with the terminal passive partners and is compared with $\tilde{a}_{\rm ta}(x)$ from equation 4.17. Figure 4.5b shows the lifetime of *all* active threadings for the entire system and is compared with $\tilde{a}(x)$ from

equation 3.25.

Because direct solution of equation 4.17 is difficult we introduce an approach based on the use of a Laplace transform defined as

$$\tilde{\psi}_n(\omega) = \int_0^\infty \mathrm{e}^{-\omega t}\psi_n(t)\, dt. \tag{4.18}$$

This can help us to reduce the complexity of the PDE by transforming it to a first order differential equation. We further note that moments of the relaxation function are related to the $\omega = 0$ value of the Laplace transformed function, as usual. This provides us with a short-cut to access these moments.

By applying the transform to the differential equation 4.11, it becomes

$$\omega\tilde{\psi}_n - \psi_n(0) = -\left(\frac{n\pi}{L}\right)^2 D\tilde{\psi}_n + \beta^\star n\frac{\partial\tilde{\psi}_n}{\partial n}. \tag{4.19}$$

Rearranging equation 4.19 and introducing dimensionless variables according to $a = \omega/\beta^\star$ and $b = \pi^2 D/2\beta^\star L^2$ we find that

$$\frac{\partial\tilde{\psi}_n}{\partial n} - \left(\frac{a}{n} + 2bn\right)\tilde{\psi}_n = -\frac{\psi_n(0)}{n\beta^\star}. \tag{4.20}$$

The parameter b is an important control parameter and can be thought of as quantifying the strength of advection compared with diffusion - the effect of advection is weak for all modes when $b \gg 1$, becoming significant for some large n modes when $b \lesssim 1$.

To compare with simulations we must account for the fact that the advective strength, reflected in the parameter b, itself depends on the number of threadings and should strictly be written $b(m)$. Broadly speaking, b is large when there are few threadings and small when there are many. This, in turn reflects the increasing strength of the network entropy as the number of threadings is increased, i.e. an increase in N (or p). We can use the definition of the quadratic potential (4.1), evaluated at $x = 0$ and $x = L/2$, to relate ΔF to β as

$$\Delta F = \frac{\beta}{8}L^2. \tag{4.21}$$

This then gives a relationship for $b = \pi^2 D/2\beta^\star L^2$ as a function of ΔF

$$b = \frac{\pi^2}{16\Delta F/k_B T}. \tag{4.22}$$

We will later use this expression to empirically approximate b from the data shown in Fig 4.4. This approach will be necessary when m is small, i.e. $m \lesssim m_c$. For larger m values one could reasonably approximate

$$\frac{\Delta F}{k_B T} = -\gamma(m - m_c), \tag{4.23}$$

where $\gamma \approx 1/20$, and hence

$$b = \frac{\pi^2}{16\gamma}\frac{1}{(m - m_c)}. \tag{4.24}$$

This expression tells us how the parameter controlling advection of the terminal-associated active threadings depends on m in the universal regime when there are many threadings. It is significant that $b \sim 1/m$ for $m \gg m_c$. This means that the advection strength increases without bound in the limit of many threadings (long rings).

We can re-state equation 4.20 to see that it can then be solved analytically using an integrating factor $\mu(n)$

$$\mu(n) = \exp[-\left(a \ln n + bn^2\right)]. \tag{4.25}$$

As usual $\frac{d}{dn}(\mu\tilde{\psi}_n) = -\mu\frac{\psi_n(0)}{n\beta^\star}$ can now be integrated to find a solution to equation 4.20

$$\tilde{\psi}_n = -\frac{1}{\mu}\Big[\int^n \mu\frac{\psi_n(0)}{n\beta^\star}dn\Big] + \frac{C}{\mu}, \tag{4.26}$$

where C is a constant of integration that must vanish to recover physical solutions in the large n limit. Thus,

$$\tilde{\psi}_n(a) = \frac{2\pi\epsilon}{\beta^\star L^2} n^a e^{bn^2} b^{\frac{a-1}{2}} \Gamma\left(\frac{1-a}{2}, bn^2\right), \tag{4.27}$$

where Γ is the incomplete gamma function.

To recap, this result corresponds to a (second) solution to the time-

evolution of the probability density of unrelaxed terminal-associated active threadings, complementing equation 4.14. The solution 4.27 is a description in terms of mode numbers n, conjugate to position x on the primitive chain, and $a = \omega/\beta^\star$, a rescaled variable conjugate to time. This result allows us to compute the time taken to relax the terminal passive penetration paired with this active threading, i.e. the time for the terminal-associated active threading to be lost. We write this as τ_p and define it in two ways.

1. One way, equivalent to taking the zeroth moment is

$$\begin{aligned}
\tau_p^\star &= \int_0^L \int_0^\infty \Psi(x,t) dt dx \\
&= \lim_{\omega\to 0} \int_0^L \int_0^\infty \Psi(x,t) e^{-\omega t} dt dx \\
&= \lim_{\omega\to 0} \sum_n \int_0^L \sin\left(\frac{n\pi x}{L}\right) dx \int_0^\infty \psi_n(t) e^{-\omega t} dt \\
&= \lim_{\omega\to 0} \sum_{n;odd} \frac{2L}{\pi} \frac{\tilde{\psi}_n(\omega)}{n}
\end{aligned} \tag{4.28}$$

where $\tilde{\psi}_n(\omega) = \int_0^\infty \psi_n e^{-\omega t} dt$. This measure of the passive threading lifetime is defined as $\tau_p^\star$, to distinguish it from the second definition defined below. We did measure a quantity that we believe to be analogous to this quantity in simulations by measuring the average lifetime of all passive threadings, rather than sampling these lifetimes after stress relaxation events. We believe that the first sampling method corresponds more closely to the zeroth moment while the second corresponds more closely to the first moment introduced below. We further find that $\tau_p^\star$ estimated in this way from the simulations corresponds to an extremely small lifetime $\tau_{p,\,\mathrm{sim}}^\star < 100 t_h$ because it is dominated by the (many) extremely short-lived active threadings, many of which don't even live long enough to hop past the terminal passive threading when it is lost/renewed. Such relaxation events are not consistent with coarse-graining the dynamics on lengthscales $\gtrsim \lambda$, where the renormalised D is appropriate, rather they often never encounter passive threadings beyond the terminal one that limits their motion to the terminal regions of size $x \sim \lambda$ and so they move with the bare diffusion constant D_c.

2. The second method used in what follows is equivalent to taking the first moment (divided by the zeroth moment)

$$\begin{aligned}\tau_p &= \frac{\int_0^L \int_0^\infty t\Psi(x,t)dtdx}{\int_0^L \int_0^\infty \Psi(x,t)dtdx} \\ &= \lim_{\omega\to 0} \frac{\int_0^L \int_0^\infty t\Psi(x,t)e^{-\omega t}dtdx}{\int_0^L \int_0^\infty \Psi(x,t)e^{-\omega t}dtdx} \\ &= \lim_{\omega\to 0} \frac{\sum_{n;odd} \int_0^L \sin(n\pi x/L)dx \int_0^\infty t\psi_n e^{-\omega t}dt}{\sum_{n;odd} \int_0^L \sin(n\pi x/L)dx \int_0^\infty \psi_n e^{-\omega t}dt} \\ &= \lim_{\omega\to 0} \frac{\sum_{n;odd}(L/n\pi) \int_0^\infty t\psi_n e^{-\omega t}dt}{\sum_{n;odd}(L/n\pi) \int_0^\infty \psi_n e^{-\omega t}dt}. \end{aligned} \tag{4.29}$$

τ_p can be rewritten in terms of ω

$$\tau_p = \lim_{\omega\to 0} \Big[\sum_{n;odd} -\frac{1}{n}\frac{\partial\tilde{\psi}_n}{\partial\omega} / \sum_{n;odd} \frac{\tilde{\psi}_n}{n} \Big] \tag{4.30}$$

and also in terms of the newly defined variable $a = \omega/\beta^\star$

$$\begin{aligned}\tau_p &= \lim_{a\to 0} \Big[\sum_{n;odd} -\frac{1}{\beta^\star n}\frac{\partial\tilde{\psi}_n}{\partial a} / \sum_{n;odd} \frac{\tilde{\psi}_n}{n} \Big] \\ &= \lim_{a\to 0} \sum_{n;odd} -\frac{1}{\beta^\star n}\frac{\partial\tilde{\psi}_n}{\partial a} / \lim_{a\to 0} \sum_{n;odd} \frac{\tilde{\psi}_n}{n}. \end{aligned} \tag{4.31}$$

We believe that this τ_p better reflects the time it takes to relax the terminal passive threadings and is approximately equivalent to the simulation τ_p^{sim}, which measures the average lifetime of the terminal threading sampled after each stress relaxation processes in the simulation. This, relatively rare, sampling convention corresponds more closely to the first moment and effectively down-weights the numerous short lived active threadings. The notation τ_p^{sim} is introduced here because I would like to distinguish between the theoretical and simulation values.

In the next part of this thesis I will analyse our finding 4.27 in two different limits, corresponding to limits in which the advection of the terminal-associated active threading due to the network entropy is (in)significant. The

first limit is where the parameter $b \gg 1$, which is believed to be an asymptote in which the active threadings move diffusively and where advection is weak, broadly when $m \ll m_c$ according to Fig 4.4. The second case is where $b \ll 1$. This is anticipated to be the advective regime and corresponds to $m \gg m_c$.

4.0.1 The weak-advection limit $b \gg 1$ (sparse threadings)

We first recall the solution 4.27, corresponding to the transform of the probability distribution for terminal-associated active threadings. We take this result and define $z = (1-a)/2$, the first argument of the gamma function, for notational simplicity to rewrite $\tilde{\psi}_n$ in terms of z as

$$\tilde{\psi}_n(z) = \frac{2\pi\epsilon}{\beta^\star L^2} n^{(1-2z)} b^{-z} e^{bn^2} \Gamma\left(z, bn^2\right). \tag{4.32}$$

In order to more conveniently take a limit of b, we define a function $G = G(z, bn^2)$ as

$$\begin{aligned} G &= e^{bn^2}\Gamma\left(z, bn^2\right) \\ &= \int_{bn^2}^{\infty} t^{z-1} e^{-t+bn^2} dt. \end{aligned} \tag{4.33}$$

By a change of variables to $u = t - bn^2$ we obtain

$$G = \int_0^{\infty} (u + bn^2)^{z-1} e^{-u} du. \tag{4.34}$$

The integral over u extends over two regimes in which $u < bn^2$ and $u > bn^2$. In order to make progress with an analytic approximation to this integral, we divide the integral into two domains accordingly.

$$G = \int_0^{u^\star} (u + bn^2)^{z-1} e^{-u} du + \int_{u^\star}^{\infty} (u + bn^2)^{z-1} e^{-u} du \tag{4.35}$$

where $u^\star = bn^2$. We first note that the integral over $u > u^\star$ becomes negligible when $bn^2 \gg 1$. We then approximate the integral over $u < u^\star$ by using a

Taylor expansion as follows

$$\begin{aligned} G &= \int_0^{u^\star} (bn^2)^{z-1} \left(1 + \frac{u}{bn^2}\right)^{z-1} e^{-u} du \\ &= \int_0^{u^\star} (bn^2)^{z-1} \left(1 + (z-1)\frac{u}{bn^2} + \cdots\right) e^{-u} du. \end{aligned} \tag{4.36}$$

Solving the integral term by term and truncating[2] gives an approximation for G of the form

$$G = (bn^2)^{z-1} \left(1 + e^{-u^\star} + \frac{(z-1)}{bn^2}(1 - e^{-u^\star} - u^\star e^{-u^\star}) + \cdots\right). \tag{4.37}$$

To first subleading order this gives

$$G = (bn^2)^{z-1} + (z-1)(bn^2)^{z-2}. \tag{4.38}$$

We then substitute this result back into 4.32 to obtain the approximate solution and first leading order correction, neglecting all higher order terms.

$$\tilde{\psi}_n(z) = \frac{2\pi\epsilon}{\beta^\star L^2} \left(\frac{1}{nb} + (z-1)\frac{1}{n^3 b^2}\right). \tag{4.39}$$

In order to calculate $\tau_p^\star$, we consider the summation appearing in equation 4.28 under the limit $a \to 0$

$$\begin{aligned} \lim_{a\to 0} \sum_{n;odd} \frac{\tilde{\psi}_n(a)}{n} &= \sum_{n;odd} \lim_{a\to 0} \frac{\tilde{\psi}_n(a)}{n} \\ &= \frac{2\pi\epsilon}{\beta^\star L^2 b} \sum_{n;odd} \left(\frac{1}{n^2} - \frac{1}{2n^4 b}\right) \\ &= \frac{2\pi\epsilon}{\beta^\star L^2 b} \left(\frac{\pi^2}{8} - \frac{\pi^4}{192b}\right) \\ &= \frac{\pi^3\epsilon}{4\beta^\star L^2 b} \left(1 - \frac{\pi^2}{24b}\right). \end{aligned} \tag{4.40}$$

[2]This truncation is possible because both (i) $bn^2 \gg 1$ in the limit $b \gg 1$ with $n \geq 1$, and (ii) we are interested in the limit $\omega \to 0$, hence $a \to 0$ in which case $z = 1/2$ and the expansion involves terms with increasing inverse powers of bn^2.

The definition of τ_p from 4.28 involves the sum calculated above. We therefore find

$$\begin{aligned}\tau_p^\star &= \frac{2L}{\pi}\frac{\pi^3\epsilon}{4\beta^\star L^2 b}\left(1-\frac{\pi^2}{24b}\right)\\ &= \frac{L\epsilon}{D}\left(1-\frac{\pi^2}{24b}\right).\end{aligned} \tag{4.41}$$

The preceding expression can be measured in τ_D unit and can be expressed as

$$\tau_p^\star = \tau_D\frac{\epsilon}{L}\left(1-\frac{\pi^2}{24b}\right), \tag{4.42}$$

giving the behaviour of the terminal threading lifetime in the diffusive limit where threadings are sparse and entropic advection of terminal-associated active threadings is weak.

Next, we will estimate the time τ_p using the second definition. To do so, we start by considering the partial derivative of $\tilde{\psi}_n$ with respect to a. It can be determined using the following expression

$$\begin{aligned}\frac{\partial\tilde{\psi}_n}{\partial a} &= \frac{\partial\tilde{\psi}_n}{\partial z}\frac{\partial z}{\partial a}\\ &= -\frac{1}{2}\frac{\partial\tilde{\psi}_n}{\partial z}\\ &= -\frac{\pi\epsilon}{\beta^\star L^2}n(bn^2)^{-z}\left(\frac{\partial G}{\partial z}-\ln(bn^2)G\right).\end{aligned} \tag{4.43}$$

Equation 4.35 provides an approximation for G in the $b \gg 1$ limit. From this we can show that

$$\begin{aligned}\frac{\partial G}{\partial z} &= \int_0^\infty (u+bn^2)^{z-1}\ln(u+bn^2)e^{-u}du\\ &= \int_0^{u^\star}(u+bn^2)^{z-1}\ln(u+bn^2)e^{-u}du + \int_{u^\star}^\infty (u+bn^2)^{z-1}\ln(u+bn^2)e^{-u}du.\end{aligned} \tag{4.44}$$

The second integral over $u > u^\star$ is negligible and the first integral over $u < u^\star$ can be determined using a similar approach to the one used previously. Using a truncated Taylor expansion for the integrand, as before, the integral becomes

$$\frac{\partial G}{\partial z} = \int_0^{u^\star} (bn^2)^{z-1} \left(1 + \frac{u}{bn^2}\right)^{z-1} \ln\left((bn^2)\left(1 + \frac{u}{bn^2}\right)\right) e^{-u} du$$
$$\sim (bn^2)^{z-1} \int_0^{u^\star} \left(1 + (z-1)\frac{u}{bn^2}\right) \left(\ln(bn^2) + \frac{u}{bn^2}\right) e^{-u} du. \qquad (4.45)$$

We only keep the linear approximated terms since the higher order terms become smaller and can be ignored. The integral becomes

$$\frac{\partial G}{\partial z} = (bn^2)^{z-1} \left(\ln(bn^2) + \frac{z-1}{bn^2}\ln(bn^2) + \frac{1}{bn^2} + \frac{2(z-1)}{(bn^2)^2}\right). \qquad (4.46)$$

Substitute this expression back to (4.43), we obtain

$$\frac{\partial \tilde{\psi}_n}{\partial a} = -\frac{\pi\epsilon}{\beta^\star L^2}\left(\frac{1}{n^3 b^2} + \frac{2(z-1)}{b^3 n^5}\right). \qquad (4.47)$$

In calculating τ_p, the numerator of equation 4.31 is calculated from

$$-\frac{1}{\beta^\star}\lim_{a\to 0}\sum_{n;odd}\frac{1}{n}\frac{\partial \tilde{\psi}_n}{\partial a} = \frac{\pi\epsilon}{\beta^{\star 2} L^2}\sum_{n;odd}\left(\frac{1}{b^2 n^4} - \frac{1}{b^3 n^6}\right)$$
$$= \frac{\pi\epsilon}{24 L^2}\tau_D^2\left(1 - \frac{\pi^2}{10b}\right). \qquad (4.48)$$

Finally, we evaluate τ_p according to equation 4.31 by dividing the above equation for the numerator of 4.31 with the denominator 4.41. Thus we obtain our second estimate (4.31) τ_p for the time taking to relax the terminal passive penetration (equal to the time taken to relax the terminal-associated active threading) as

$$\tau_p = \frac{\tau_D}{12}\,\frac{1 - \frac{\pi^2}{10b}}{1 - \frac{\pi^2}{24b}} = \frac{\tau_D}{12}\left(1 - \frac{7\pi^2}{120b}\right) \qquad (4.49)$$

In the next subsection, I will perform an analysis of the lifetime of the terminal passive threading in the other limit. This is the strongly advective regime in which the parameter $b \ll 1$.

4.0.2 The strong advection limit $b \ll 1$ (numerous threadings)

We again seek to calculate the lifetime of the terminal passive threading from the corresponding lifetime of the terminal-associated active threading but now in the regime where advection of the terminal-associated active threading due to the threading network entropy is strong. This corresponds to the case $m \gg m_c$ and $b \ll 1$. As before our analysis is based on our solution for the probability distribution for terminal-associated active threadings, through its transformed version equation 4.27.

We consider the function G in its integral form and again divide it into two regimes $u < u^\star$ and $u > u^\star$ with $u^\star = bn^2$ as before according to equation 4.35 to obtain

$$G = \int_0^{u^\star} (bn^2)^{z-1} \left(1 + u/bn^2\right)^{z-1} e^{-u} du + \int_{u^\star}^{\infty} u^{z-1} \left(1 + \frac{bn^2}{u}\right)^{z-1} e^{-u} du. \tag{4.50}$$

We now Taylor expand and truncating the integrand in each regime, as before. After some algebra we obtain

$$\begin{aligned} G = {} & u^{\star z-1} \left(1 - e^{-u^\star} + \frac{z-1}{u^\star} \left(1 - e^{-u^\star}(1 + u^\star)\right)\right) \\ & + \Gamma\left(z, u^\star\right) + u^\star(z-1)\Gamma\left(z-1, u^\star\right). \end{aligned} \tag{4.51}$$

Using the fact that

$$u^\star(z-1)\Gamma\left(z-1, u^\star\right) = u^\star\Gamma\left(z, u^\star\right) - u^{\star z} e^{-u^\star}. \tag{4.52}$$

We rewrite the expression as

$$\begin{aligned} G = {} & u^{\star z-1} \left(1 - e^{-u^\star} + \frac{z-1}{u^\star} \left(1 - e^{-u^\star}(1 + u^\star)\right)\right) \\ & + (1 + u^\star)\Gamma\left(z, u^\star\right) + (z - e^{-u^\star})u^{\star z}. \end{aligned} \tag{4.53}$$

In order to make further progress in obtaining an approximation for G, and hence the probability distribution for the terminal-associated active threadings, we examine $u^\star$ and ask when it is large $u^\star \gg 1$ or small $u^\star \ll 1$.

Recalling $u^\star = bn^2$ and $b \ll 1$ we see that there is a characteristic n value, written $n^\star$, that separates these two regimes, defined according to $bn^{\star 2} = 1$. This mode number is significant. The regime $b \ll 1$ should more properly be defined as the regime in which *some* n-modes are strongly advected and others are not. The modes $n < n^\star$ arse strongly advected while higher n-modes are weakly advected (approximately diffusive). This has a physical interpretation. The longer wavelength, slowly relaxing modes $n < n^\star$ feel the effect of the entropy from the threading network more strongly and respond to it as a result. The shorter wavelength, rapidly relaxing modes $n > n^\star$ do not live long enough to experience significant advection.

For the specific case of $n \ll n^\star$, corresponding to the strongly advected modes, we have $u^\star \ll 1$. For these modes we can show that equation 4.53 becomes

$$G = (z-1)(bn^2)^z + \Gamma(z) - \frac{(bn^2)^z}{z} + \frac{(bn^2)^{z+1}}{z+1} - \frac{(bn^2)^{z+2}}{2(z+2)} + \cdots . \tag{4.54}$$

We thereby obtain an approximation for equation 4.32 in this limit

$$\tilde{\psi}_n(z) = \frac{2\pi\epsilon}{\beta^\star L^2} n^{(1-2z)} b^{-z} \left(\Gamma(z) + \left(z - 1 - \frac{1}{z} \right) (bn^2)^z + \frac{(bn^2)^{z+1}}{z+1} \right) \text{ for } n \ll n^\star. \tag{4.55}$$

We now seek the corresponding expression for the diffusive modes $n \gg n^\star$, corresponding to $u^\star \gg 1$. In this case we again expand, truncate and integrate to show

$$G = u^{\star z-1} + (z-1)u^{\star z-2}. \tag{4.56}$$

Hence

$$G = (bn^2)^{z-1} + (z-1)(bn^2)^{z-2}. \tag{4.57}$$

Reassuringly, this is exactly the same as equation 4.38. This is because they both represent the same expression in the case of diffusive modes. In the previous section (4.0.1) the advection of active threadings was assumed to be sufficiently weak that *all* modes were diffusive while in the present section it is only the modes $n \gg n^\star$ that are diffusive in character. This leads to the

approximate result

$$\tilde{\psi}_n(z) = \frac{2\pi\epsilon}{\beta^\star L^2} n^{(1-2z)} b^{-z} \left((bn^2)^{z-1} + (z-1)(bn^2)^{z-2} \right). \tag{4.58}$$

Hence

$$\tilde{\psi}_n(z) = \frac{2\pi\epsilon}{\beta^\star L^2} n \left(\frac{1}{bn^2} + (z-1)\frac{1}{b^2 n^4} \right) \quad \text{for} \quad n \gg n^\star. \tag{4.59}$$

Reassuringly, this is identical to equation 4.39 for the same reasons as described above.

In summary, we have now calculated the transform of the probability distribution for the terminal-associated active threadings when threadings are numerous and (some) modes are advected by the entropy associated with the network of threadings. The corresponding solution is the combination of equations 4.55 and 4.59.

We are interested in the lifetime of the terminal active threading in this regime. This is related to the lifetime of the terminal-associated active threading, as previously described. We will examine the expressions for this lifetime using both definitions (4.28) and (4.31). We focus first on definition 1, according to (4.28).

In order to compute (4.28) we need to evaluate the summation that appears in its definition in the limit $a \to 0$, corresponding to $z \to 1/2$. This summation takes the form

$$\begin{aligned} \lim_{z\to\frac{1}{2}} \sum_{n=1;odd}^{m} \frac{\tilde{\psi}_n(z)}{n} &= \sum_{n=1;odd}^{m} \lim_{z\to\frac{1}{2}} \frac{\tilde{\psi}_n(z)}{n} \\ &= \frac{2\pi\epsilon}{\beta^\star L^2 \sqrt{b}} \sum_{n=1;odd}^{n^\star} \frac{1}{n} \left(\Gamma\left(\frac{1}{2}\right) - \frac{5}{2}\sqrt{b}n + \frac{2}{3} b^{\frac{3}{2}} n^3 \right) \\ &\quad + \frac{2\pi\epsilon}{\beta^\star L^2} \sum_{n=n^\star;odd}^{m} \left(\frac{1}{bn^2} - \frac{1}{2b^2 n^4} \right). \end{aligned} \tag{4.60}$$

Here we have first identified that the largest mode consistent with our coarse graining at the scale of the threadings is the $n = m$ mode. Modes with $n > m$ would correspond to diffusion on length scales less than the distance between threadings. They would therefore proceed with the bare curvilinear diffusion constant D_c, rather than the renormalised diffusion that takes into account

the "hopping" process corresponding to the loss/renewal of terminal passive threadings. We further split the summation into two domains, one for $n < n^\star$ (the second line) and the other for $n^\star < n < m$ (the third line). The summands in each of these terms come from the approximations given in equations 4.55 and 4.59 respectively. Thus equation 4.60 gives us an approximation to $\tau_p^\star$.

Using integral approximations to calculate the summations and setting the upper limit as a number of threadings m. Here, we are using the fact that the number of penetrations limits the number of possible modes.

$$\begin{aligned}\lim_{z\to\frac{1}{2}} \sum_{n;odd} \frac{\tilde{\psi}_n(z)}{n} &\approx \frac{\pi\epsilon}{\beta^\star L^2}\left(\sqrt{\frac{\pi}{b}}\ln n^\star + \frac{1}{b}\left(\frac{1}{n^\star}-\frac{1}{m}\right) + \frac{1}{6b^2}\left(\frac{1}{n^{\star 3}}-\frac{1}{m^3}\right)\right) \\ &= \frac{2\tau_D b\epsilon}{\pi L^2}\left(\sqrt{\frac{\pi}{b}}\ln n^\star + \frac{1}{b}\left(\frac{1}{n^\star}-\frac{1}{m}\right) + \frac{1}{6b^2}\left(\frac{1}{n^{\star 3}}-\frac{1}{m^3}\right)\right).\end{aligned} \tag{4.61}$$

The above result allows us to derive an expression for 4.28, giving the first definition of the removal time of the terminal passive threadings

$$\tau_p^\star = \frac{4\tau_D}{\pi^2}\left(\frac{\epsilon}{L}\right)\left(\sqrt{\pi}\sqrt{b}\ln b^{-\frac{1}{2}} + \left(b^{\frac{1}{2}}-\frac{1}{m}\right) + \frac{1}{6b}\left(b^{\frac{3}{2}}-\frac{1}{m^3}\right)\right). \tag{4.62}$$

The limit of small b implies high values of $n^\star = 1/\sqrt{b}$ and also a high number of penetrations m. The leading order scaling can be shown to be

$$\frac{\tau_p^\star}{\tau_D} \sim b^{\frac{1}{2}}\ln b, \tag{4.63}$$

or writing in terms of m,

$$\frac{\tau_p^\star}{\tau_D} \sim \frac{\ln m}{m^{\frac{1}{2}}}. \tag{4.64}$$

We apply the same of approach as we did in case of $\tau_p^\star$ to the case of τ_p by separating the summation into two regimes where $n \le n^\star$ and $n^\star < n \le m$. We then determine τ_p by considering the numerator

$$
\begin{aligned}
-\frac{1}{\beta^\star}\sum_{n;odd}\frac{1}{n}\frac{\partial\tilde{\psi}_n}{\partial a} &= \frac{\pi\epsilon}{\beta^{\star 2}L^2}\sum_{n;odd}(bn^2)^{-z}\left(\frac{\partial G}{\partial z}-\ln(bn^2)G\right)\\
&= \frac{\pi\epsilon}{\beta^{\star 2}L^2}\Big[\sum_{n=1}^{n^\star}(bn^2)^{-z}\left(\frac{\partial G}{\partial z}-\ln(bn^2)G\right)\\
&+ \sum_{n=n^\star;odd}^{m}(bn^2)^{-z}\left(\frac{\partial G}{\partial z}-\ln(bn^2)G\right)\Big]. \qquad (4.65)
\end{aligned}
$$

Using the integral approximation, we can express the numerator in terms of b as follows

$$
\begin{aligned}
-\frac{1}{\beta^\star}\sum_{n;odd}\frac{1}{n}\frac{\partial\tilde{\psi}_n}{\partial a} &\sim \frac{\pi\epsilon}{2\beta^{\star 2}L^2}\left[\sqrt{\frac{\pi}{b}}\left(0.98\ln b+\frac{1}{4}(\ln b)^2\right)+\frac{1}{3b^2}\left(b^{\frac{3}{2}}-\frac{1}{m^3}\right)\right]\\
&= \frac{2\tau_D^2 b^2\epsilon}{\pi^3 L^2}\left[\sqrt{\frac{\pi}{b}}\left(0.98\ln b+\frac{1}{4}(\ln b)^2\right)+\frac{1}{3b^2}\left(b^{\frac{3}{2}}-\frac{1}{m^3}\right)\right]. \qquad (4.66)
\end{aligned}
$$

We only consider the dominant terms and ignore the parts involving the high value of m as well as small b. By combining the preceding numerator with the denominator 4.61. Finally, we achieve τ_p in the form of the parameter b

$$
\tau_p \approx -\frac{\tau_D}{\pi^2}b\left(1.96+0.5\ln b\right), \qquad (4.67)
$$

or scales with the number of penetrations

$$
\frac{\tau_p}{\tau_D}\sim\frac{\ln m}{m}. \qquad (4.68)
$$

It is always a good idea to compare the analysis with the simulation results. So far, we already acquired the expressions for the lifetime of the terminal passive threading with two different definitions. The first definition is defined using the zeroth moment 4.28 and the second definition implementing the first-moment 4.31. It is possible to construct some numerical results regarding these two solutions. Moreover, as we did the analysis on the possible asymptotic limits of the solution, which are the advective limit (small b) and the diffusive limit (large b), we can also check the validity of our analysis. The detailed description will be discussed in the next section.

4.1 Comparison between the analytical result and the simulation

The first definition of τ_p is not what we measured in the present simulations. Therefore, what we can do with this value is to compare its numerical solution with the asymptotic analysis. Figure 4.6 shows the plot between the normalised $\tau_p^\star$ and the parameter b. The result reveals the analytic solution of $\tau_p^\star$ converges to the numerical results in the diffusive limit. This is not surprising since in that limit the number of threading is converging to zero, leaving the ring follows the standard reptation. It also implies the scaling $\tau_p^\star \sim \tau_D$. On the other hands, the advective region (small b) presents the lifetime of the terminal passive penetration depending on the stress relaxation time in such a way that $\tau_p^\star/\tau_D \sim m^{-\frac{1}{2}} \ln m$.

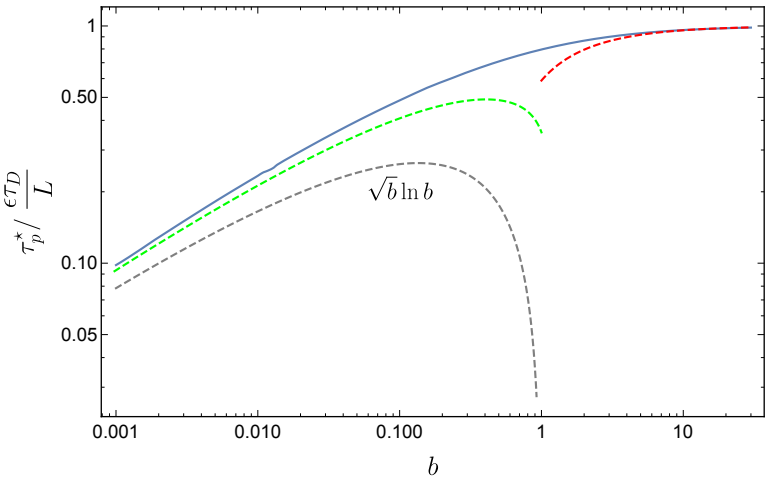

Figure 4.6: Full numerical results for the dimensionless lifetime of passive threadings $\tau_p^\star$ (shown in blue) converges to two asymptotic limits: $b \ll 1$ (green dashed line) indicating an advective regime and $b \gg 1$ (red dashed line) showing a diffusive regime. The black-dashed line shows the crude approximation $\tau_p^\star \sim \sqrt{b} \ln b$.

Next, we compare the second definition of τ_p with the simulation result τ_p^{sim}, see Fig. 4.7. This requires us to adopt some form of $b(m)$. Because we would also like to include the regime $m < m_c$ in our results we need a way of estimating $b(m)$ in this regime and we would like to avoid the overly crude approximation $\Delta F = 0$, corresponding to $b \to \infty$. We therefore utilise equation 4.22 to directly interpolate b from the simulation results shown in

Fig. 4.4. This has the advantage that we recover (4.24) for large m but also a smoothly increasing b for $m < m_c$ that only diverges in the limit $m \to 0$. In Fig. 4.7, the simulation data is presented in red with error bars and is also normalised by the average stress relaxation time of ring polymer τ_d while the analytical result is shown on a different axis and is normalised by τ_D. It is worth to clarify here that τ_d is not the same as τ_D defined by equation 4.16. From the graph, the two cases agree in the diffusive regime ($\tau_p/\tau_D = \tau_p^{sim}/\tau_D$). However, decreasing of b reveals the simulation data falling much faster than the numerical results. This gives us the idea that we might not measure the same relaxation time. The minimum value of the threading time from the simulation data, around $b \approx 0.5$, is most different to the numerical result when normalised in this way, involving a large factor of about $\mathcal{O}(10^2)$.

4.2 Chapter conclusion

Throughout this chapter, I provided an alternative analysis of the stress relaxation process of the threaded ring network. In the previous chapter, we introduced the scaling $\tau_d \simeq (m/2)^2\tau_p$, which was shown to be self-contradictory with the age of the threadings $\tau_p \simeq \tau_d$. To reconcile this, we seek to analyse the relaxation of rings differently by considering the distribution of terminal-associated active penetrations. The result reported in Fig.4.3 revealed a thermodynamic bias of the active threading towards the ends of the duplex ring. The proposal in this thesis is that the active penetrations experience the repulsive force pushing them away from the centre and this fundamentally affects the decay process of terminal-associated active threadings. The identification of an entropy, arising from the network topology, is a new discovery. We believe that it may play an important role here by providing a force that biases the decay of the terminal-associated active threadings. The approximation that we used for the thermodynamic potential arising from the network topology, as used in the analysis, was chosen to have the most simple form - a harmonic potential with symmetry around the middle of the chain. The harmonic potential tends to drive the active threadings towards the ends and thus has the opposite sign compared to what we usually think of as a harmonic (confining) potential in Physics. The potential should really be thought of as a free energy,

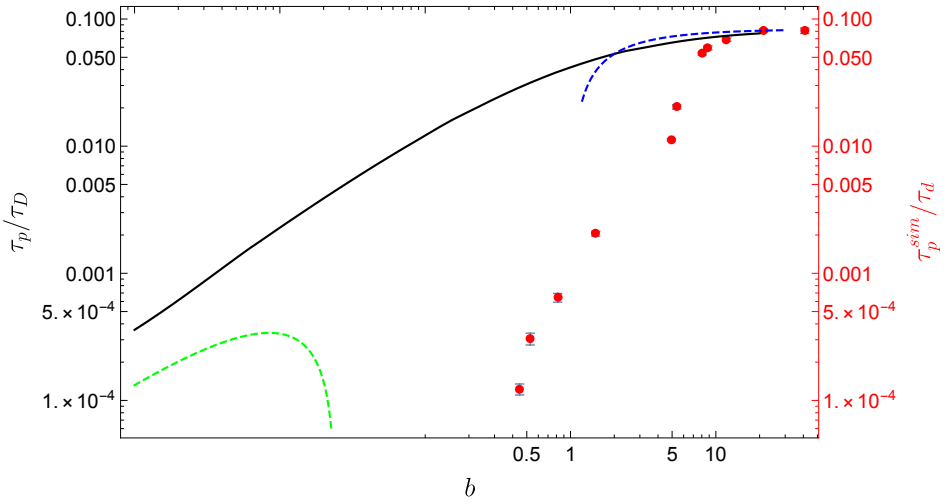

Figure 4.7: The characteristic lifetime of the terminal passive threadings τ_p is important in setting the rate for stress relaxation and evolution of the threading network. τ_p is related to b, a parameter that controls the strength of advection of terminal-associated active threadings towards the chain end due to the effect of the threading network entropy. When $b < 1$ there are many threadings and the advection is strong, while $b > 1$ corresponds to the case in which there are few threadings and the motion of the terminal-associated active threading is nearly diffusive. The solid black line represents the approximation for the lifetime of the terminal passive threadings τ_p given by (4.31) with (4.27), together with an interpolation for b from equation 4.22 and the data shown in Fig 4.4. This time appears in units of τ_D. The simulation results for the lifetime of the terminal passive threadings are shown by red data points and are normalised by the stress relaxation time τ_d. Both results shows consistency in the limit that the value of b is large as the motion is diffusive and $\tau_D \approx \tau_d$. However, the simulation result deviates from the analytic results for smaller b as the number of penetrations increases. This may be related to the fact that τ_D and τ_d may represent rather different times in this regime. The blue and green dashed lines refer to the analytic approximations in the two limits given by equations 4.49 and 4.67, respectively.

since it can be traced purely to the network entropy.

The diffusion of the active penetration was studied using the Fokker-Planck equation incorporating the free energy difference as a driving term. This problem could be approached using the initial condition that the active threading segment is inserted to the system at either end together with the absorbing boundaries. The modified condition 4.5 with the extended domain reduced the problem to the partial differential equation of the time-dependent coefficient $\psi_n(t)$. The PDE could be solved analytically using the method of

characteristics. A Laplace transform approach allowed us to solve for the transformed coefficient $\tilde{\psi}(\omega)$ and hence to calculate the lifetime of a terminal passive penetration. We defined two simple definitions, e.g., the zeroth-moment 4.28 ($\tau_p^\star$) and the first-moment 4.31 (τ_p). They were analysed in two asymptotes, small b (advective) and large b (diffusive). The parameter b is related to the strength of the potential and scales with the number of penetrations such that $b \sim 1/m$. As a consequence, $\tau_p^\star$ and $\tau_p \sim \tau_D$ in the diffusive limit. The advective regime suggested that $\tau_p^\star/\tau_D \sim m^{-\frac{1}{2}} \ln m$ and $\tau_p/\tau_D \sim m^{-1} \ln m$. Ultimately the agreement with the simulation data had right trend but a much stronger dependence on b than predicted by the theory. One interpretation of this is that it further reflects the non mean-field character of the problem in which an approach based on a Fokker-Plank equation for a (representative) active threading is inadequate. While this is an essentially negative result it may be significant in informing future studies. It suggests that an approach based on retaining information at the level of, e.g. distribution functions over the network, rather than only mean quantities may be more promising. Ultimately, it may be that analytic approaches simply remain very difficult and we need to rely primarily on simulation results, either of the sort presented in this thesis or using full MD. The former has the approach that it is easier to access large values of m but has drawbacks, including the use of a rather restrictive duplex assumption.

Chapter 5

Conclusion

Understanding the physics of highly entangled ring polymers has become a primary interest of a growing number of polymer physicists. A proper understanding of this topic remains unresolved. One of the most challenging problems is to understand the role of threading between ring polymers, the existence of which has only recently been unambiguously established in MD simulations. One finding reported in this literature is that threadings slow down the dynamics of rings. This motivated us to study a system of threading ring polymers by re-purposing well-established conceptual tools, such as Tube model and reptation dynamics. The main objective of this research was to study a system of ring polymers embedded in a gel and to understand the role of threading in controlling the dynamics of ring polymers. While the presence of a gel is required to ensure a duplex character for the rings, in which each gel mesh volume contains both an outgoing and a returning ring polymer segment, it may be that these results could also bring some understanding to the canonical problem of ring melts. Our investigation involved performing computer simulations using Monte Carlo sampling to simulate the motion of the polymers. Inter-ring penetration, or threadings, are introduced in a simple manner by postulating the existence of some probability to insert a new (pair of) threading(s) after each successful microscopic move. Our study also extended to theoretical work taking inspiration from the simulations. Our goal was to build an analytical model that helped us to understand more about the dynamics of rings.

The new results from this work were mainly presented in chapter 3 and

4. In chapter 3 Monte Carlo dynamics of identical ring polymers in a non-fluctuating gel were studied using computer simulations. The framework of this study is limited to the problem of flexible, unlinked and unknotted ring polymers. Above all, rings are assumed to retain the duplex structure, allowing them to explore space by a reptation-like motion, reminiscent of linear polymers. The existence of terminal segments in the duplex configuration means that the motion is end-directed and, as a result, it is only the motion of these ends that can (sometimes) thread through the contour of another duplex chain to create a threading. These threadings generate the only inter-ring interactions in the simulations: ring polymers can now protrude into or be threaded by other chains. We measured the variation of the stress relaxation time with increasing polymer length and the number of threadings. The concentration of the system was considered above the overlap concentration to ensure that rings were in close proximity to other rings. Increasing the polymer concentration could change two of our parameters. Firstly, its reasonable to expect that the threading probability p could depend on the local polymer concentration. Calibrating this is beyond the scope of this work but could be achieved, e.g. by running microscopically realistic (3D) polymer simulations, noting that the rate depends on the local environment of a duplex end and so these simulations could be performed at modest chain lengths. Secondly, changing the concentration changes the tube diameter. Within our model this has the effect of renormalising N, defined as the number of tube-sized segments, or "blobs" in the chain. For ideal chains the approximate scaling is $N \sim c^2$, corresponding to blobs containing $g \sim 1/c^2$ monomers [de Gennes, 1979].

We believe that it is primarily the number of threadings that controls the complexity of the network of inter-ring threadings, and hence the relaxation time. In this work, we extended our simulations into an extreme regime in which a new pair of threading is formed with probability $p = 1$ following every successful microscopic chain displacement move. Although this regime is likely unphysical, in a strict sense, what it allows us to do is reach the largest possible number of threadings m at fixed length N. Our simulations are then most efficiently focussed on exploring the role of threadings, rather than expending the computing time moving longer inter-threading sections of polymer. Our simulation results reveal that the mean stress relaxation time

increases exponentially with polymer length $\tau_d \sim \exp(\alpha N)$. This is in contrast to the more usual power-law behaviour for unthreaded polymers, here $\tau_d \sim N^2$ (an additional power of N is absorbed into the microscopic "hop" time, by which all dimensionless times are scaled). This exponential stress relaxation, with an origin in the topology of the ring polymers, has been referred to as a topological glass.

We also examined the statistics of the stress relaxation process and found that it exhibits heavy-tailed statistics with a long late-time tail. These rare, extremely slow, relaxation events are likely due to correspondingly rare network topologies that can be undone in only a few different long and "obscure" move sequences. We tested the conjecture that the dynamics of the rings might follow the Doi-Edwards behaviour of linear polymers, but with a renormalised (much slower) diffusion constant. This was shown not to be the case by comparing the moments of the stress relaxation function obtained by simulation with the Doi-Edwards theory. The slowing of ring polymers is also reflected in the polymers mean square displacement in time, with the emergence of a long, sub-diffusive regime for intermediate times. This finding also underlines that the dynamics of threaded ring polymers cannot as simple as Fickian diffusion with an effective diffusion constant. We anticipated that the stress relaxation time τ_d might depend on the time taken to relax terminal passive penetrations τ_p such that $\tau_d \sim (m/2)^2\tau_p$. This was shown to be inconsistent with another seemingly natural assumption that the relaxation of active (and hence passive) threadings and the relaxation of stress have similar timescales. It was also shown to be inconsistent with the simulation results. On the other hand, an equivalent scaling argument based on the *rates* rather than the times of these relaxation processes is compatible with the simulations. Here the relationship $1/k_d \simeq (m/2)^2/k_p$ was preserved, even in the limit of a large number of threadings. This indicates that some simple understanding may be associated with these rates.

In chapter 4 we studied the statistics of the threadings and worked to construct a better analytical understanding of the dynamics controlling the lifetime of threadings. We confirmed that active threadings residing near the ends of the active polymer that carries them are shorter-lived in contrast to the ones located near the middle of the chain. Our study of threading lifetimes was

motivated by the significance of terminal passive penetrations, since they are the mechanism that blocks the motion of double-folded rings. Significantly, we discovered a non-uniform distribution of terminal-associated active threadings - the partners to the terminal passive threadings on another chain. A naive view of active threadings is that they should be uniformly distributed (if rare, and hence non-interacting) because they are injected at, and removed from, the chain ends. Like any (featureless) equilibrium system with this character they might be expected to adopt a uniform distribution, e.g. a tube of water open to a reservoir of dye at each end or a conducting rod with its ends at constant temperature: at equilibrium the distribution of dye, or heat, will become uniform. The breakdown of uniformity in the distribution of active threadings therefore has thermodynamic significance. We associate this with an entropy associated with the (accessible) configurations of the threading network: There are more topologically accessible threading networks with terminal-associated active threadings near the chain ends than the middle, a somewhat non-trivial result. One can relate a potential, or free energy, with this non-uniform distribution. This drives terminal-associated active threadings to the chain ends. We find evidence that the free energy difference between such a threading at the end and near the middle increases linearly with m. While the regime of m accessible to us was limited, resulting in a free energy difference of order $k_{B}T$, the linear scaling of free energy with the number of penetrations suggests that for longer rings with more threadings this energy could become arbitrarily large. Even $k_{B}T$ is enough to quantitatively bias the distribution. The diffusion of the terminal-associated active penetration (actually the chain moves, the tube segment associated with the threading remains stationary) was studied using a Fokker-Planck equation with appropriate (absorbing) boundaries. The potential arising from the network entropy was chosen to be harmonic, with symmetry around the middle of the chain. This gave a good fit to the distribution of positions of terminal-associated active threadings. This allowed us to calculate the time τ_{p}, which is the lifetime of the terminal passive threadings and an (unknown) renormalised diffusion constant. In the analysis, we defined this relaxation time in two ways, first as the zeroth and then the first moment of the relaxation function. These were analysed in two asymptotic limits. The first of these is a "diffusive" regime, in which the entropy difference

of the network is negligible, and the dynamics of the duplex rings reduces to Doi-Edward curvilinear diffusion, as for linear polymers (unthreaded duplex rings can be treated as linear polymers). The other asymptote is the "advective" regime in which the force due to the network entropy becomes large enough to dominate diffusion. Here the simulation results are rather different from the numerical calculation. In the simulation, we measured the lifetime of the terminal passive penetration at the end of any relaxation processes. The discrepancy may signify that any attempt at a mean-field analysis may fail, signifying that the system is inherently non mean-field (the use of a Fokker Plank equation represents a mean field approach). In spite of the fact that this might be viewed as a negative result it may prove extremely useful in informing the construction of future theories. These may have to be based on a full distribution function, rather than average quantities alone.

The simulation model implemented in our research is promising for the study of the dynamics of ring polymers in a gel due to the ability to access the highly threaded regime. This will remain inaccessible to brute-force MD approaches for the foreseeable future and so any progress relies on the development of simplified models, such as the Monte Carlo approach employed here. A possible extension of our work would be to integrate its results into a more traditional MD simulation. Our simulations are very efficient at creating equilibrated networks of threadings that are far larger than can be accessed using existing MD simulations, indeed this is the main advantage of our approach. It may then be possible to transplant the duplex networks that we can generate into MD simulations. This would be in the spirit of an initial condition - the MD simulations would be initialised to resemble a network of duplex rings with the specified threading network. This approach would allow us to investigate the properties of such equilibrated networks on shorter timescales but using more microscopically faithful techniques and may be advantageous, both for efficiently pre-equilibrating MD simulations but also verifying the results of our work, e.g. in the way the network changes. Other possible extensions include introducing gel imperfections, such as dangling ends, that would be present in any real gel and potentially protrude through the ring polymers, generating passive gel-ring threadings. Another possible extension would be to include the possibility of self-threaded rings. However, the most pressing

extension would be to understand a system of double-folded ring polymers that are permitted to extend branches, forming lattice animals. It would be fascinating to study the effect of this on threading and stress lifetimes, and dynamics in general.

Bibliography

[Anderson, 1995] Anderson, P. W. (1995). Through the glass lightly. *Science*, 267(5204):1615–1616.

[Bates and Maxwell, 2005] Bates, A. and Maxwell, T. (2005). *DNA Topology*. Oxford bioscience. Oxford University Press.

[Berne and Pecora, 2000] Berne, B. J. and Pecora, R. (2000). *Dynamic Light Scattering: With Applications to Chemistry, Biology, and Physics*. John Wiley & Sons, Ltd.

[Bhattacharjee et al., 2013] Bhattacharjee, S. M., Giacometti, A., and Maritan, A. (2013). Flory theory for polymers. *Journal of Physics: Condensed Matter*, 25(50):503101.

[Birshtein and Ptitsyn, 1966] Birshtein, T. M. and Ptitsyn, O. B. (1966). *Conformations of Macromolecules*. NY, Wiley.

[Carraher, 2017] Carraher, C. (2017). *Introduction to Polymer Chemistry, Fourth Edition*. Taylor & Francis.

[Cates and Deutsch, 1986] Cates, M. and Deutsch, J. (1986). Conjectures on the statistics of ring polymers. *Journal de Physique*, 47(12):2121–2128.

[Christiansen et al., 1973] Christiansen, C., Christiansen, G., Bak, A. L., and Stenderup, A. (1973). Extrachromosomal deoxyribonucleic acid in different enterobacteria. *Journal of bacteriology*, 114(1):367–377.

[Cotton, 1980] Cotton, J. P. (1980). Polymer excluded volume exponent v : An experimental verification of the n vector model for n = 0. *Journal De Physique Lettres*, 41:231–234.

[de Gennes, 1971] de Gennes, P. G. (1971). Reptation of a polymer chain in the presence of fixed obstacles. *The Journal of Chemical Physics*, 55(2):572–579.

[de Gennes, 1979] de Gennes, P. G. (1979). *Scaling concepts in polymer physics*. Cornell University Press, 1 edition.

[Doi, 1996] Doi, M. (1996). *Introduction to Polymer Physics*, chapter 5, pages 93–113. Oxford science publications. Clarendon Press.

[Doi and Edwards, 1986] Doi, M. and Edwards, S. F. (1986). *The Theory of Polymer Dynamics*. International series of monographs on physics. Clarendon Press.

[Domb et al., 1965] Domb, C., Gillis, J., and Wilmers, G. (1965). On the shape and configuration of polymer molecules. *Proceedings of the Physical Society*, 85(4):625–645.

[Drew et al., 2004] Drew, H., Luisi, B., Travers, A., and Calladine, C. R. (2004). *Understanding DNA : The Molecule and How It Works*. Elsevier Science & Technology.

[Edwards, 1967] Edwards, S. F. (1967). The statistical mechanics of polymerized material. 92(1):9–16.

[Edwards, 1977] Edwards, S. F. (1977). The theory of rubber elasticity. *British Polymer Journal*, 9(2):140–143.

[Einstein, 1905] Einstein, A. (1905). Über die von der molekularkinetischen theorie der wärme geforderte bewegung von in ruhenden flüssigkeiten suspendierten teilchen. *Annalen der Physik*, 322(8):549–560.

[Flory, 1949] Flory, P. J. (1949). The configuration of real polymer chains. *The Journal of Chemical Physics*, 17(3):303–310.

[Flory, 1953] Flory, P. J. (1953). *Principles of Polymer Chemistry*. Cornell University Press.

[Flory, 1969] Flory, P. J. (1969). *Statistical Mechanics of Chain Molecules*. NY, Interscience Publishers.

[Grosberg, 2014] Grosberg, A. Y. (2014). Annealed lattice animal model and flory theory for the melt of non-concatenated rings: towards the physics of crumpling. *Soft Matter*, 10:560–565.

[Grosberg et al., 1988] Grosberg, A. Y., Nechaev, S., and Shakhnovich, E. (1988). The role of topological constraints in the kinetics of collapse of macromolecules. *Journal de Physique*, 49(12):2095–2100.

[Halverson et al., 2011a] Halverson, J. D., Lee, W. B., Grest, G. S., Grosberg, A. Y., and Kremer, K. (2011a). Molecular dynamics simulation study of nonconcatenated ring polymers in a melt. i. statics. *The Journal of Chemical Physics*, 134(20):204904.

[Halverson et al., 2011b] Halverson, J. D., Lee, W. B., Grest, G. S., Grosberg, A. Y., and Kremer, K. (2011b). Molecular dynamics simulation study of nonconcatenated ring polymers in a melt. ii. dynamics. *The Journal of Chemical Physics*, 134(20):204905.

[Kapnistos et al., 2008] Kapnistos, M., Lang, M., Vlassopoulos, D., Pyckhout-Hintzen, W., Richter, D., Cho, D., Chang, T., and Rubinstein, M. (2008). Unexpected power-law stress relaxation of entangled ring polymers. *Nature Materials*, 7(12):997–1002.

[Karayiannis et al., 2009] Karayiannis, N. C., Foteinopoulou, K., and Laso, M. (2009). The structure of random packings of freely jointed chains of tangent hard spheres. *The Journal of Chemical Physics*, 130(16):164908.

[Kavassalis and Noolandi, 1987] Kavassalis, T. A. and Noolandi, J. (1987). New view of entanglements in dense polymer systems. *Phys. Rev. Lett.*, 59:2674–2677.

[King et al., 1974] King, T. A., Knox, A., and McAdam, J. D. G. (1974). Polymer dynamics in solutions and gels from rayleigh light-scattered linewidths. *Journal of Polymer Science: Polymer Symposia*, 44(1):195–202.

[Kuhn, 1934] Kuhn, W. (1934). Über die gestalt fadenförmiger moleküle in lösungen. *Kolloid-Zeitschrift*, 68(1):2–15.

[Kuhn, 1936] Kuhn, W. (1936). Beziehungen zwischen molekülgröße, statistischer molekülgestalt und elastischen eigenschaften hochpolymerer stoffe. *Kolloid-Zeitschrift*, 76(3):258–271.

[Kuhn, 1939] Kuhn, W. (1939). Molekülkonstellation und kristallitorientierung als ursachen kautschukähnlicher elastizität. *Kolloid-Zeitschrift*, 87(1):3–12.

[Lo and Turner, 2013] Lo, W. and Turner, M. S. (2013). The topological glass in ring polymers. *Europhysics Letters*, 102(5):58005.

[Lodish et al., 2008] Lodish, H., Berk, A., Matsudaira, P., Kaiser, C. A., Krieger, M., Scott, M. P., Zipursky, L., and Darnell, J. (2008). *Molecular Cell Biology*. W. H. Freeman, fifth edition edition.

[Lopatina et al., 2011] Lopatina, L. M., Olson Reichhardt, C. J., and Reichhardt, C. (2011). Jamming in granular polymers. *Phys. Rev. E*, 84:011303.

[Michieletto, 2016] Michieletto, D. (2016). On the Tree-like Structure of Rings in Dense Solutions. *Soft Matter*.

[Michieletto et al., 2014] Michieletto, D., Marenduzzo, D., Orlandini, E., Alexander, G. P., and Turner, M. S. (2014). Threading dynamics of ring polymers in a gel. *ACS Macro Letters*, 3(3):255–259.

[Michieletto et al., 2017a] Michieletto, D., Nahali, N., and Rosa, A. (2017a). Glassiness and heterogeneous dynamics in dense solutions of ring polymers. *Phys. Rev. Lett.*, 119:197801.

[Michieletto et al., 2017b] Michieletto, D., Orlandini, E., Marenduzzo, D., and Turner, M. S. (2017b). Ring polymers: Threadings, knot electrophoresis and topological glasses. *Polymers*, 9:349.

[Michieletto and Turner, 2016] Michieletto, D. and Turner, M. S. (2016). A Topologically Driven Glass in Ring Polymers. *Proceedings of the National Academy of Sciences of the United States of America*, 113:5195–200.

[Milner and Newhall, 2010] Milner, S. T. and Newhall, J. D. (2010). Stress relaxation in entangled melts of unlinked ring polymers. *Phys. Rev. Lett.*, 105:208302.

[Nose and Chu, 1979] Nose, T. and Chu, B. (1979). Static and dynamical properties of polystyrene in trans-decalin. 1. nbs 705 standard near theta conditions. *Macromolecules*, 12(4):590–599.

[Rosa and Everaers, 2014] Rosa, A. and Everaers, R. (2014). Ring polymers in the melt state: The physics of crumpling. *Phys. Rev. Lett.*, 112:118302.

[Rosa and Everaers, 2019] Rosa, A. and Everaers, R. (2019). Conformational statistics of randomly branching double-folded ring polymers. *The European Physical Journal E*, 42(1):7.

[Rouse, 1953] Rouse, P. E. (1953). A theory of the linear viscoelastic properties of dilute solutions of coiling polymers. *The Journal of Chemical Physics*, 21(7):1272–1280.

[Rubinstein, 1986] Rubinstein, M. (1986). Dynamics of ring polymers in the presence of fixed obstacles. *Phys. Rev. Lett.*, 57:3023–3026.

[Rubinstein and Colby, 2003] Rubinstein, M. and Colby, R. H. (2003). *Polymer Physics*. Chemistry. Oxford University Press, 1 edition.

[Sakaue, 2012] Sakaue, T. (2012). Statistics and geometrical picture of ring polymer melts and solutions. *Phys. Rev. E*, 85:021806.

[Shapiro et al., 1999] Shapiro, T. A., Klein, V. A., and Englund, P. T. (1999). Isolation of kinetoplast dna. In Bjornsti, M.-A. and Osheroff, N., editors, *DNA Topoisomerase Protocols: Volume I: DNA Topology and Enzymes*, pages 61–67. Humana Press, Totowa, NJ.

[Smrek et al., 2020] Smrek, J., Chubak, I., Likos, C. N., and Kremer, K. (2020). Active topological glass. *Nature Communications*, 11(1):26.

[Smrek and Grosberg, 2015] Smrek, J. and Grosberg, A. Y. (2015). Understanding the dynamics of rings in the melt in terms of the annealed tree model. *Journal of Physics: Condensed Matter*, 27(6):064117.

[Smrek and Grosberg, 2016] Smrek, J. and Grosberg, A. Y. (2016). Minimal surfaces on unconcatenated polymer rings in melt. *ACS Macro Letters*, 5(6):750–754.

[Smrek et al., 2019] Smrek, J., Kremer, K., and Rosa, A. (2019). Threading of unconcatenated ring polymers at high concentrations: Double-folded vs time-equilibrated structures. *ACS Macro Letters*, 8(2):155–160.

[Vettorel et al., 2009] Vettorel, T., Grosberg, A. Y., and Kremer, K. (2009). Statistics of polymer rings in the melt: a numerical simulation study. *Physical Biology*, 6(2):025013.

[Volkenstein, 1958] Volkenstein, M. V. (1958). The configurational statistics of polymeric chains. *Journal of Polymer Science*, 29(120):441–454.

[Wall et al., 1963] Wall, F. T., Windwer, S., and Gans, P. J. (1963). Monte carlo study of coiling type molecules. i. macromolecular configurations. *The Journal of Chemical Physics*, 38(9):2220–2227.

[Zimm, 1956] Zimm, B. H. (1956). Dynamics of polymer molecules in dilute solution: Viscoelasticity, flow birefringence and dielectric loss. *The Journal of Chemical Physics*, 24(2):269–278.